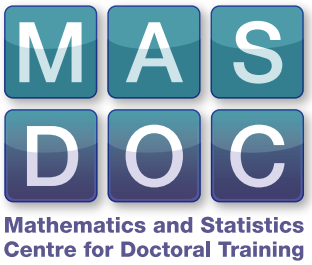

Phase Field Models on Evolving Surfaces

by

David O'Connor

Thesis

Submitted for the degree of

Doctor of Philosophy

Mathematics Institute

The University of Warwick

September 2016

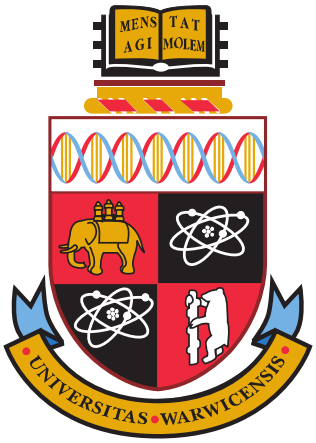

Contents

Acknowledgments

This work was supported by the UK Engineering and Physical Sciences Research Council (EPSRC) Grant EP/H023364/1 within the MASDOC Centre for Doctoral Training at the University of Warwick.

Thank you to my supervisor, Björn Stinner for all of his help and guidance throughout this project. Thank you, also, to everyone in MASDOC and Warwick who have made my time here a pleasure, especially my workmates Graham, Jorge and Ben.

To Mum, Dad, Nathan and Dominic, thank you for all of your support and help to get me to this point.

Declarations

This thesis is submitted to the University of Warwick in support of my application for the degree of Doctor of Philosophy. It has been composed by myself and has not been submitted in any previous application for any degree. The work presented was carried out solely by the author, under the supervision of Björn Stinner.

Part of this thesis has been submitted for publication by the author. Chapter 2, Chapter 3 (except for Section 3.5) and the numerical simulations of Chapter 4 have been submitted in a paper co-authored with Björn Stinner, *The Cahn-Hilliard Equation on an Evolving Surface, O'Connor and Stinner [2016].*

Abstract

We study the asymptotic limit of some evolving surface partial differential equations. We first examine the setting of an evolving surface with prescribed velocity, extending the method of formally matched asymptotic expansions to account for the movement of the domain. We apply this method to the Cahn-Hilliard equation, considering various forms for the mobility and potential functions. In particular looking at different scalings of the mobility with respect to the interface thickness parameter. Mullins-Sekerka type problems are derived with additional terms which are due to the domain evolution.

We then consider the evolving surface finite element method and applying it to the Cahn-Hilliard equation in an evolving surface setting. We do this so as to support the theoretical findings as well as to further explore some interesting behaviour of solutions.

We finally examine the setting of an evolving surface with an unknown surface velocity, described by a geometric evolution equation coupled to intrinsic fields on the surface. The method of formally matched asymptotic expansions is further extended to account for the unknown surface. We apply the technique to a derived model for focal cell adhesion which aims to extend a known model from the literature. We finish with simulations of a reduced model of our derived version.

Chapter 1

Introduction

1.1 Overview

In Section 1.1.1 we introduce the notion of phase field models, discussing some of their history and appearances in the literature as well as motivating their uses. In Section 1.1.2 we introduce the method of matched asymptotics and explain its relation to the phase field methodology. We will give an account of some known works in the area. In Section 1.2 we give an outline of the structure of this thesis and highlight the novel results in each chapter.

1.1.1 The Phase Field Methodology

The phase field methodology is a powerful tool for simulating phase separation and interfacial evolution in a wide variety of applications. Partial differential equations describing phase separation on evolving surfaces occur, for example, in de-alloying of binary alloys Eilks and Elliott [2008], in two-phase flow Hohenberg and Halperin [1977] (potentially with soluble surfactants H. Garcke and Stinner [2013]), in pattern formation on growing organisms Leung and Berzins [2003], or in phase separation on biomembranes Elliott and Stinner [2010b,a, 2013].

The types of situation modelled by phase field models typically consist of large regions, or phases, that are by some measure distinct from each other and immiscible. For example in binary alloys Eilks and Elliott [2008] the phases are the distinct regions of pure components of the alloy, or in two-phase flow the phases Hohenberg and Halperin [1977] are the different immiscible fluids. Conventional modelling techniques, those that generate free boundary problems, stipulate that the interfaces between these different phases are modelled by moving hypersurfaces and are thus *sharp*. They thus decompose the domain into a multi-domain structure

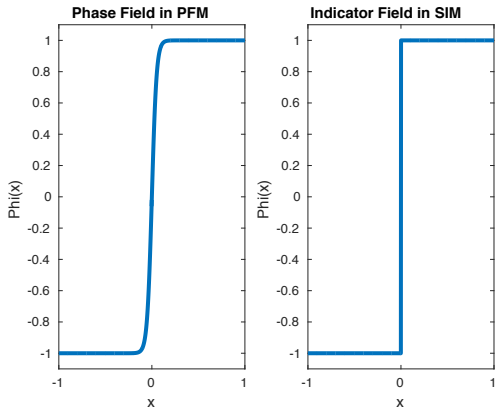

Figure 1.1: Comparison of sharp versus diffuse interface approach for a function ϕ which describes the regions. In the diffuse interface method ϕ changes continuously between equilibrium values rather than making a discontinuous jump. The interface in both exists at $x = 0$ with the interfacial region existing for $|x| < 0.1$ in the diffuse interface approach.

described by the position of the interfacial boundaries. Usually a set of differential equations is solved in each domain subject to flux conditions and constitutive laws at the interfaces.

In contrast, using the phase field technique, also known as a diffuse interface approach, a phase field variable is introduced to keep track of the boundaries between pure phases. Typically the phase field variable will take distinct values in the different phases with the phases now separated by a narrow region where the phase field variable transitions between the values associated to each phase. The sharp interface is then approximated as some level set of the phase field variable. See Figure 1.1 for a pictorial representation of the two settings.

When solving free boundary problems the a priori unknown interface must be computed in addition to the solution of the governing differential equations in each region. Popular methods include level set methods Xu et al. [2006]; Gross and Reusken [2011]; Xu et al. [2014], front-tracking methods Muradoglu and Tryggvason [2008]; Lai et al. [2008]; Khatri and Tornberg [2011] and arbitrary Lagrangian-Eulerian methods Yon and Pozrikidis [1998]; Yang and James [2007]; Ganesan and Tobiska [2009]; Barrett et al. [2015], however these methods can break down when topological changes occur. The power of the phase field methodology arises from the implicit description of the interface through the phase field variable. Thus in modelling time dependent problems there is no need to explicitly track the interface.

The evolution of the interface will usually be described by a set of partial

differential equations, possibly derived as a minimiser of some energy Elliott and Stinner [2013] or through a gradient flow dynamic involving the variation of an energy Cahn and Hilliard [1958]; Cahn [1961]. As early as 1893, van der Waals used the idea of continuous variations in density across an interface to model a liquid-gas system. In 1950 Landau and Ginzburg [1950], Ginzburg and Landau used a complex valued phase field variable to model superconductivity and in 1958 Cahn and Hilliard [1958] Cahn and Hilliard published their seminal paper utilising a thermodynamic formulation to account for the inclusion of gradients in thermodynamic properties.

Phase field models need not be restricted to binary systems, with notable works by Steinbach et al. Steinbach et al. [1996]; Tiaden et al. [1998] and Garcke et al. Stinner et al. [2004]; Nestler et al. [2005] considering multiphase systems for arbitrary numbers of components. These multicomponent models naturally arise in the setting of material analysis, in particular in the solidification of alloys Cha et al. [2005].

Central to many phase field models is the use of the Ginzburg-Landau energy functional, which is an integral over the region under consideration of the following integrand:

$$\delta(\phi, \nabla\phi) := \frac{\varepsilon}{2}|\nabla\phi|^2 + \frac{1}{\varepsilon}F(\phi), \tag{1.1}$$

with ϕ the phase field variable, ε the interfacial thickness parameter and F a potential function. It has been used in the derivation of the Allen-Cahn equation Allen and Cahn [1979], the Cahn-Hilliard equation Cahn and Hilliard [1958] and for the modelling of two phase biomembranes Elliott and Stinner [2010a]. At the heart of this energy functional is the Landau term represented by the potential function, F.

Differing choices of potential function offer variations in the dynamics of each model. In many applications, F, is chosen to be of either double well type Elliott and Zheng [1986] or double obstacle type Blowey and Elliott [1991a]. As double well potential, it is standard to assume the form $F(\phi) = \frac{1}{4}(1-\phi^2)^2$, with this particular choice known as the standard double well potential. For a double obstacle type potential one might choose

$$F(\phi) = \frac{1}{2}(1-\phi^2) + I_{[-1,1]}(\phi) \tag{1.2}$$

with $I_{[-1,1]}(\phi)$ the indicator function of the interval $[-1,1]$ which takes value 0 when ϕ is in the interval, and value ∞ otherwise. Common to all potential functions are the minima, u_a and u_b, characterising the value of the phase field variable in the bulk regions. The gradient term of the Ginzburg-Landau energy is the part penalising large jumps in the gradient and thus generating the narrow interfacial

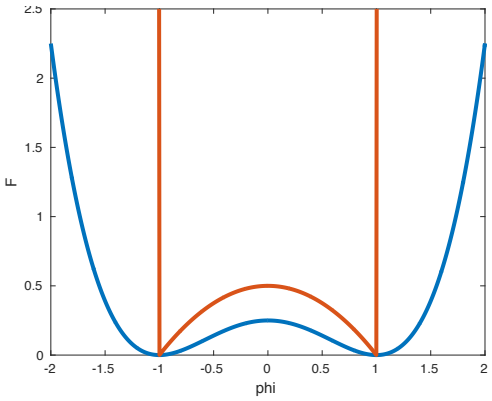

Figure 1.2: Two choices of potential. In blue the standard double well potential and in red the double obstacle type potential as in equation (1.2).

regions between the phase values.

The advantage of double-well type potentials are their smoothness properties but this is also their disadvantage since this can mean that the phase field variable does not always lie between the minima of the potential. In examples where a phase field model is used purely for interface tracking, Elliott and Stinner [2010a], this may not be a problem but in examples where the phase field variable has a physical interpretation, such as a density or concentration Eilks and Elliott [2008], it may not make sense for the phase variable to exceed it's bulk values. The obvious difficulty of using a double-obstacle type potential is that the governing equations must be expressed in terms of variational inequalities and can be difficult to solve. In Elliott and Garcke [1996], the following logarithmic potential was considered:

$$F(\phi) = \frac{\theta}{2}\left[(1+\phi)\log(1+\phi) + (1+\phi)\log(1-\phi)\right] + \frac{1}{2}(1-\phi^2) \tag{1.3}$$

which has the advantage of being smooth but in the limit $\theta \to 0$ tends to the double obstacle potential (1.2).

1.1.2 The Method of Matched Asymptotic Expansions

In each of the phase field models that we have discussed the interfacial layer, in which the phase field variable transitions between bulk values, has a thickness characterised by some scalar parameter in the model. Often this parameter is denoted ε. It is reasonable to ask under what conditions the phase field model can be related to a free boundary problem and to ask if in the limit $\varepsilon \to 0$, thus sending the interface width to zero, the solutions of the diffuse interface problems approximate in some

way the solutions of a free boundary problem. In some instances this is the case and the phase field model can be considered purely as an approximation of a free boundary problem. This limit of sending the interface width parameter to zero is known as an asymptotic limit or a sharp interface limit.

In the literature there are two types of asymptotic results on limits of phase field models. In works such as that of Pego Pego [1989] and Cahn et al. Cahn et al. [2006], the results are formal ones based on the method of formally matched asymptotics. The other type is of rigorous convergence as in the works of Bates et al. N. Alikakos and Chen [1994] or Le Le [2008]. In the former a rigorous justification was made of the asymptotics analysis and in the latter a Gamma-Convergence approach was used with an energy based argument, exploiting the gradient flow based structure of the model.

The method of matched asymptotics is formal in that it assumes the existence of a limiting free boundary problem. That is if ϕ^ε solves the diffuse interface problem, it is assumed that there is a sensible limit ϕ^0 in the sharp interface limit. The question becomes then what problem should this sharp interface solution satisfy. By assuming a possible decomposition of the domain, asymptotic expansions are made in the interface width variable, for both the bulk or outer regions (areas ϕ is approximately constant) and the interfacial or inner regions (where ϕ rapidly transitions). It is an assumption of the method that these expansions exist. These two expansions are then assumed to agree in some intermediate region and sets of matching conditions can be derived.

The need for two different expansions is due to the rapid transitions of the phase field variable in the inner region. By considering a new set of co-ordinates and rescaling them appropriately with respect to ε, the interface is effectively blown up to unitary width so that sensible limits of quantities dependent on ε can be established.

The method of matched asymptotics has been carefully detailed in the work of Fife and Penrose Fife and Penrose [1995] and can also be found in Caginalp Caginalp [1989]. The method has been used for multi-component systems in Garke and Stinner [2006a] and has been extended to elliptic problems on stationary surfaces Elliott and Stinner [2010a]. Much of the work in this thesis involves further extensions of the standard technique.

Although we cannot use the method of Gamma-Convergence to identify a free boundary problem, for reasons explained in Chapter 3, we briefly discuss the approach here for the sake of completeness. For systems derived using a gradient flow structure, such as the Cahn-Hilliard equation Cahn and Hilliard [1958] which is the

H^{-1} gradient flow of (1.1), or the Allen-Cahn equation Allen and Cahn [1979] which is its L^2 gradient flow, the convergence of the energy functional used in the gradient flow structure, in some appropriate manner, can be used to show convergence of solutions to the underlying gradient flows. The abstract framework can be found in the work of Serfaty Serfaty [2011].

It is known that the Ginzburg-Landau energy functional converges, in an appropriate sense, to the perimeter function i.e. the area function on the interface, and thus the L^2 gradient flow of this functional results in mean curvature flow, and the H^{-1} gradient flow gives the Mullins-Serkerka flow.

1.2 Outline of the Thesis

We briefly describe the organisation of this thesis with a short summary of the contents of each chapter.

In Chapter 2 we define the common notation used throughout this work. In particular we discuss the notion of surface calculus, then introduce the framework for adding a time dependence to these surfaces and discuss some of the important identities that can be found in this area's literature. There is also some discussion on useful results from differential geometry that we employ to look at curves on evolving surfaces. The main result that we investigate in this chapter is the effects of a time dependent surface on the change of variables formulae for use in our asymptotic analysis.

In Chapter 3 we consider a specific example of a phase field model on an evolving surface, namely the Evolving Surface Cahn-Hilliard (ESCH) equation. We use the results of the previous chapter alongside the method of matched asymptotic expansions to investigate the ESCH equations sharp interface limit. We consider general forms for its mobility and potential functions, initially restricting to smooth potentials, before looking at the case of a double obstacle potential. The novelty of this work comes from the postulation of an evolving surface and its effects on the asymptotic analysis and limiting models

In Chapter 4 we numerically investigate the evolving surface Cahn-Hilliard equation under the setting of a constant mobility function and a smooth quartic potential function. We provide supporting evidence of some of the results in Chapter 3 as well as displaying some examples which exhibit interesting behaviour caused by the surface movement. We give a general overview of the numerical methods used and also explain how we have applied it in our setting.

The subject of Chapter 5 is a phase field approach to a model for focal cell

adhesion. We extend a known model by Freund and Lin [2004], building on their observations regarding the process by which fronts propagate, in particular, we apply the phase field methodology to generate an intrinsic model on a surface. We also analyse the resultant model in the sharp interface limit to be able to compare it with the Freund and Lin model as well as other known literature results on two phase surface flows. This analysis is more complex than that presented in Chapter 3 due to the surface being an unknown. We also consider a reduced model and simulate it's solutions, looking to validate our model by qualitatively recovering some adhesion growth behaviour from the model of Freund and Lin [2004].

Chapter 2

Calculus on Evolving Surfaces

In this Chapter we discuss the elementary geometric analysis required throughout the remainder of this thesis. We first introduce the notation we have used in the context of surface calculus, introducing such structures as the surface gradient and the material derivative. We then look at how we can describe curves on evolving surfaces, introducing several different distance functions as well as the Darboux frame that we later use to reparameterise space locally around a given curve. Finally we present the result from O'Connor and Stinner [2016] with regards the change of variable formula for the signed distance function.

2.1 Notation

In this subsection we will discuss the notation and essential concepts of calculus on evolving surfaces required to describe partial differential equations in moving and curved space. A more detailed introduction can be found in Dziuk and Elliott [2013] and Dziuk and Elliott [2007]. Since we have in mind physical systems we present the following under a setting of two-dimensional hypersurfaces evolving in a three dimensional ambient space. However some of the facts presented in this section can be generalised to other dimensions.

More specifically we consider a smooth, closed, compact and connected evolving two-dimensional submanifold $\{\Gamma(t)\}_{t\in[0,T]}$ embedded in $\mathbb{R}^3$ for $t \in [0,T]$. We assume that it is orientable and denote by $\boldsymbol{\nu}(\cdot,t) : \Gamma(t) \to \mathbb{R}^3$, $t \in [0,T]$, a spatial unit normal vector field. By $\Gamma(0)$ we denote the initial hypersurface. The space-time manifold for the moving surface is denoted by

$$\mathcal{G}_T := \bigcup_{t\in[0,T]} \Gamma(t) \times \{t\}. \tag{2.1}$$

We have time-dependent *material surfaces* in mind, thus a material particle p located at $\boldsymbol{x}_p(t) \in \Gamma(t)$ at a time $t \in [0,T)$ has an associated velocity $\dot{\boldsymbol{x}}_p(t)$ which determines the evolution of the shape. In addition we assume a smooth velocity field $\boldsymbol{v}(\cdot,t) : \Gamma(t) \to \mathbb{R}^3$, $t \in [0,T)$, such that $\dot{\boldsymbol{x}}_p(t) = \boldsymbol{v}(\boldsymbol{x}_p(t),t)$.

For a function $f : \mathcal{G}_T \to \mathbb{R}$ the material derivative at a point $(\boldsymbol{x},t)$ with $\boldsymbol{x} \in \Gamma(t)$ and $t \in (0,T)$ is defined by

$$\partial_t^\bullet f(\boldsymbol{x},t) := \frac{d}{dt} f(\boldsymbol{x}_p(t),t) = \frac{\partial \tilde{f}}{\partial t}(\boldsymbol{x},t) + \boldsymbol{v}(\boldsymbol{x},t) \cdot \nabla \tilde{f}(\boldsymbol{x},t) \tag{2.2}$$

where $\boldsymbol{x} = \boldsymbol{x}_p(t)$ for a material particle p located at $\boldsymbol{x}$ at time t. Note that for the expressions on the right hand side to be well-defined a smooth extension $\tilde{f}$ of f to a neighbourhood of $\mathcal{G}_T$ is required however the value of $\partial_t^\bullet f$ is independent of this extension Dziuk and Elliott [2013]. The normal time derivative $\partial_t^\circ f$ can be similarly defined by considering particle paths $\boldsymbol{x}_{\boldsymbol{\nu}}(t)$ that move in a direction normal to the surface at all times. Thus if $\boldsymbol{x} = \boldsymbol{x}_{\boldsymbol{\nu}}(t)$ then

$$\partial_t^\circ f(\boldsymbol{x},t) := \frac{d}{dt} f(\boldsymbol{x}_{\boldsymbol{\nu}}(t),t) = \frac{\partial \tilde{f}}{\partial t}(\boldsymbol{x},t) + v_{\boldsymbol{\nu}}(\boldsymbol{x},t)\boldsymbol{\nu}(\boldsymbol{x},t) \cdot \nabla \tilde{f}(\boldsymbol{x},t) \tag{2.3}$$

where $v_{\boldsymbol{\nu}} = \boldsymbol{v} \cdot \boldsymbol{\nu}$ is the normal component of the velocity. The normal time derivative represents time rate of change due to the normal motion of the surface and is related to the material derivative by the identity $\partial_t^\bullet f = \partial_t^\circ f + \boldsymbol{v}_\tau \cdot \nabla \tilde{f}$, with $\boldsymbol{v}_\tau$ the tangential velocity. The tangential or surface gradient is defined as the projection of the standard derivative onto the tangent plane of the surface so that

$$\nabla_{\Gamma(t)} f(\boldsymbol{x},t) := \nabla \tilde{f}(\boldsymbol{x},t) - (\nabla \tilde{f}(\boldsymbol{x},t) \cdot \boldsymbol{\nu}(\boldsymbol{x},t))\boldsymbol{\nu}(\boldsymbol{x},t).$$

This quantity again makes use of any extension of f to a neighbourhood of $\Gamma(t)$ and is also independent of this choice of extension. We denote by $\underline{D}_i$ the i'th component of the surface gradient.

If $\boldsymbol{w} = (\boldsymbol{w}_i)_{i=1}^3, \boldsymbol{z} = (\boldsymbol{z}_i)_{i=1}^3 : \Gamma(t) \to \boldsymbol{R}^3$ are smooth vector fields then $\nabla_{\Gamma(t)}\boldsymbol{w}$ is the matrix with components $(\nabla_{\Gamma(t)}\boldsymbol{w})_{ij} = \underline{D}_j \boldsymbol{w}_i$ and we write $(\nabla_{\Gamma(t)}\boldsymbol{w})^T = (\underline{D}_i \boldsymbol{w}_j)_{ij}$ for its transpose and use the scalar product $\nabla_{\Gamma(t)}\boldsymbol{w} : \nabla_{\Gamma(t)}\boldsymbol{z} = \sum_{i,j} \underline{D}_j \boldsymbol{w}_i \underline{D}_j \boldsymbol{z}_i$. We will furthermore use the notation $\boldsymbol{w} \otimes \boldsymbol{z}$ for the matrix with entries $\boldsymbol{w}_i \boldsymbol{z}_j$. The surface divergence is defined by $\nabla_{\Gamma(t)} \cdot \boldsymbol{w} = \operatorname{tr}(\nabla_{\Gamma(t)}\boldsymbol{w})$ and the surface curl is defined with components $\left(\nabla_{\Gamma(t)} \times \boldsymbol{w}\right)_i = \epsilon^{ijk} \underline{D}_j \boldsymbol{w}_k$ with ϵ the permutation tensor.

At any point $\boldsymbol{x} \in \Gamma(t)$ we define the projection $\boldsymbol{P}(\boldsymbol{x},t) := \boldsymbol{I} - \boldsymbol{\nu}(\boldsymbol{x},t) \otimes \boldsymbol{\nu}(\boldsymbol{x},t) \in \mathbb{R}^{3\times 3}$, with $\boldsymbol{I}$ the identity matrix, to the tangent space $T_{\boldsymbol{x}}\Gamma(t)$. Observe that this is a symmetric matrix. With the help of $\boldsymbol{P}$ we can write $\nabla_{\Gamma(t)} f = \boldsymbol{P}\nabla f$,

$\nabla_{\Gamma(t)}\boldsymbol{w} = \nabla\boldsymbol{w}\boldsymbol{P}$, $\nabla_{\Gamma(t)} \cdot \boldsymbol{w} = \boldsymbol{P} : \nabla_{\Gamma(t)}\boldsymbol{w}$. The Laplace-Beltrami operator on $\Gamma(t)$ is defined as the tangential divergence of the tangential gradient, $\Delta_{\Gamma(t)}f = \nabla_{\Gamma(t)} \cdot \nabla_{\Gamma(t)}f$.

In contrast with the directional derivatives in planar space, the components of the gradient operator in curved space do not commute. For the commutation of derivatives we have the following result Dziuk and Elliott [2013]

$$\underline{D}_i\underline{D}_j f - \underline{D}_j\underline{D}_i f = \left(\nabla_{\Gamma(t)}\boldsymbol{\nu}\nabla_{\Gamma(t)}f\right)_j \boldsymbol{\nu}_i - \left(\nabla_{\Gamma(t)}\boldsymbol{\nu}\nabla_{\Gamma(t)}f\right)_i \boldsymbol{\nu}_j. \tag{2.4}$$

The symmetric matrix $\nabla_{\Gamma(t)}\boldsymbol{\nu}$ of the tangential derivatives of the normal field is known as the Weingarten map or shape operator. And the mean curvature of $\Gamma(t)$ with respect to $\boldsymbol{\nu}$ is defined as the negative of the trace of the Weingarten map:

$$\kappa_m(\boldsymbol{x}, t) = -\nabla_{\Gamma(t)} \cdot \boldsymbol{\nu}(\boldsymbol{x}, t). \tag{2.5}$$

We denote by κ_g the Gaussian curvature. With κ_i the principle curvatures, $i = 1, 2$, it is the case that $\kappa_m = \kappa_1 + \kappa_2$ and $\kappa_g = \kappa_1\kappa_2$. In addition we may write

$$\kappa_g = \frac{1}{2}(\kappa_m^2 - |\nabla_\Gamma\boldsymbol{\nu}|^2) \tag{2.6}$$

with $|\nabla_\Gamma\boldsymbol{\nu}|^2 = \nabla_\Gamma\boldsymbol{\nu} : \nabla_\Gamma\boldsymbol{\nu}$. Furthermore, Elliott and Stinner [2010a]

$$\Delta_\Gamma\boldsymbol{\nu} = -|\nabla_\Gamma\boldsymbol{\nu}|^2\boldsymbol{\nu} - \nabla_\Gamma\kappa_m. \tag{2.7}$$

2.2 Some Important Identities

For an arbitrary open subset $V(t) \subset \Gamma(t)$ and a function $f(t) \in C^1(\overline{V(t)})$ we have that Dziuk and Elliott [2013]

$$\int_{V(t)} \nabla_{\Gamma(t)}f = -\int_{V(t)} f\kappa_m\boldsymbol{\nu} + \int_{\partial V(t)} f\boldsymbol{\mu}_{ext}. \tag{2.8}$$

Here, $\boldsymbol{\mu}_{ext}$ is the exterior co-normal on the boundary $\partial V(t)$ that is tangent to $\Gamma(t)$, pointing away from $V(t)$ and orthogonal to $\boldsymbol{\nu}$.

Reynolds Transport Formula, also referred to as the Leibniz Formula, enables us to compute the time derivative of a time dependent surface integral. For a material test volume, that is a subset $V(t) \subset \Gamma(t)$ for which no material enters or

leaves and so points $\boldsymbol{x}$ move with speed $\boldsymbol{v}(\boldsymbol{x},t)$, it reads Dziuk and Elliott [2007]

$$\frac{d}{dt}\int_{V(t)} f = \int_{V(t)} \partial_t^\bullet f + f\nabla_{\Gamma(t)}\cdot\boldsymbol{v}. \tag{2.9}$$

If $V(t)\subset\Gamma(t)$ is not a material volume and so material may enter or leave the region and thus the boundary moves with a speed $\boldsymbol{v}_{\partial V}$ which may be different from $\boldsymbol{v}$, then Betounes [1986]

$$\frac{d}{dt}\int_{V(t)} f = \int_{V(t)} \left(\partial_t^\circ f - f\kappa_m v_{\boldsymbol{\nu}}\right) + \int_{\partial V(t)} f\boldsymbol{v}_{\partial V}\cdot\boldsymbol{\mu}_{ext}. \tag{2.10}$$

Observe that the case (2.10) is a generalisation of (2.9). In the specific setting that $\boldsymbol{v}_{\partial V}=\boldsymbol{v}$ an integration by parts argument on the velocity terms shows that (2.9) can be recovered. The time derivative of the Dirichlet inner product reads Dziuk and Elliott [2007]:

$$\begin{aligned}\frac{d}{dt}\int_{\Gamma(t)} \nabla_{\Gamma(t)}f\cdot\nabla_{\Gamma(t)}g = &\int_{\Gamma(t)} \nabla_{\Gamma(t)}f\cdot\nabla_{\Gamma(t)}\partial_t^\bullet g + \nabla_{\Gamma(t)}\partial_t^\bullet g\cdot\nabla_{\Gamma(t)}f \\ &+\int_{\Gamma(t)}\left(\nabla_{\Gamma(t)}\cdot\boldsymbol{v}\mathbb{I} - 2D_\Gamma\boldsymbol{v}\right)\nabla_{\Gamma(t)}f\cdot\nabla_{\Gamma(t)}g\end{aligned} \tag{2.11}$$

where $D_\Gamma\boldsymbol{v} := \frac{1}{2}\boldsymbol{P}\left(\nabla_{\Gamma(t)}\boldsymbol{v}+\nabla_{\Gamma(t)}\boldsymbol{v}^T\right)\boldsymbol{P}$ is the tangential deformation tensor or symmetric gradient.

2.3 Curves on evolving surfaces

2.3.1 Notation

Let $\{\Lambda(t)\}_{t\in[0,T]}$ denote a smooth, closed, and connected evolving curve on $\{\Gamma(t)\}_{t\in[0,T]}$. For all $t\in[0,T]$ it splits the surface $\Gamma(t)$ into two domains which we denote $\Gamma^b(t)$ and $\Gamma^a(t)$. Using the notion of the intrinsic distance between points $\boldsymbol{x},\boldsymbol{y}\in\Gamma(t)$ ($|\cdot|_2$ being the standard Euclidean norm),

$$d_\Gamma(\boldsymbol{x},\boldsymbol{y},t) := \inf\left\{\int_0^1 \|g'\|_2 \,\middle|\, g\in C^1([0,1],\Gamma(t)),\, g(0)=\boldsymbol{x},\, g(1)=\boldsymbol{y}\right\},$$

we can define the distance to the curve $\Lambda(t)$ for a point $\boldsymbol{x}\in\Gamma(t)$ as

$$d_{\Lambda(t)}(\boldsymbol{x},t) := \inf_{\boldsymbol{y}\in\Lambda(t)} d_\Gamma(\boldsymbol{x},\boldsymbol{y},t) \tag{2.12}$$

and then the *signed distance function* by

$$d(\boldsymbol{x},t) := \begin{cases} d_{\Lambda(t)}(\boldsymbol{x},t) & \text{if } \boldsymbol{x} \in \Gamma^b(t), \\ -d_{\Lambda(t)}(\boldsymbol{x},t) & \text{if } \boldsymbol{x} \in \Gamma^a(t). \end{cases} \tag{2.13}$$

If we assume that $\Lambda(t)$ and $\Gamma(t)$ are sufficiently smooth then there is a narrow tubular region of thickness $\bar{\varepsilon} > 0$ (independent of t) such that for all points in this region there is a unique geodesic (modulo reparametrisation) which realises the distance. Define now the unit tangent vector along the geodesic by

$$\boldsymbol{\mu}(\boldsymbol{x},t) := \nabla_{\Gamma(t)} d(\boldsymbol{x},t), \quad \boldsymbol{x} \in \Gamma(t)$$

which is a smooth function close to $\Lambda(t)$ (by which we mean in the tubular region). Its derivative along the geodesic, $(\nabla_{\Gamma(t)}\boldsymbol{\mu})\boldsymbol{\mu} = \nabla_{\Gamma(t)}(\nabla_{\Gamma(t)} d)\boldsymbol{\mu}$, then is normal to $\Gamma(t)$. We now choose the unique $\boldsymbol{\tau}(\boldsymbol{x},t)$ such that $(\boldsymbol{\tau},\boldsymbol{\mu},\boldsymbol{\nu})$ is a positively oriented orthonormal basis of $\mathbb{R}^3$ on $\Gamma(t)$ close to $\Lambda(t)$. Then

$$\boldsymbol{\mu} \cdot (\nabla_{\Gamma(t)}\boldsymbol{\mu})\boldsymbol{\mu} = 0, \quad \boldsymbol{\tau} \cdot (\nabla_{\Gamma(t)}\boldsymbol{\mu})\boldsymbol{\mu} = 0. \tag{2.14}$$

For the restrictions of $\boldsymbol{\tau}$ and $\boldsymbol{\mu}$ to $\Lambda(t)$ we will write

$$\boldsymbol{\tau}_\Lambda(\boldsymbol{x},t) := \boldsymbol{\tau}(\boldsymbol{x},t), \quad \boldsymbol{\mu}_\Lambda(\boldsymbol{x},t) := \boldsymbol{\mu}(\boldsymbol{x},t), \qquad \boldsymbol{x} \in \Lambda(t).$$

Let now $\lambda(s,t) : R_{\Lambda(t)}S^1 \times [0,T] \to \mathbb{R}$ denote a parametrisation of $\Lambda(t)$ by arc-length. Here, $R_{\Lambda(t)}S^1$ is the circle around the origin of radius $R_{\Lambda(t)}$ which is such that $2\pi R_{\Lambda(t)}$ is the length of $\Lambda(t)$. Assume that the orientation of the parametrisation is such that $\lambda_s(s,t) = \boldsymbol{\tau}(\lambda(s,t),t)$. Let us introduce

$$\boldsymbol{\tau}_\lambda(s,t) := \boldsymbol{\tau}_\Lambda(\lambda(s,t),t), \quad \boldsymbol{\mu}_\lambda(s,t) := \boldsymbol{\mu}_\Lambda(\lambda(s,t),t).$$

The curvature vector of $\Lambda(t)$ is given by $\boldsymbol{\kappa}_\Lambda(s,t) := \partial_s \boldsymbol{\tau}_\lambda(s,t)$ and, as $\boldsymbol{\tau}_\lambda \cdot \partial_s \boldsymbol{\tau}_\lambda = \frac{1}{2}\partial_s |\boldsymbol{\tau}_\lambda|^2 = 0$, can be decomposed up into a portion normal to $\Gamma(t)$ with coefficient $\kappa_{\boldsymbol{\nu}} := \boldsymbol{\kappa}_\Lambda(s,t) \cdot \boldsymbol{\nu}(\lambda(s,t),t)$. This coefficient is called the *normal curvature*, similarly we define the tangential coefficient

$$\kappa_\Lambda(\lambda(s,t),t) =: \kappa_\lambda(s,t) := \boldsymbol{\kappa}_\Lambda(s,t) \cdot \boldsymbol{\mu}_\lambda(s,t) = \partial_s \boldsymbol{\tau}_\lambda(s,t) \cdot \boldsymbol{\mu}_\lambda(s,t) = -\boldsymbol{\tau}_\lambda(s,t) \cdot \partial_s \boldsymbol{\mu}_\lambda(s,t) \tag{2.15}$$

which is known as the *geodesic curvature* of $\Lambda(t)$ with respect to $\Gamma(t)$. One can show that $\kappa_\Lambda(t) : \Lambda(t) \to \mathbb{R}$ is independent of the parametrisation.

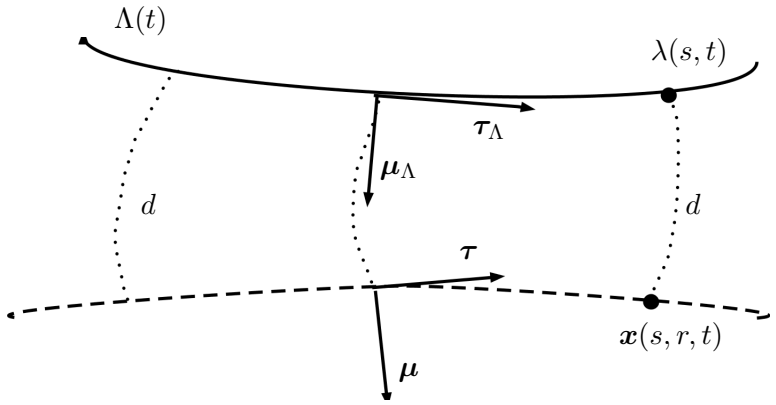

Figure 2.1: Sketch of geometric quantities describe in Section 2.3

2.3.2 Local Surface Reparameterisation

In Chapter 3 when employing the method of matched asymptotic expansions we will look to parametrise space locally around the interfacial curve so that we have a variable that scales with the interface width. We will then blow this variable up so that it scales independently from the interface width so that we can sensibly study the limit of fields in the sharp interface limit.

We may parametrise $\Gamma(t)$ close to $\Lambda(t)$ as $\boldsymbol{x}_\Gamma(s,r,t)$ by extending the parametrisation $\lambda(s,t)$ where $\boldsymbol{x}_\Gamma(s,r,t)$ is the solution of

$$\tilde{\boldsymbol{x}}(s,0,t) = \lambda(s,t), \qquad \tilde{\boldsymbol{x}}_r(s,r,t) = \boldsymbol{\mu}(\tilde{\boldsymbol{x}}(s,r,t),t), \quad r \in [-\bar{\varepsilon},\bar{\varepsilon}].$$

For fixed s and t the curve $r \mapsto \boldsymbol{x}_\Gamma(s,r,t)$ then is a geodesic and

$$d(\boldsymbol{x}_\Gamma(s,r,t)) = r. \tag{2.16}$$

With $\boldsymbol{v}_\Lambda(t) : \Lambda(t) \to \mathbb{R}^3$ we denote the (intrinsic) normal velocity of $\Lambda(t)$, i.e., it can have a portion in direction $\boldsymbol{\nu}(t)$ and in direction $\boldsymbol{\mu}_\Lambda(t)$ but $\boldsymbol{v}_\Lambda(x,t)\cdot\boldsymbol{\tau}_\Lambda(x,t) = 0$ for all $\boldsymbol{x} \in \Lambda(t)$, $t \in [0,T]$. Note that as $\Lambda(t) \subset \Gamma(t)$ for all $t \in [0,T]$ the velocity of $\Lambda(t)$ in the direction $\boldsymbol{\nu}(t)$ normal to the surface coincides with the one of the surface,

$$\boldsymbol{v}_\Lambda(\boldsymbol{x},t)\cdot\boldsymbol{\nu}(\boldsymbol{x},t) = \boldsymbol{v}(\boldsymbol{x},t)\cdot\boldsymbol{\nu}(\boldsymbol{x},t) \quad \forall \boldsymbol{x} \in \Lambda(t).$$

However, the portion of $\boldsymbol{v}_\Lambda(t)$ which is tangential to $\Gamma(t)$ may be different from the tangential portion of $\boldsymbol{v}(t)$. Observe that

$$\lambda_t(s,t)\cdot\boldsymbol{\mu}_\lambda(s,t) = \boldsymbol{v}_\Lambda(\lambda(s,t),t)\cdot\boldsymbol{\mu}_\lambda(s,t). \tag{2.17}$$

ss assumptions on $\Gamma(t)$, the differentials $\nabla_{\Gamma(t)}\boldsymbol{\tau}$, $\nabla_{\Gamma(t)}\boldsymbol{\mu}$ and $\nabla_{\Gamma(t)}\boldsymbol{\nu}$ then have limits when approaching $\Lambda(t)$. If we define $\nabla_{\Lambda(t)} := \nabla_{\Gamma(t)} - \boldsymbol{\mu}\otimes\boldsymbol{\mu}\nabla_{\Gamma(t)}$ to be the projection

of the surface gradient onto the curve $\Lambda(t)$ then on $\Lambda(t)$ it holds that:

$$\boldsymbol{\tau} \cdot \nabla_{\Gamma(t)} \boldsymbol{\nu}\boldsymbol{\tau} = \boldsymbol{\tau} \cdot \nabla_{\Lambda(t)} \boldsymbol{\nu}\boldsymbol{\tau} = -\boldsymbol{\nu} \cdot \nabla_{\Lambda(t)} \boldsymbol{\tau}\boldsymbol{\tau} = -\boldsymbol{\nu} \cdot \boldsymbol{\kappa}_\Lambda = -\kappa_{\boldsymbol{\nu}} \tag{2.18}$$

where we use that $\boldsymbol{\nu} \cdot \boldsymbol{\tau} = 0$ for the interchange of derivative and have used that the surface gradient on $\Lambda(t)$, given by $\nabla_{\Lambda(t)}$ coincides with the derivative ∂_s. This gives us a method by which we may extend the normal curvature of $\Lambda(t)$ to the surrounding tube. Thus in the tubular region surrounding $\Lambda(t)$ we define $\kappa_{\boldsymbol{\nu}} := -\boldsymbol{\tau} \cdot \nabla_{\Gamma(t)} \boldsymbol{\nu}\boldsymbol{\tau}$. We also define the quantities

$$\kappa_p := -\boldsymbol{\mu} \nabla_{\Gamma(t)} \boldsymbol{\nu}\boldsymbol{\mu}, \qquad \kappa_d := -\boldsymbol{\tau} \cdot \nabla_{\Gamma(t)} \boldsymbol{\nu}\boldsymbol{\mu} \; (= -\boldsymbol{\mu} \cdot \nabla_{\Gamma(t)} \boldsymbol{\nu}\boldsymbol{\tau}). \tag{2.19}$$

Thus near the interface we can write the Weingarten map as

$$\nabla_{\Gamma(t)} \boldsymbol{\nu} = -\kappa_{\boldsymbol{\nu}} \boldsymbol{\tau} \otimes \boldsymbol{\tau} - \kappa_p \boldsymbol{\mu} \otimes \boldsymbol{\mu} - \kappa_d \boldsymbol{\tau} \otimes \boldsymbol{\mu} - \kappa_d \boldsymbol{\mu} \otimes \boldsymbol{\tau}. \tag{2.20}$$

It can easily be shown that

$$\kappa_m = \kappa_{\boldsymbol{\nu}} + \kappa_p, \qquad |\nabla_{\Gamma(t)} \boldsymbol{\nu}|^2 = \kappa_{\boldsymbol{\nu}}^2 + \kappa_p^2 + 2\kappa_d^2, \qquad \kappa_g = \kappa_{\boldsymbol{\nu}} \kappa_p - \kappa_d^2. \tag{2.21}$$

Some other useful formulae are

$$\partial_t^\circ \boldsymbol{\nu} = -\nabla_{\Gamma(t)} (\boldsymbol{v} \cdot \boldsymbol{\nu}), \quad \partial_t^\bullet \boldsymbol{\nu} = -(\nabla_{\Gamma(t)} \boldsymbol{v})^T \boldsymbol{\nu} \tag{2.22}$$

$$\partial_t^\circ \kappa_m = \Delta_{\Gamma(t)} (\boldsymbol{v} \cdot \boldsymbol{\nu}) + |\nabla_{\Gamma(t)} \boldsymbol{\nu}|^2 \nabla_{\Gamma(t)} \boldsymbol{v} \cdot \boldsymbol{\nu} \tag{2.23}$$

Using the reparameterisation of space $\boldsymbol{x} \mapsto (s, r)$ around a curve $\Lambda(t)$, we can rewrite a function $f : \Gamma(t) \to \mathbb{R}$ as $F : R_\Lambda S^1 \times [-\bar{\varepsilon}, \bar{\varepsilon}] \to \mathbb{R}$. Of importance later on is the time rate of change of the signed distance function (2.13).

Let us consider a piont $\boldsymbol{x} \in \Gamma(t)$ with a distance of order ε to $\Lambda(t)$ at a fixed time t, such that, without loss of generality, $r(\boldsymbol{x}, t) > 0$. Let $\tilde{t} \mapsto \boldsymbol{x}_p(\tilde{t})$ be the path of a material point p such that $\boldsymbol{x} = \boldsymbol{x}_p(t)$. For all $\tilde{t}$ close to t denote by $\rho \mapsto g^m(\rho, \tilde{t}) \in \Gamma(\tilde{t})$ the geodesic which realises the distance $d_{\Lambda(\tilde{t})}(\boldsymbol{x}_p(\tilde{t}))$ defined in (2.12), and denote by $\boldsymbol{x}_\Lambda(\tilde{t}) \in \Lambda(\tilde{t})$ the initial point.

Then $\partial_t^\bullet r(\boldsymbol{x}, t)$ is the instantaneous change of the length of g^m when varying the time whilst staying on the surface. The length can change by adding (or subtracting) length at the initial point. This instantaneous change is given by the velocity of the initial point in the tangential direction of the geodesic, i.e., by

$$\partial_t \boldsymbol{x}_\Lambda(t) \cdot (-\boldsymbol{\mu}_\Lambda(\boldsymbol{x}_\Lambda(t), t)) = -\boldsymbol{v}_\Lambda(\boldsymbol{x}_\Lambda(t), t) \cdot \boldsymbol{\mu}_\Lambda(\boldsymbol{x}_\Lambda(t), t)$$

where the minus sign comes from the fact that $r(\boldsymbol{x},t) > 0$ so that $\boldsymbol{\mu}_\Lambda(\boldsymbol{x}(t),t)$ is an inward oriented unit tangential vector of the geodesic. The length of g^m can also change by adding length at the end point. Analogously, this instantaneous change is given by

$$\partial_t \boldsymbol{x}_p(t) \cdot \boldsymbol{\mu}(\boldsymbol{x},t) = \boldsymbol{v}(\boldsymbol{x},t) \cdot \boldsymbol{\mu}(\boldsymbol{x},t).$$

By the ε closeness of $\boldsymbol{x}$ to $\Lambda(t)$ we can expand the last term in $\boldsymbol{x}_\Lambda(t)$ and altogether obtain

$$\partial_t^\bullet r(\boldsymbol{x},t) = \big(\boldsymbol{v}(\boldsymbol{x}_\Lambda,t) - \boldsymbol{v}_\Lambda(\boldsymbol{x}_\Lambda,t)\big) \cdot \boldsymbol{\mu}_\Lambda(\boldsymbol{x}_\Lambda,t) + \mathcal{O}(\varepsilon). \tag{2.24}$$

Observe that further contributions to the change of the length of the geodesic, g_m, for instance, by movement in the direction of it's curvature, are of order ε thanks to the closeness of $\boldsymbol{x}$ to $\Lambda(t)$.

Chapter 3

Asymptotics for the Evolving Surface Cahn-Hilliard Equation

3.1 Introduction to the Cahn-Hilliard Equation

The subject of this chapter is the Evolving Surface Cahn-Hilliard (ESCH) equation

$$\partial_t^\bullet \phi + \phi \nabla_{\Gamma(t)} \cdot \boldsymbol{v} = -\nabla_{\Gamma(t)} \cdot \boldsymbol{j}, \tag{3.1}$$

$$\boldsymbol{j} = -M(\phi)\nabla_{\Gamma(t)} w, \qquad w = -\varepsilon \Delta_{\Gamma(t)}\phi + \frac{1}{\varepsilon} f(\phi). \tag{3.2}$$

Here, $\{\Gamma(t)\}_t \subset \mathbb{R}^n$ is a closed, smoothly evolving surface with a prescribed surface velocity $\boldsymbol{v} : \Gamma(t) \to \mathbb{R}^3$, for material points of $\Gamma(t)$. The scalar function $\phi : \Gamma(t) \to \mathbb{R}$ is the phase field variable, ε is the variable representing interfacial width, the function $f(\phi) = F'(\phi)$ is the derivative of a double-well potential, and $M(\phi)$ is a mobility function. The vector $\boldsymbol{j} : \Gamma(t) \to \mathbb{R}^n$ is the flux and $w : \Gamma(t) \to \mathbb{R}$, known as the chemical potential, is the variation of the Ginzburg-Landau energy

$$\mathcal{E}_\varepsilon(\phi(t)) = \int_{\Gamma(t)} \frac{\varepsilon}{2} |\nabla_{\Gamma(t)}\phi(t)|^2 + \frac{1}{\varepsilon} F(\phi(t)) dx \tag{3.3}$$

and in the case $\boldsymbol{v} = 0$ the system (3.1), (3.2) is the $M(\phi)$-weighted H^{-1} gradient flow of (3.3).

As discussed in Chapter 1 with regards to $F(\phi)$, in most applications a double-well or double-obstacle type potential is chosen Blowey and Elliott [1991a], Bates and Fife [1993], we consider potentials with two stable non-degenerate minima denoted by $\phi_a < \phi_b$ which is twice continuously differentiable on an interval (α, β) containing $[\phi_a, \phi_b]$. We consider second order phase transitions such that $F(\phi_a) =$

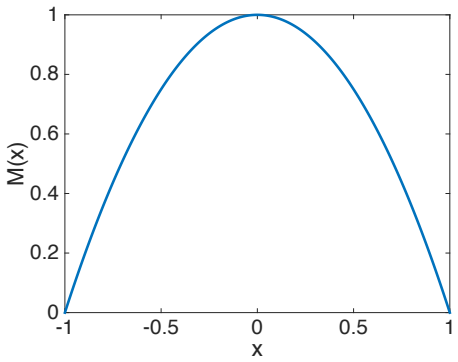

Figure 3.1: Example of a mobility function, M_{deg} as defined in (3.6) with $\alpha = -1$ and $\beta = 1$.

$F(\phi_b)$. Specifically, we have a quartic potential and a logarithmic potential in mind defined by

$$F_{log}(\phi) = \tfrac{\theta}{2k_1}\left((\beta-\phi)\log(\beta-\phi) + (\phi-\alpha)\log(\phi-\alpha)\right) - \tfrac{\theta_c}{2k_2}(\beta-\phi)(\phi-\alpha) \qquad \text{(logarithmic)}, \quad (3.4)$$

$$F_q(\phi) = \frac{1}{4}(\phi_b-\phi)^2(\phi-\phi_a)^2 \qquad \text{(quartic)}, \quad (3.5)$$

where $\theta, \theta_c, k_1, k_2 > 0$ are parameters, but we stress that the results are not restricted to these two cases. Qualitative examples of quartic type potentials can be seen in Figure 1.2.

We assume that the mobility $M(\phi)$ is Lipschitz on $[\alpha, \beta]$ and positive and continuously differentiable on (α, β) (the latter for simplicity, a slightly smaller open interval comprising $[\phi_a, \phi_b]$ would be sufficient). Qualitative examples can be seen in Figure 3.1 We have in mind the two specific mobility functions:

$$M_{deg}(\phi) = |\bar{M}(\phi-\alpha)(\beta-\phi)| \qquad \text{(degenerate)}, \quad (3.6)$$

$$M_c(\phi) = \bar{M} \qquad \text{(constant)}, \quad (3.7)$$

where $\bar{M} > 0$ is a constant. Let us introduce the pairings (F_q, M_c) and (F_{log}, M_{deg}), the former we refer to as the *constant mobility ESCH equation* and the later as the *degenerate ESCH equation*.

On a stationary, flat domain the Cahn-Hillard equation has been introduced to model phase separation under a mass constraint in binary alloy systems Cahn and Hilliard [1958]; Cahn [1961]. As a prototype model for segregation of two components in a mixture it has been applied in many areas beyond materials science.

We refer to Novick-Cohen [2008] for a recent review of the equation. The field ϕ usually stands for the (mass or volume) concentration of one of the components, sometimes also their difference. Cahn and Hilliard motivated the logarithmic double-well potential (3.4) in their original works Cahn and Hilliard [1958]; Cahn [1961] by theories of mixing. The parameter $\theta > 0$ is the (constant) temperature of the system and $\theta_c > 0$ is a critical temperature dependent on the material which determines the onset of phase separation. In the shallow quench limit ($\theta \nearrow \theta_c$), the logarithmic potential can be well approximated by the quartic potentials of the form (3.5). Non-constant mobilities were motivated by Cahn and Hilliard in the original derivation, see also Gurtin [1996]. But also the case of a constant mobility (3.7) has been of interest Elliott and Zheng [1986]; Bates and Fife [1993]; Novick-Cohen [1985]. In the limit $\theta \to 0$ the logarithmic potentials converges to the double obstacle type potential

$$F_\infty(\phi) = \frac{1}{2}(\beta - \phi)(\alpha - \phi) + I_{[\alpha,\beta]}(\phi). \tag{3.8}$$

As mentioned in the introduction partial differential equations describing phase separation on evolving surfaces occur in many examples. In contrast to the usual notion of the phase variable, ϕ, as a concentration, we here take an abstract point of view choosing not to physically interpret the phase variable. We only assume that ϕ is a conserved quantity for which (3.1) is a mass balance on the moving surface $\Gamma(t)$. In Section 3.1.1, we see how this assumption of mass conservation is used to derive the ESCH equation. By mass conservation we mean global mass conservation such that, $\int_{\Gamma(t)} \phi(t) = \int_{\Gamma(0)} \phi(0)$ at all times t. This can be seen to hold by considering the weak form of (3.1) which reads

$$\frac{d}{dt}\int_{\Gamma(t)} \phi\eta = -\int_{\Gamma(t)} M(\phi)\nabla_{\Gamma(t)} w \cdot \nabla_{\Gamma(t)}\eta \qquad \text{for all } \eta \in H^1(\Gamma(t)) \text{ a.e. } t \in [0,T].$$

Choosing as an admissible test function, $\eta = 1$, gives the result. The essential difference to the standard Cahn-Hilliard equation is the $\phi\nabla_\Gamma \cdot \boldsymbol{v}$ term in (3.1) which accounts for local stretching if $\nabla_\Gamma \cdot \boldsymbol{v} > 0$ (or compressing in case of the opposite sign).

After the initial stage of separation, solutions ϕ to the Cahn-Hilliard equation exhibit large domains (or *phases*) in which ϕ is almost constant and close to one of the minima ϕ_a, ϕ_b of F. These phases are separated by moving layers with a thickness that scales with ε. This behaviour of solutions is a general feature of phase field models. We refer to Rubinstein and Sternberg [1992] for an analysis of a phase field model with regards to the different time scales at which the phase separation and the movement of the interfacial layers take place. In the latter

solution regime, by using formally matched asymptotics expansions, limiting free boundary problems (or *sharp interface models*) as $\varepsilon \to 0$ have been derived. For the Cahn-Hilliard equation in a stationary, flat domain, the pairing (F_q, M_c) has been considered by Pego [1989] whilst Cahn et al. [2006] have studied the pairing (F_{log}, M_{deg}) including the deep quench limit $\theta \searrow 0$. The method has also been applied to elliptic equations on fixed hypersurfaces in Elliott and Stinner [2010a] where also the underlying surface depends on the solution and, thus, on ε. In some cases such expansions have been rigorously shown to converge, for instance, see Matthieu et al. [2008]; N. Alikakos and Chen [1994]. In N. Alikakos and Chen [1994] it is required that the resultant free boundary problem admits a smooth solution, thus imposing regularity assumptions on the initial condition. In Stoth [1996] these regularity assumptions are relaxed but with the restriction to radially symmetric solutions. Regarding other approaches to assess the sharp interface limit, the H^{-1}-gradient flow (of the Ginzburg-Landau energy (3.3)) structure has been used in the context of Γ-convergence to show asymptotic convergence to the Mullins-Sekerka problem in Le [2008] for the pairing (F_q, M_c). However, when working with a deformable domain, without some relation coupling the surface velocity to the solution, the system does not necessarily have a gradient flow structure.

By considering the time derivative of (3.3) we see that

$$
\begin{aligned}
\frac{d}{dt}\mathcal{E}_\varepsilon(\phi(t)) &\overset{(2.11)}{=} \int_{\Gamma(t)} \varepsilon \nabla_{\Gamma(t)}\phi \cdot \nabla_{\Gamma(t)} \partial_t^\bullet \phi - \varepsilon D_\Gamma \boldsymbol{v} \nabla_{\Gamma(t)}\phi \cdot \nabla_{\Gamma(t)}\phi + \frac{\varepsilon}{2}|\nabla_{\Gamma(t)}\phi|^2 \nabla_{\Gamma(t)} \cdot \boldsymbol{v} \\
&\quad + \int_{\Gamma(t)} \frac{1}{\varepsilon} f(\phi)\partial_t^\bullet \phi + \frac{1}{\varepsilon} F(\phi) \nabla_{\Gamma(t)} \cdot \boldsymbol{v} \\
&\overset{(2.8)}{=} \int_{\Gamma(t)} -\varepsilon \left(\Delta_{\Gamma(t)}\phi\right) \partial_t^\bullet \phi - \varepsilon D_\Gamma \boldsymbol{v} \nabla_{\Gamma(t)}\phi \cdot \nabla_{\Gamma(t)}\phi + \frac{\varepsilon}{2}|\nabla_{\Gamma(t)}\phi|^2 \nabla_{\Gamma(t)} \cdot \boldsymbol{v} \\
&\quad + \int_{\Gamma(t)} \frac{1}{\varepsilon} f(\phi)\partial_t^\bullet \phi + \frac{1}{\varepsilon} F(\phi) \nabla_{\Gamma(t)} \cdot \boldsymbol{v} \\
&\overset{(3.2)}{=} \int_{\Gamma(t)} \varepsilon w \partial_t^\bullet \phi - \varepsilon D_\Gamma \boldsymbol{v} \nabla_{\Gamma(t)}\phi \cdot \nabla_{\Gamma(t)}\phi + \frac{\varepsilon}{2}|\nabla_{\Gamma(t)}\phi|^2 \nabla_{\Gamma(t)} \cdot \boldsymbol{v} \\
&\quad + \int_{\Gamma(t)} \frac{1}{\varepsilon} F(\phi) \nabla_{\Gamma(t)} \cdot \boldsymbol{v} \\
&\overset{(3.1)}{=} \int_{\Gamma(t)} w \left(\nabla_{\Gamma(t)} \cdot (M(\phi)\nabla_{\Gamma(t)} w) - \phi \nabla_{\Gamma(t)} \cdot \boldsymbol{v}\right) - \varepsilon D_\Gamma \boldsymbol{v} \nabla_{\Gamma(t)}\phi \cdot \nabla_{\Gamma(t)}\phi \\
&\quad + \int_{\Gamma(t)} \frac{\varepsilon}{2}|\nabla_{\Gamma(t)}\phi|^2 \nabla_{\Gamma(t)} \cdot \boldsymbol{v} + \frac{1}{\varepsilon} F(\phi) \nabla_{\Gamma(t)} \cdot \boldsymbol{v}
\end{aligned}
$$

$$\overset{(2.8)}{=} \int_{\Gamma(t)} -M(\phi)|\nabla_{\Gamma(t)} w|^2 + \int_{\Gamma(t)} \left(\frac{\varepsilon}{2}|\nabla_{\Gamma(t)}\phi|^2 + \frac{1}{\varepsilon}F(\phi) - \phi w \right) \nabla_{\Gamma(t)} \cdot \boldsymbol{v} - \varepsilon D_\Gamma \boldsymbol{v} \nabla_{\Gamma(t)}\phi \cdot \nabla_{\Gamma(t)}\phi$$

The first term is strictly dissipative, however it should be clear that examples can be constructed such that the term on the final line increases the energy. See for example the energy outputs in Section 4.4.3 or Section 4.4.5 for examples where the energy is increased due to the motion of the surface. Thus the potential for local compressing/stretching to increase the system energy means that the Cahn-Hilliard system does not posses a gradient flow structure unless some more assumptions are made on the velocity.

The general aim of this chapter is to investigate the impact of the motion of the underlying domain $\Gamma(t)$. Via a formal asymptotic analysis (for instance, see Fife and Penrose [1995]) we investigate the effects of the surface motion on the limiting problem that is obtained as $\varepsilon \to 0$. The methodology has been applied to surface phase field models in the stationary case where also the surface depends on ε in Elliott and Stinner [2010a]. We have further extended the technique so that we can deal with moving surfaces and can apply it to the ESCH equation. As usual, a coordinate change using the signed distance function to the limiting moving phase interface is performed in the narrow interfacial region which blows up its thickness to unit length. But since the underlying space, $\Gamma(t)$, is time dependent, the scaled distance function must take account of transport due to the surface velocity. Technically, the challenge is to expand the material time derivative $\partial_t^\bullet$ in the new coordinates. The analysis is carried out for the case of hypersurfaces in the three-dimensional space ($n = 3$) but the ideas should carry through to the case $n > 3$. The only difficulty should consist in dealing with several tangential coordinates along the limiting phase interface rather than one.

The scaling of $M(\phi)$ (or rather $\bar{M}$) with respect to ε turns out to be crucial when attempting to derive limiting free boundary problems. In the case of a stationary, flat domain ($\boldsymbol{v} = 0$) it is equivalent to study the Cahn-Hilliard equation at different time scales as in Pego [1989]. Specific scalings have been considered in Novick-Cohen [2008] where $\bar{M} \sim \varepsilon^1$ and Elliott and Ranner [2013] where $\bar{M} \sim \varepsilon^0$. The former appears as a model for early time phase separation when the interfaces form and the latter as a long time model for interface evolution. The scaling $\bar{M} \sim \varepsilon^{-1}$ appears in Cahn et al. [2006] for the degenerate mobility in the regime of the deep quench limit, $\theta \searrow 0$, of the logarithmic potential. Each of these time scales has been considered in Dai and Du [2014]. Different scales have also been

discussed in Caginalp [1989] in the context of a more general phase field model. We here consider a fixed time scale given by the evolution of the surface, namely one given by (a) a typical velocity at which the domains evolves and (b) a length scale given by the typical size of the surface. Different scalings of $\bar{M}$ in ε then relate to the speed at which diffusion effects are taking place in comparison with transport effects.

Not for all scalings were we able to identify sensible limiting free boundary problems. If the mobility is too small, i.e., $\bar{M}$ is of a high order in ε, then the limiting problems do not see the long time behaviour resulting from the evolution of the phase field variable, whence the dynamics are purely governed by the transport with the given velocity field $\boldsymbol{v}$. If the mobility is too high so that $\bar{M}$ is of a low (negative) order in ε then the asymptotic limits are forced towards equilibrium states with respect to the phases which are barely affected by the transport.

In the interesting intermediate case in which $\bar{M}$ is of order ε^0 we obtain the following evolving surface Mullins-Sekerka problem:

$$\left.\begin{aligned} \phi &= \phi_i \\ \nabla_{\Gamma(t)} \cdot \big(M(\phi)\nabla_{\Gamma(t)} w(t)\big) &= \phi \nabla_{\Gamma(t)} \cdot \boldsymbol{v}(t) \end{aligned}\right\} \text{ in } \Gamma^i(t),\ i = a, b, \tag{3.9}$$

$$\left.\begin{aligned} [w(t)] &= 0 \\ w(t) &= S\kappa_\Lambda(t) \\ \tfrac{1}{\phi_b - \phi_a}[M(\phi)\nabla_{\Gamma(t)} w(t)] \cdot \boldsymbol{\mu}_\Lambda(t) &= \big(\boldsymbol{v}(t) - \boldsymbol{v}_\Lambda(t)\big) \cdot \boldsymbol{\mu}_\Lambda(t) \end{aligned}\right\} \text{ on } \Lambda(t). \tag{3.10}$$

With, $\Lambda(t)$ the moving boundary separating the bulk phases $\Gamma^b(t)$ and $\Gamma^a(t)$, $[\cdot]$ stands for the jump across $\Lambda(t)$ when moving from $\Gamma^a(t)$ to $\Gamma^b(t)$, $S > 0$ is a constant depending on the double-well potential F, $\kappa_\Lambda(t)$ is the geodesic curvature of $\Lambda(t)$ with respect to $\Gamma(t)$, $\boldsymbol{v}_\Lambda(t)$ is the normal velocity of $\Lambda(t)$, and $\boldsymbol{\mu}_\Lambda(t)$ is the co-normal of $\Lambda(t)$ with respect to $\Gamma(t)$ which points into $\Gamma^b(t)$. A sketch of the physical setup described by this free boundary problem can be seen in Figure 3.2

Observe that, in general, $\phi \nabla_\Gamma \cdot \boldsymbol{v}$ is a non-trivial right hand side in the limiting elliptic equation for the chemical potential. This fact causes problems when attempting to pass to the deep quench limit $\theta \to 0$ for the degenerate ESCH equation. In that limit, the degenerate mobility switches off the elliptic equation in the bulk. On a stationary domain a purely geometric equation is obtained in the sharp interface limit, namely surface diffusion Cahn et al. [2006]. But in the present case a nontrivial term persists in the bulk if $\nabla_\Gamma \cdot \boldsymbol{v} \neq 0$, and there is no mechanism to account for the mass density changes due to this local stretching or compressing.

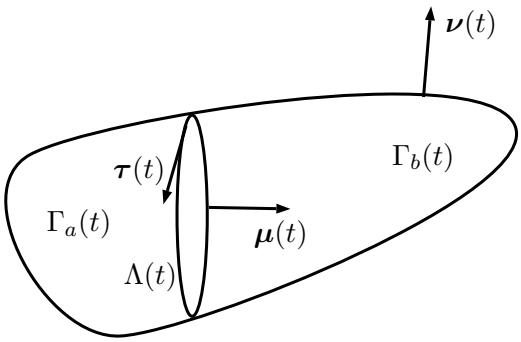

Figure 3.2: Sketch of physical setting for Mullins-Sekerka type problems with important quantities identified.

If $\nabla_{\Gamma(t)} \cdot \boldsymbol{v} = 0$ then the procedure of Cahn et al. [2006] works however.

The remainder of this Chapter is set out as follows. We begin with a derivation of the ESCH equation and some remarks on the effects of rescaling the double-well potential. We then present our assumptions for performing an asymptotic analysis on an evolving surface. In particular we discuss the necessary expansion of the material derivative, $\partial_t^\bullet$, in the inner co-ordinate system using the results from the previous chapter. Under the set up described we perform the asymptotic analysis on the ESCH equation for the slow mobility, when $\bar{M} \sim \varepsilon^0$, and interpret the results for specific mobility and potential functions. We then turn our attention to the fast mobility, when $\bar{M} \sim \varepsilon^{-1}$ and compare the result with the slow mobility. Finally we consider the deep quench limit $\theta \to 0$ of the logarithmic potential (3.4) and analyse the resulting problem.

3.1.1 Motivation of and remarks on the ESCH equation

Following the lines of Elliott and Ranner [2013] we briefly derive the Cahn-Hilliard equation in the form (3.1), (3.2). Let $\phi(\cdot, t) : \Gamma(t) \to \mathbb{R}$, $t \in [0, T]$, be some scalar conserved quantity which means that for any test volume $V(t) \subset \Gamma(t)$ with external co-normal $\boldsymbol{\mu}_{ext}$:

$$\frac{d}{dt} \int_{V(t)} \phi = - \int_{\partial V(t)} \boldsymbol{j} \cdot \boldsymbol{\mu}_{ext} \tag{3.11}$$

with a flux $\boldsymbol{j}(\cdot, t) : \Gamma(t) \to \mathbb{R}^m$, $t \in [0, T]$ which is (spatially) tangential to $\Gamma(t)$. Using (2.8) and the transport formula (2.9) yields

$$\int_{V(t)} \partial_t^\bullet \phi + \phi \nabla_\Gamma \cdot \boldsymbol{v} + \nabla_\Gamma \cdot \boldsymbol{j} = 0.$$

As this must hold for any choice of $V(t)$, we obtain (3.1). One may now postulate that the flux is driven by the gradient of the chemical potential w given as the first

variation of the Ginzburg-Landau energy functional (3.3) so that

$$\boldsymbol{j} = -M(\phi)\nabla_\Gamma w.$$

Many results in the literature on the Cahn-Hilliard equation are obtained for a dimensionless version where the minima of the double well potential are located at ± 1. Our system can be transformed to such a setting as follows. Setting

$$\tilde{\phi} = \frac{\phi - \phi_b}{\phi_b - \phi_a} + \frac{\phi - \phi_a}{\phi_b - \phi_a} \quad \Leftrightarrow \quad \phi = \tfrac{1}{2}\big((1+\tilde{\phi})\phi_b + (1-\tilde{\phi})\phi_a\big)$$

to be the dimensionless form we define $\tilde{F}(\tilde{\phi}) := F(\phi)$ and $\tilde{M}(\tilde{\phi}) := M(\phi)$. Then $f(\phi) = F'(\phi) = \frac{2}{\phi_b - \phi_a}\tilde{F}'(\tilde{\phi}) = \frac{2}{\phi_b - \phi_a}\tilde{f}(\tilde{\phi})$, and a short calculation shows that (3.1), (3.2) takes the form

$$\partial_t^\bullet \tilde{\phi} + \tilde{\phi}\nabla_\Gamma \cdot \boldsymbol{v} + c_1 \nabla_\Gamma \cdot \boldsymbol{v} = \nabla_\Gamma \cdot \left(\tilde{M}(\tilde{\phi})\nabla_\Gamma \frac{\tilde{w}}{c_2^2}\right) \tag{3.12}$$

$$\tilde{w} = -\varepsilon c_2 \Delta_\Gamma \tilde{\phi} + \frac{\tilde{f}(\tilde{\phi})}{c_2 \varepsilon} \tag{3.13}$$

where $c_1 = \frac{\phi_b + \phi_a}{2}$, $c_2 = \frac{\phi_b - \phi_a}{2}$ and $\tilde{w}$ is the chemical potential corresponding to the first variation of the energy $\tilde{\mathcal{E}}_\varepsilon(\tilde{\phi}) := \mathcal{E}_\varepsilon(\phi)$.

We remark that in Elliott and Ranner [2013] the case $c_1 = 0$, $c_2 = 1$ is considered. The essential difference is the source term proportional to the divergence of the surface velocity in (3.12).

Existence and uniqueness of the ESCH equation with constant mobility and standard double well potential was shown in Elliott and Ranner [2013] (in which the surface velocity was assumed C^2, for a stationary planar setting with degenerate mobilities and a double well type potentials in Elliott and Garcke [1996], and for constant mobilities and double obstacle type potentials in Blowey and Elliott [1991a].

3.2 Assumptions for the asymptotic analysis

The goal is now to identify the sharp interface problem from the diffuse interface problem by matching appropriate asymptotic ε-expansions. The technique has been carefully detailed in Fife and Penrose [1995]. We can also make use of an extension to elliptic problems on stationary surfaces Elliott and Stinner [2010a]. A novel extension to the technique concerns the parabolic case and, in particular, consists in accounting for the time dependence of the domain and re-writing the material time derivative $\partial_t^\bullet$ in inner coordinates close to the phase interface. Recall the result and

techniques introduced in Section 2.3.2.

3.2.1 Solution regime

We consider solution regimes to (3.1)-(3.2) where phases have formed, in each of which ϕ is close to one of the two minima of F and which are separated by layers with a thickness that scales with ε. Let $(\phi_\varepsilon, w_\varepsilon)_{\varepsilon>0}$ denote a family of such solutions and assume that it converges to some pairing (u_0, w_0) such that, at each time t, the spatial domain $\Gamma(t)$ is split up into domains $\Gamma^a(t) = \{\phi_0(t) = \phi_a\}$ and $\Gamma^b(t) = \{\phi_0(t) = \phi_b\}$ which are separated by a smooth, closed, and connected evolving curve $\Lambda(t)$ to which the level sets $\{\phi_\varepsilon(t) = (\phi_b + \phi_a)/2\}$ converge. The asymptotic analysis below, in principle, also works for several curves; however note that topological changes cannot be dealt with as they destroy the validity of the change of coordinates employed in the inner region. The aim is now to identify the equations that govern the evolution of $\Lambda(t)$, $\phi_0(t)$, and $w_0(t)$.

3.2.2 Outer expansions

We assume that away from the interfacial layer around the curve $\Lambda(t)$ we can expand the phase field variable and the chemical potential in the form

$$\phi(\boldsymbol{x}, t) = \sum_i \phi_i(\boldsymbol{x}, t)\varepsilon^i, \quad w(\boldsymbol{x}, t) = \sum_i w_i(\boldsymbol{x}, t)\varepsilon^i \tag{3.14}$$

in each domain $\Gamma^{a,b}(t)$.

3.2.3 Inner coordinates

As the thickness of the interfacial layer scales with ε it makes sense to blow it up to unit length in order to be able to study the limit of fields and functions as $\varepsilon \to 0$ in a meaningful way. We therefore introduce the scaled (geodesic) distance on $\Gamma(t)$ to the interface $\Lambda(t)$ by

$$z := \frac{r}{\varepsilon}. \tag{3.15}$$

It is with respect to the new coordinates (s, z, t) we choose to work with in the interfacial layer. But before we state the (inner) expansions of the fields in these coordinates and state the matching conditions with the outer expansions in the adjacent domains we need to discuss how the differential operators transform by the change of coordinates.

With regards to the spatial differential operators we may proceed as in Elliott

and Stinner [2010a]. For fixed t consider the inversion of the map $R_\Lambda(t)S^1\times[-\bar\varepsilon,\bar\varepsilon]\ni(s,r)\to\boldsymbol{x}_{\Gamma(t)}(s,r,t)\in\Gamma(t)$ and let $\boldsymbol{x}\in\Gamma(t)$ be a point with a distance to $\Lambda(t)$ which is $\mathcal{O}(\varepsilon)$. The identity (2.16) implies that $\varepsilon\nabla_{\Gamma(t)}z(\boldsymbol{x},t)=\nabla_{\Gamma(t)}r(\boldsymbol{x},t)=\boldsymbol{\mu}(\boldsymbol{x},t)$. Taylor expanding in $\boldsymbol{x}_\Lambda:=\lambda(s,t)$ then yields

$$\nabla_{\Gamma(t)}z(\boldsymbol{x},t)=\frac{1}{\varepsilon}\boldsymbol{\mu}_\Lambda(\boldsymbol{x}_\Lambda,t)+\nabla_{\Gamma(t)}\boldsymbol{\mu}(\boldsymbol{x}_\Lambda,t)\boldsymbol{\mu}_\Lambda(\boldsymbol{x}_\Lambda,t)z(\boldsymbol{x},t)+\mathcal{O}(\varepsilon).$$

Similarly we see that

$$\nabla_{\Gamma(t)}s(\boldsymbol{x},t)=\boldsymbol{\tau}_\Lambda(\boldsymbol{x}_\Lambda,t)+\mathcal{O}(\varepsilon).$$

For a scalar field $\psi:\Gamma(t)\to\mathbb{R}$ and a vector field $\boldsymbol{\psi}:\Gamma(t)\to\mathbb{R}^3$ define $\psi(\boldsymbol{x},t)=\Psi(s,z,t)$ and $\boldsymbol{\psi}(\boldsymbol{x},t)=\boldsymbol{\Psi}(s,z,t)$ close to $\Lambda(t)$. Then we obtain for the surface gradient and the surface divergence in the new coordinates

$$\begin{aligned}
\nabla_{\Gamma(t)}\psi(\boldsymbol{x},t) &= \Psi_s(s,z,t)\nabla_{\Gamma(t)}s+\Psi_z(s,z,t)\nabla_{\Gamma(t)}z\\
&= \tfrac{1}{\varepsilon}\Psi_z(s,z,t)\boldsymbol{\mu}_\Lambda(\boldsymbol{x}_\Lambda,t) \qquad (3.16a)\\
&\quad +\Psi_s(s,z,t)\boldsymbol{\tau}_\Lambda(\boldsymbol{x}_\Lambda,t)+\Psi_z(s,z,t)\nabla_{\Gamma(t)}\boldsymbol{\mu}(\boldsymbol{x}_\Lambda,t)\,\boldsymbol{\mu}_\Lambda(\boldsymbol{x}_\Lambda,t)z+\mathcal{O}(\varepsilon),\\
\nabla_{\Gamma(t)}\cdot\boldsymbol{\psi}(\boldsymbol{x},t) &= \boldsymbol{\Psi}_s(s,z,t)\cdot\nabla_{\Gamma(t)}s+\boldsymbol{\Psi}_z(s,z,t)\cdot\nabla_{\Gamma(t)}z\\
&= \tfrac{1}{\varepsilon}\boldsymbol{\Psi}_z(s,z,t)\cdot\boldsymbol{\mu}_\Lambda(\boldsymbol{x}_\Lambda,t) \qquad (3.16b)\\
&\quad +\boldsymbol{\Psi}_s(s,z,t)\cdot\boldsymbol{\tau}_\Lambda(\boldsymbol{x}_\Lambda,t)+\boldsymbol{\Psi}_z(s,z,t)\cdot\nabla_{\Gamma(t)}\boldsymbol{\mu}(\boldsymbol{x}_\Lambda,t)\boldsymbol{\mu}_\Lambda(\boldsymbol{x}_\Lambda,t)z+\mathcal{O}(\varepsilon).
\end{aligned}$$

Using these identities, (2.14), and (2.15), a short calculation shows that we can write for the Laplace-Beltrami operator

$$\Delta_{\Gamma(t)}\psi(\boldsymbol{x},t)=\frac{1}{\varepsilon^2}\Psi_{zz}(s,z,t)-\frac{1}{\varepsilon}\kappa_\Lambda(\boldsymbol{x}_\Lambda,t)\Psi_z(s,z,t)+\mathcal{O}(\varepsilon^0). \qquad (3.17)$$

With regards to the operator $\partial_t^\bullet$ it will turn out that knowledge of the term to lowest order in ε is sufficient for the asymptotic analysis. As

$$\partial_t^\bullet\psi(\boldsymbol{x},t)=\Psi_s(s,z,t)\partial_t^\bullet s(\boldsymbol{x},t)+\Psi_z(s,z,t)\partial_t^\bullet z(\boldsymbol{x},t)$$

and $\partial_t^\bullet z=\frac{1}{\varepsilon}\partial_t^\bullet r$ we need to focus on computing the leading order term of $\partial_t^\bullet r$. Recall (2.24)

$$\partial_t^\bullet r(\boldsymbol{x},t)=\big(\boldsymbol{v}(\boldsymbol{x}_\Lambda,t)-\boldsymbol{v}_\Lambda(\boldsymbol{x}_\Lambda,t)\big)\cdot\boldsymbol{\mu}_\Lambda(\boldsymbol{x}_\Lambda,t)+\mathcal{O}(\varepsilon)$$

so that

$$\partial_t^\bullet\psi(\boldsymbol{x},t)=\frac{1}{\varepsilon}\Psi_z(s,z,t)\big(\boldsymbol{v}(\boldsymbol{x}_\Lambda,t)-\boldsymbol{v}_\Lambda(\boldsymbol{x}_\Lambda,t)\big)\cdot\boldsymbol{\mu}_\Lambda(\boldsymbol{x}_\Lambda,t)+\mathcal{O}(\varepsilon^0). \qquad (3.18)$$

3.2.4 Inner expansions

In conjunction with the outer region we will employ two ε-expansions in the inner region. However, in contrast with the outer region, we will use the inner variables discussed in the previous section so that the expansions take the form

$$\psi(\boldsymbol{x},t)=\sum_{i=0}^{\infty}\Psi_i(s,z,t)\varepsilon^i,\quad w(\boldsymbol{x},t)=\sum_{i=0}^{\infty}W_i(s,z,t)\varepsilon^i. \tag{3.19}$$

The use of capitals is to distinguish between inner and outer variables.

3.2.5 Matching conditions

The above two expansions valid in the inner and outer regions should match in some intermediary region. Given an arbitrary outer field, ψ, with expansion functions ψ_i and Ψ_i there are a set of matching conditions that these functions should satisfy. These conditions are related to the spatial coordinates only and, thus, are independent of the movement of the domain. Therefore, and because a full derivation can be found in the literature (for instance, see Garke and Stinner [2006a]), we only state them here: In the limit as $z\to\pm\infty$

$$\begin{aligned}
\Psi_0(s,z,t) &\sim \psi_0^{\pm}(\boldsymbol{x}_\Lambda,t), && \text{(3.20a)}\\
\partial_z\Psi_0(s,z,t) &\sim 0, && \text{(3.20b)}\\
\Psi_1(s,z,t) &\sim \psi_1^{\pm}(\boldsymbol{x}_\Lambda,t)\pm\nabla_{\Gamma(t)}\psi_0^{\pm}(\boldsymbol{x}_\Lambda,t)\cdot\boldsymbol{\mu}_\Lambda(\boldsymbol{x}_\Lambda,t)z, && \text{(3.20c)}\\
\partial_z\Psi_1(s,z,t) &\sim \pm\nabla_{\Gamma(t)}\psi_0^{\pm}(\boldsymbol{x}_\Lambda,t)\cdot\boldsymbol{\mu}_\Lambda(\boldsymbol{x}_\Lambda,t), && \text{(3.20d)}\\
\partial_z\Psi_2(s,z,t) &\sim \pm\nabla_{\Gamma(t)}\psi_1^{\pm}(\boldsymbol{x}_\Lambda,t)\cdot\boldsymbol{\mu}_\Lambda(\boldsymbol{x}_\Lambda,t)+\big(\boldsymbol{\mu}_\Lambda(\boldsymbol{x}_\Lambda,t)\cdot\nabla_{\Gamma(t)}\big)^2\psi_0^{\pm}(\boldsymbol{x}_\Lambda,t), && \text{(3.20e)}
\end{aligned}$$

3.3 Slow Mobility

We begin identifying free boundary problems with the case $\bar{M}\sim\varepsilon^0$. As we will briefly discuss below this is the highest scaling of the mobility in ε (or the slowest mobility) for which a sensible free boundary problem occurs.

3.3.1 Outer solutions

Inserting the expansions (3.14) into (3.1) and (3.2), we match orders of ε. To order ε^{-1} (3.2) yields

$$f(\phi_0)=0, \tag{3.21}$$

which has $\phi_0 = \phi_a$ and $\phi_0 = \phi_b$ as stable stationary solutions. Motivated by the assumptions on the setting at the beginning of Section 3.2.1 we can conclude that $\phi_0 = \phi_a$ in Γ^a and $\phi_0 = \phi_b$ in Γ^b which is the first equation of (3.9). To order ε^0 combining (3.1) with the flux term in (3.2) we obtain a bulk problem for the leading order term of the chemical potential:

$$\phi_0 \nabla_\Gamma \cdot \boldsymbol{v} = \nabla_\Gamma \cdot (M(\phi_0) \nabla_\Gamma w_0) \,. \tag{3.22}$$

This is the PDE in (3.9). It remains to derive the interface conditions (3.10). For being able to apply the matching conditions we need to know whether ϕ_1 is a suitable field. So we briefly look at the equation to next order of (3.2) which reads

$$w_0 = f'(\phi_0)\phi_1.$$

3.3.2 Inner solutions

We now insert the expansions (3.19) into (3.1) and (3.2) and employ the change of variables formula (3.16). To the lowest order, ε^{-2}, (3.1) yields

$$0 = \partial_z \left(M(\Phi_0) \partial_z W_0 \right). \tag{3.23}$$

Thus there exists a function $\delta(s,t)$ such that $M(\Phi_0)\partial_z W_0 = \delta(s,t)$. Using the matching condition (3.20b) and that $M > 0$ on (ϕ_a, ϕ_b) we see that $\delta = 0$ and $\partial_z W_0 = 0$. This implies that w_0 is continuous across the interface $\Lambda(t)$ in the limiting problem which is the first condition of (3.10).

To the order ε^{-1} (3.2) yields

$$0 = -\partial_{zz}\Phi_0 + f(\Phi_0). \tag{3.24}$$

The matching condition (3.20a) implies that $\Phi_0 \to \phi_a$ as $z \to -\infty$ and $\Phi_0 \to \phi_b$ as $z \to \infty$. The solution is the phase field profile. Well-posedness of the boundary value problem is discussed in Fife et al. [1979] and its references.

At the same order ε^{-1} (3.1) gives thanks to the new expansion (3.18)

$$\partial_z \Phi_0 (\boldsymbol{v} - \boldsymbol{v}_\Lambda) \cdot \boldsymbol{\mu}_\Lambda + \Phi_0 \partial_z \boldsymbol{v} \cdot \boldsymbol{\mu}_\Lambda = \partial_z \left(M(\Phi_0) \partial_z W_1 \right). \tag{3.25}$$

Here, $\boldsymbol{v}$, $\boldsymbol{v}_\Lambda$, $\boldsymbol{\mu}_\Lambda$, and $\partial_z \boldsymbol{v}$ are evaluated at $(\boldsymbol{x}_\Lambda, t)$ with the usual $\boldsymbol{x}_\Lambda \in \Lambda$ introduced in Section 3.2.3. Using that $\boldsymbol{\mu}_\Lambda$ and $\boldsymbol{v}_\Lambda$ are independent of z the left hand side reads $\partial_z(\Phi_0(\boldsymbol{v} - \boldsymbol{v}_\Lambda) \cdot \boldsymbol{\mu}_\Lambda)$. We may integrate with respect to z over the interfacial region,

i.e., from $-\infty$ to $+\infty$, to obtain the last condition of (3.10),

$$(\phi_b - \phi_a)\big(\boldsymbol{v} - \boldsymbol{v}_\Lambda\big) \cdot \boldsymbol{\mu}_\Lambda = [M(\phi_0)\nabla_\Gamma w_0]. \tag{3.26}$$

Note that we have applied the matching conditions (3.20a) and (3.20d) to Φ_0 and $\partial_z W_1$, respectively.

To the order ε^0 (3.2) gives thanks to (3.17)

$$W_0 = -\partial_{zz}\Phi_1 - \partial_z\Phi_0\kappa_\Lambda + f'(\Phi_0)\Phi_1 \tag{3.27}$$

where κ_Λ is evaluated at $(\boldsymbol{x}_\Lambda, t)$. We multiply by $\partial_z\Phi_0$ and integrate over the interfacial region. By differentiating (3.24) with respect to z we see that $\partial_z\Phi_0$ lies in the kernel of the operator $\partial_{zz} - f'(\Phi_0)$. Using this after an integration by parts argument we obtain the following solvability condition:

$$w_0 = S(\Phi_0)\kappa_\Lambda \tag{3.28}$$

where

$$S(\Phi_0) = \Big(\int_{\mathbb{R}} (\partial_z\Phi_0)^2\Big)/(\phi_b - \phi_a)$$

is a constant depending on the phase profile of Φ_0 and, thus, on the double-well potential. This is the last condition of (3.10) so that we have derived the complete free boundary problem (3.9), (3.10).

3.3.3 Discussion

Let us discuss the limiting problem (3.9), (3.10) for some specific choices of mobilities and potentials and compare with previous results for a stationary flat domain in the literature. We shall also briefly discuss the case of an even slower mobility scaling with ε^1.

- **Mass conservation:** In the limiting problem (3.9), (3.10) the total mass is preserved (as it is in the ESCH equation):

$$\begin{aligned}
&\frac{d}{dt}\Big(\int_{\Gamma^b}\phi_b+\int_{\Gamma^a}\phi_a\Big)\\
&\overset{(2.10)}{=}\int_{\Gamma^b}\phi_b\kappa_m\boldsymbol{v}\cdot\boldsymbol{\nu}+\int_{\Lambda}\phi_b\boldsymbol{v}_\Lambda\cdot(-\boldsymbol{\mu}_\Lambda)+\int_{\Gamma^b}\phi_a\kappa_m\boldsymbol{v}\cdot\boldsymbol{\nu}+\int_{\Lambda}\phi_a\boldsymbol{v}_\Lambda\cdot\boldsymbol{\mu}_\Lambda\\
&\overset{(2.8)}{=}\int_{\Gamma^b}\phi_b\nabla_\Gamma\cdot\boldsymbol{v}+\int_{\Lambda}\phi_b(\boldsymbol{v}_\Lambda-\boldsymbol{v})\cdot(-\boldsymbol{\mu}_\Lambda)+\int_{\Gamma^a}\phi_a\nabla_\Gamma\cdot\boldsymbol{v}+\int_{\Lambda}\phi_a(\boldsymbol{v}_\Lambda-\boldsymbol{v})\cdot\boldsymbol{\mu}_\Lambda\\
&\overset{(3.9)}{=}\int_{\Gamma^b}\nabla_\Gamma\cdot(M(\phi_b)\nabla_\Gamma w)+\int_{\Gamma^a}\nabla_\Gamma\cdot(M(\phi_a)\nabla_\Gamma w)+\int_{\Lambda}(\phi_a-\phi_b)(\boldsymbol{v}_\Lambda-\boldsymbol{v})\cdot\mu_\Lambda\\
&\overset{(2.8),(3.10)}{=}\int_{\Lambda}[M(\phi)\nabla_\Gamma w]\cdot(-\boldsymbol{\mu}_\Lambda)+\int_{\Lambda}[M(\phi)\nabla_\Gamma w]\cdot\boldsymbol{\mu}_\Lambda\quad=0. \qquad (3.29)
\end{aligned}$$

  Thus, if $\phi_b>\phi_a\geq 0$ there is a bound on the maximal and minimal surface area where the bounds depend on the initial mass. This implies a restriction on the surface velocity $\boldsymbol{v}$ or the length of the time interval $[0,T]$ for which the solution exists.
  Observe that such a restriction also applies to the phase field model if the logarithmic potential (3.4) is used as then the value of Φ is bounded from above by β and from below by α so that the total mass has to remain between $\int_\Gamma\alpha$ and $\int_\Gamma\beta$. However, there is no such restriction in the case of a smooth, globally defined potential such as (3.5).
  In turn, there is no restriction in either case, that is for the limiting free boundary problem nor the phase field model, if $\phi_a<0<\phi_b$.

- **Constant mobility:** For the case of a constant mobility and a smooth double-well potential such as F_q, Pego [1989] has shown that the sharp interface limit of the Cahn-Hilliard equation is the Mullins-Sekerka problem Mullins and Sekerka [1963]. It corresponds to (3.9), (3.10) with a flat and stationary surface. One difference is that the curvature, κ_Λ, now is the *geodesic curvature* of the interface. Another difference is the addition of the transport term $\boldsymbol{v}\cdot\boldsymbol{\mu}_\Lambda$ in the evolution law for the interface given in (3.26). The most important difference to the Mullins-Sekerka problem is the surface divergence of the surface velocity in (3.22). In general, the chemical potential is no longer harmonic, and changes over time can occur due to the time dependence of the surface velocity.

- **Non-constant mobility:** With a non-constant but positive (on (α,β)) mobility we obtain a limiting Mullins-Sekerka type problem where the diffusivities

of the chemical potential in the bulk can differ (see (3.22)) which also impacts on the jump term in (3.26). This result is independent of the choice of the double-well potential as long as the smoothness assumptions on (α, β) are met and the minima are located at ϕ_a and ϕ_b. However, the choice of F influences the leading order profile (solution to (3.24)) and, thus, the values of $S(\Phi_0)$ in (3.28). But by appropriate choice of coefficients such as k_1 and k_2 in F_{log} (or a suitable prefactor for F_q) one can ensure that $S(\Phi_0) = 1$.

- **Slower mobility:** Let us briefly consider the case of an even slower mobility $\bar{M} \sim \varepsilon^1$. Equation (3.21) still holds true while (3.1) yields to leading order that $\phi_0 \nabla_\Gamma \cdot \boldsymbol{v} = 0$. Within the solution regime defined in Section 3.2.1, which implies that ϕ_0 is constant in the bulk, we thus obtain the solvability condition $\nabla_\Gamma \cdot \boldsymbol{v} = 0$. This is a strong restriction on the motion of the surface as it corresponds to local incompressibility. In (3.25) then W_0 features instead of W_1. With the matching condition (3.20b) we then see that $\boldsymbol{v}_\Lambda \cdot \boldsymbol{\mu}_\Lambda = \boldsymbol{v} \cdot \boldsymbol{\mu}_\Lambda$. So the interface is simply transported with the surface velocity and any subtle front propogation due to the Cahn-Hilliard dynamics is lost. We remark that this is no contradiction to the results in Pego [1989] where, for the slow mobility, a Stefan type problem is shown to emerge because that limit is established at the next higher order in ε.

3.4 Fast mobility

A fast mobility scaling $\bar{M} \sim \varepsilon^{-1}$ has been used in Cahn et al. [2006] to derive surface diffusion in the deep quench limit $\theta \searrow 0$ of the Cahn-Hilliard equation with (F_{log}, M_{deg}) on a flat and stationary domain. We will discuss this problem below but first consider the general, non-degenerate case $\theta > 0$ or (F_q, M_c).

3.4.1 Asymptotic analysis

As previously we insert the expansions (3.14) and (3.19) into (3.1) and (3.2) and match orders of ε.

From the outer expansion of (3.2) to order ε^{-1} we obtain again that $\phi_0 = \phi_b$ or $\phi_0 = \phi_a$ in Γ^b and Γ^a, respectively. Combining (3.1) with the flux term in (3.2) we obtain to order ε^{-1}

$$0 = \nabla_\Gamma \cdot (M(\phi_0) \nabla_\Gamma w_0) \,. \tag{3.30}$$

Multiplying by w_0 and integrating over $\Gamma^b(t) \cup \Gamma^a(t)$ we obtain using (2.8)

$$\begin{aligned} 0 &= \int_{\Gamma^b(t)} w_0 \nabla_\Gamma \cdot \big(M(\phi_0)\nabla_\Gamma w_0\big) + \int_{\Gamma^a(t)} w_0 \nabla_\Gamma \cdot \big(M(\phi_0)\nabla_\Gamma w_0\big) \qquad (3.31) \\ &= -\int_{\Gamma^b(t)} M(\phi_0)|\nabla_\Gamma w_0|^2 - \int_{\Gamma^a(t)} M(\phi_0)|\nabla_\Gamma w_0|^2 - \int_{\Lambda(t)} \big[w_0 M(\phi_0)\nabla_\Gamma w_0\big] \cdot \boldsymbol{\mu}_\Lambda. \end{aligned}$$

To get an idea of what the jump term is we require information from the inner solutions.

The inner expansion of equation (3.2) yields the equation (3.24) to order ε^{-1} and that Φ_0 is again the phase transition profile. From (3.1) we obtain to order ε^{-3} the equation (3.23) for W_0 again, and as before using the matching conditions (3.20b) and (3.20a) we can conclude that

$$\partial_z W_0 = 0 \quad \text{and} \quad [w_0] = 0. \qquad (3.32)$$

Using this and the orthogonality of $\boldsymbol{\mu}_\Lambda$ and $\boldsymbol{\tau}_\Lambda$, to order ε^{-2} the same equation yields

$$0 = \partial_z\big(M(\Phi_0)\partial_z W_1\big).$$

Similarly, we can conclude that $\partial_z W_1 = 0$ and, using the matching conditions (3.20d) and (3.20c),

$$0 = [M(\phi_0)\nabla_\Gamma w_0] \cdot \boldsymbol{\mu}_\Lambda \quad \text{and} \quad [w_1] = 0. \qquad (3.33)$$

Together with (3.32) we see that the last term of (3.31) vanishes, and we can conclude that $\nabla_\Gamma w_0 = 0$ in $\Gamma^b(t)$ and $\Gamma^a(t)$ so that

$$w_0(t) \text{ is constant on } \Gamma^b(t) \cup \Gamma^a(t). \qquad (3.34)$$

We have explicitly noted the time dependence to clarify that w_0 can and, in general, will change over time (see below).

From equation (3.2) to order ε^0, which is (3.27) again, we can conclude as before that (3.28) holds true. With (3.34) we obtain that also

$$\kappa_\Lambda(t) = \frac{1}{S(\Phi_0)} w_0(t) \text{ is constant along } \Lambda(t) \text{ at all times } t. \qquad (3.35)$$

Continuing with the outer expansions, (3.2) to order ε^0 yields $w_0 = f'(\phi_0)\phi_1$ so that also ϕ_1 is constant where we recall that $F''(\phi_0) = f'(\phi_0) \neq 0$ for $\phi_0 \in \{\phi_a, \phi_b\}$ thanks to the assumption that F has non-degenerate minima. Using that $\nabla_\Gamma w_0 = 0$,

equation (3.1) to order ε^0 yields the following elliptic bulk problem for w_1:

$$\phi_0 \nabla_\Gamma \cdot \boldsymbol{v} = \nabla_\Gamma \cdot (M(\phi_0) \nabla_\Gamma w_1) \,. \tag{3.36}$$

One boundary condition is given by (3.33). In order to determine a second one, consider the inner expansion of (3.1) to order ε^{-1}. Using (3.18) and that $\partial_z W_0 = 0$, $\partial_s W_0 = 0$ (thanks to (3.34)), and $\partial_z W_1 = 0$ as well as the orthogonality of $\boldsymbol{\mu}_\Lambda$ and $\boldsymbol{\tau}_\Lambda$, a short calculation shows that it greatly simplifies to

$$\partial_z \Phi_0 (\boldsymbol{v} - \boldsymbol{v}_\Lambda) \cdot \boldsymbol{\mu}_\Lambda + \Phi_0 \partial_z \boldsymbol{v} \cdot \boldsymbol{\mu}_\Lambda = \partial_z \left(M(\Phi_0) \partial_z W_2 \right). \tag{3.37}$$

It reads as (3.26) except that W_1 is replaced by W_2. Integrating with respect to z over $\mathbb{R}$, treating the left hand side in the same manner as done for (3.26), and applying (3.20e) to the right hand side where we use that $\nabla_\Gamma w_0 = 0$ we arrive at

$$(\phi_b - \phi_a)\big(\boldsymbol{v} - \boldsymbol{v}_\Lambda\big) \cdot \boldsymbol{\mu}_\Lambda = [M(\phi_0) \nabla_\Gamma w_1]. \tag{3.38}$$

Returning to the higher order inner expansions, from equation (3.2) to order ε^0, we obtain (3.27) again, and conclude as before that (3.28) holds true. With (3.34) we obtain that also

$$\kappa_\Lambda(t) = \frac{1}{S(\Phi_0)} w_0(t) \text{ is constant along } \Lambda(t) \text{ at all times } t. \tag{3.39}$$

Since $W_0 = S(\Phi_0)\kappa_\Lambda$, writing $\Phi_1 = \tilde{\phi}\kappa_\Lambda$ and substituting into (3.27), then $\tilde{\phi}$ can be determined as the unique function solving

$$-\partial_{zz}\tilde{\phi} + f'(\Phi_0)\tilde{\phi} = S(\Phi_0) + \partial_z \Phi_0 \tag{3.40}$$

subject to the boundary condition $\lim_{z \to \pm\infty} \partial_z \tilde{\phi} = 0$ from (3.20b).

Finally at order ε we obtain

$$W_1 = -\partial_{zz}\Phi_2 + \partial_z \Phi_1 \kappa_\Lambda + f'(\Phi_0)\Phi_2 + f''(\Phi_0)\frac{\Phi_1^2}{2} \tag{3.41}$$

This gives us a method to determine the interface condition for the first order term of the chemical potential. Multiplying by $\partial_z \Phi_0$ and integrating as before we can determine w_1 to be:

$$w_1 = \frac{\kappa^2}{\phi_b - \phi_a} \int_{-\infty}^{\infty} \partial_z \tilde{\phi} \partial_z \Phi_0 - \frac{\tilde{\phi}^2}{2} \partial_z f'(\Phi_0).$$

We may express this in a short from as

$$w_1 = T(\Phi_0)\kappa_\Lambda^2,$$

where $T(\Phi_0)$ is a constant depending on the leading order phase profile in the inner region. We have suppressed the dependence on $\tilde{\phi}$ by noting the dependence of $\tilde{\phi}$ on the phase profile Φ_0 (see (3.40)).

3.4.2 Discussion

To summarise the findings of the preceding section: The phase interface is in spatial equilibrium in the sense that the geodesic curvature is constant, see (3.39). In the thus split domain we have the set of equations:

$$\left.\begin{aligned} \phi &= \phi_i \\ \nabla_\Gamma \cdot (M(\phi)\nabla_\Gamma \tilde{w}(t)) &= \phi \nabla_\Gamma \cdot \boldsymbol{v}(t) \end{aligned}\right\} \text{ in } \Gamma^i(t), i = a, b, \tag{3.42}$$

$$\left.\begin{aligned} [\tilde{w}(t)] &= 0 \\ \tilde{w}(t) &= T(t)\kappa_\Lambda^2 \\ \tfrac{1}{\phi_b - \phi_a}\left[M(\phi)\nabla_\Gamma \tilde{w}(t)\right] \cdot \boldsymbol{\mu}_\Lambda(t) &= \big(\boldsymbol{v}(t) - \boldsymbol{v}_\Lambda(t)\big) \cdot \boldsymbol{\mu}_\Lambda(t) \end{aligned}\right\} \text{ on } \Lambda(t). \tag{3.43}$$

- **Restrictions due to compatibility condition:** From (3.35) we have a compatibility condition that the curvature should remain constant, in addition we assumed a general surface evolution so that $\boldsymbol{v}$ was arbitrary. However, this causes a problem as a general arbitrary velocity could drive the interface in different ways along its length so as to alter the geodesic curvature. Thus for a solution of the free boundary problem, in the fast mobility regime, to exist we cannot assume an arbitrary surface velocity but must instead assume that the evolution is such that the (spatially) constant curvature persists. This compatibility condition is thus rather restrictive.

- **Mass conservation:** First, observe that the total mass is still preserved in the sharp interface limit potentially implying a restrictions on the velocity $\boldsymbol{v}$. In the identity (3.29) w has to be replaced by $\tilde{w}$ for this purpose.

- **Interface evolution:** The solvability condition (3.39) is an equilibrium condition with respect to the phase separation. This restriction seems reasonable since the fast scaling of the mobility acts to blow up the effects of the Cahn-Hilliard dynamics. But the equilibrium condition (3.39) alone doesn't tell us

much about the evolution of $\Lambda(t)$. In fact, at a given time t there may be several possible curves $\Lambda(t)$ of constant geodesic curvature such that the mass side condition is satisfied. For instance, if $\Gamma(t)$ is a sphere one will find an infinite number. By the assumptions in Section 3.2.1 the interface is approximated by level sets of the phase field solutions. Thus, one may expect it to evolve smoothly, and one will also expect that a specific curve is picked in the sharp interface limit. We leave this question open for future studies.

3.5 The Deep Quench Limit

The deep quench limit of (3.1) and (3.2) for the degenerate ESCH equation corresponds to the limit as $\theta \searrow 0$. Then $\phi_a \to \alpha$ and $\phi_b \to \beta$ so that the degenerate mobility $M_{deg}(\phi)$ is switched off in the bulk. In the case of a stationary, flat domain the limiting problem is surface diffusion and has been derived in Cahn et al. [2006]. There, the flux $\boldsymbol{j}$ is expanded in addition to the fields and some matching conditions are replaced by assumptions on the limits of the fluxes when approaching the boundaries of the interfacial layer. This is due to a lack of equations for the bulk fields.
Indeed, also in our case, (3.30) does not exist so that we have no equation for w_0 in the bulk. In particular, we cannot conclude any more that $\nabla_\Gamma w_0 = 0$. Similarly, there is no bulk equation for w_1: Equation (3.36) reduces to $\phi_0 \nabla_\Gamma \cdot \boldsymbol{v} = 0$. Within the solution regime defined in Section 3.2.1 this means necessarily that

$$\nabla_{\Gamma(t)} \cdot \boldsymbol{v}(t) = 0$$

in the bulk phases, the implication of which has been discussed in the context of a very slow mobility already (see Section 3.3.3). As we also cannot conclude any more that $\partial_s W_0 = 0$ another term of the form $M(u_0)\partial_{ss} W_0$ appears on the right hand side of (3.37). Integrating and using suitable assumptions for the flux $M(\phi_0)\partial_z W_2$ as in Cahn et al. [2006] we obtain

$$(\phi_b - \phi_a)\big(\boldsymbol{v}(t) - \boldsymbol{v}_\Lambda(t)\big) \cdot \mu_\Lambda(t) = \tilde{S}(\Phi_0)\Delta_{\Lambda(t)}\kappa_\Lambda(t) \tag{3.44}$$

instead of (3.38). Here, $\Delta_{\Lambda(t)}$ corresponds to ∂_{ss} after parametrisation and stands for the Laplace-Beltrami operator on the curve $\Lambda(t)$, and $\tilde{S}(\Phi_0) = S(\Phi_0)\int_{\mathbb{R}} M(\Phi_0)$. Equation (3.44) is *surface diffusion* for a curve on a moving surface where the velocity $\boldsymbol{v}$ of the underlying surface manifests by an additional transport term.

It thus seems that surface diffusion might be a sensible sharp interface limit

of the deep quench limit problem in an appropriate setting. In this section we will look to alter the asymptotic analysis to derive surface diffusion more rigorously. Since we have in mind recovering something akin to (3.44), and bearing in mind the compatibility condition resulting from (3.36) we will consider a different system that we will call the non-conservative evolving surface Cahn-Hilliard equation (NESCH). Note that this is not a limit of our previous form for the ESCH. The non-conservative ESCH equation replaces (3.1) with the following

$$\partial_t^\bullet \phi = \nabla_{\Gamma(t)} \cdot \left(M(\phi) \nabla_{\Gamma(t)} w \right). \tag{3.45}$$

The dropping of the term $\phi \nabla_{\Gamma(t)} \cdot \boldsymbol{v}$ from (3.1) results in a relaxation of the conservation assumption with regards the phase field variable, inspiring our naming it the non-conservative ESCH equation. Observe that in weak form (3.45) reads:

$$\frac{d}{dt} \int_{\Gamma(t)} \phi\eta = \int_{\Gamma(t)} \phi\eta \nabla_{\Gamma(t)} \cdot \boldsymbol{v} - M(\phi) \nabla_{\Gamma(t)} w \nabla_{\Gamma(t)} \eta \qquad \text{for all } \eta \in H^1(\Gamma(t)) \text{ a.e. } t \in [0,T]. \tag{3.46}$$

Upon testing with the admissible test function $\eta = 1$ we obtain

$$\frac{d}{dt} \int_{\Gamma(t)} \phi = \int_{\Gamma(t)} \phi \nabla_{\Gamma(t)} \cdot \boldsymbol{v}. \tag{3.47}$$

In the case of local incompressibility, $\nabla_{\Gamma(t)} \cdot \boldsymbol{v} = 0$, we obtain mass conservation again, however in the case of a non-divergence free velocity the total mass can change. Although we take the point of view of referring to the nESCH as a non-conservative form of the ESCH, a possible alternative interpretation is that conservation still holds, but that there is balancing of mass supply by adding the term $\phi \nabla_{\Gamma(t)} \cdot \boldsymbol{v}$ to the right hand side of (3.1) so that mass is added to the system at exactly the rate with which it would appear to be lost due to local stretching/compression.

Since we wish to study the deep quench limit of the logarithmic potential, (3.4), we consider the double obstacle type potential, (3.8). Since this is not differentiable (3.2) must be expressed in the following form:

$$w + \varepsilon \Delta_{\Gamma(t)} \phi + \frac{1}{\varepsilon} (\phi - \frac{\beta + \alpha}{2}) \in \partial \mathcal{I}_{[\alpha,\beta]}(\phi). \tag{3.48}$$

In (3.48), $\partial \mathcal{I}_{[\alpha,\beta]}(\cdot)$ is the subdifferential of the indicator function $I_{[\alpha,\beta]}$ for the interval $[\alpha, \beta]$.

Existence of solutions of (3.45) and (3.48) have been considered in Blowey and Elliott [1991b] in the case of a constant mobility, $M(\phi) = 1$ and a planar setting. It was shown in Elliott and Luckhaus [1991] that under the same setting as

in Blowey and Elliott [1991b] that (3.45) and (3.48) result as the deep quench limit when considering the Ginzburg-Landau energy with the logarithmic potential (3.4), however it must be assumed that this result still holds for the case of a degenerate mobility and an evolving surface.

3.5.1 Assumptions on the Solution Regime

Solutions, $\phi \in C^0(\Gamma(t))$, of (3.45) and (3.48) decompose the surface, $\Gamma(t)$, in the following manner $\Gamma(t) = \Gamma^\alpha(t) \cup \Gamma^\Lambda(t) \cup \Gamma^\beta(t)$ such that

$$\phi \in (\alpha, \beta), \quad w = -\varepsilon \Delta_{\Gamma(t)} \phi - \frac{1}{\varepsilon} \left(\phi - \frac{\alpha + \beta}{2} \right), \quad \boldsymbol{x} \in \Gamma^\Lambda(t) \tag{3.49}$$

$$\phi = \alpha, \quad \boldsymbol{x} \in \Gamma^\alpha(t) \tag{3.50}$$

$$\phi = \beta, \quad \boldsymbol{x} \in \Gamma^\beta(t). \tag{3.51}$$

In line with the assumptions made in Section 3.2.1 and following the lines of Cahn et al. [2006], we assume that our solutions roughly mimic the characteristic features of minimisers of the Ginzburg-Landau energy (with double obstacle potential) so that $\Gamma^\Lambda(t)$ is an annular subsection of the surface $\Gamma(t)$ and that both $\Gamma^\alpha(t)$ and $\Gamma^\beta(t)$ are of non-zero measure.

Furthermore, since there is no bulk problem the matching conditions (3.20a) to (3.20e) can no longer be used. Due to the fact that there are no outer expansions the standard practice of describing an intermediary region where inner and outer expansions match cannot be applied. For this reason we must deal with the boundary of the interfacial region explicitly. We will denote these boundaries by $\Lambda^\alpha(t) = \partial\Gamma^\Lambda(t) \cap \Gamma^\alpha(t)$ and $\Lambda^\beta(t) = \partial\Gamma^\Lambda(t) \cap \Gamma^\beta(t)$, and will assume they can be expressed as a graph so that the scaled distance function takes values $z \in [Z_\varepsilon^-(s,t), Z_\varepsilon^+(s,t)]$ with

$$Z_\varepsilon^\pm(s,t) = Z_0^\pm(s,t) + \varepsilon Z_1^\pm(s,t) + \mathcal{O}(\varepsilon^2). \tag{3.52}$$

Since the matching conditions cannot be applied we must make constitutive assumptions on the fluxes at the boundary. Motivated by the natural flux conditions that are usually associated with the Cahn-Hilliard equation we assume the following

boundary conditions on the inner region.

$$\lim_{x\to\Lambda^i(t)} \nabla_{\Gamma(t)}\phi\cdot\boldsymbol{\mu} = 0, \tag{3.53}$$

$$\lim_{x\to\Lambda^i(t)} M(\phi)\nabla_{\Gamma(t)}w\cdot\boldsymbol{\mu} = 0 \tag{3.54}$$

with $i\in\{\alpha,\beta\}$ and $\boldsymbol{\mu}$ the extension of the co-normal to $\Lambda(t)$.

For the ease of the reader we collect the principal equations from the above for use in the asymptotic analysis.

$$\left.\begin{aligned}\phi(x,t) &= \alpha\end{aligned}\right\} x\in\Gamma^\alpha(t) \tag{3.55}$$

$$\left.\begin{aligned}\phi(x,t) &= \beta\end{aligned}\right\} x\in\Gamma^\beta(t) \tag{3.56}$$

$$\left.\begin{aligned}\partial_t^\bullet\phi &= \nabla_{\Gamma(t)}\cdot\left(M(\phi)\nabla_{\Gamma(t)}w\right)\\ w &= -\varepsilon\nabla_{\Gamma(t)}\phi - \tfrac{1}{\varepsilon}\left(\phi-\tfrac{\alpha+\beta}{2}\right)\end{aligned}\right\} x\in\Gamma^\Lambda(t) \tag{3.57}$$

$$\left.\begin{aligned}0 &= \nabla_{\Gamma(t)}\phi\cdot\boldsymbol{\mu}\\ 0 &= M(\phi)\nabla_{\Gamma(t)}w\cdot\boldsymbol{\mu}\end{aligned}\right\} x\in\Lambda^i(t),\ i\in\{\alpha,\beta\} \tag{3.58}$$

We will employ the same inner expansions used previously, (3.19). The upshot of the boundary conditions, (3.58), together with (3.55)-(3.56) implies the following boundary conditions for the individual terms of the inner expansion.

$$\lim_{z\to Z_0^+}\Phi_0 = \beta \tag{3.59}$$

$$\lim_{z\to Z_0^-}\Phi_0 = \alpha \tag{3.60}$$

$$\lim_{z\to Z_0^\pm}\partial_z\Phi_0(s,z,t) = 0 \tag{3.61}$$

$$\lim_{z\to Z_0^\pm}\Phi_1(s,z,t) = 0 \tag{3.62}$$

$$\lim_{z\to Z_0^\pm} M(\Phi_0)\partial_z W_0 = 0 \tag{3.63}$$

$$\lim_{z\to Z_0^\pm}\Phi_1 M'(\Phi_0)\partial_z W_0 + M(\Phi_0)\partial_z W_1 = 0 \tag{3.64}$$

3.5.2 Asymptotic Analysis

From the second equation of (3.57), to order ε^{-1}, we obtain the equation

$$0 = -\partial_{zz}\Phi_0 - \Phi_0. \tag{3.65}$$

With the boundary conditions (3.59), (3.60) and (3.65), this equation is solvable if $Z_0^{\pm} = \frac{\pi}{2}$, thus we make this assumption about the relative width of the inner region and thus conclude that the phase profile takes the form:

$$\Phi_0(z,s,t) = \frac{\beta-\alpha}{2}\sin(z) + \frac{\beta+\alpha}{2}. \tag{3.66}$$

To lowest order, ε^{-3} from (3.57) we see that

$$0 = \partial_z \left(M(\Phi_0)\partial_z W_0 \right). \tag{3.67}$$

Arguing as with (3.23), identifying that $M(\Phi_0)\partial_z W_0$ is a function of s and t only, we use the boundary condition (3.63) instead of matching conditions to infer that this constant is in fact zero. Thus noting (3.66), and recalling the assumed positivity of the mobility function in this region, we may infer that

$$\partial_z W_0 = 0, \quad W_0 = \delta_1(s,t) \tag{3.68}$$

so that W_0 is independent of z and a function of s and t only. To the next order, ε^{-2}, we have

$$0 = \partial_z \left(M'(\Phi_0)\Phi_1 \partial_z W_0 + M(\Phi_0)\partial_z W_1 \right). \tag{3.69}$$

Using the boundary condition (3.64) we can argue as at the previous order to see that the term in the brackets is independent of z and then use (3.68) to proceed to the conclusion that

$$\partial_z W_1 = 0, \quad W_1 = \delta_2(s,t) \tag{3.70}$$

and so W_1 is also independent of z and is also a function of s and t only. To order ε^{-1} from the first equation of (3.57), we obtain the following

$$\partial_z \Phi_0 (\boldsymbol{v} - \boldsymbol{v}_\Lambda) \cdot \boldsymbol{\mu}_\Lambda = \partial_z \left(M(\Phi_0)\partial_z W_2 \right) + M(\Phi_0)\Delta_s W_0 \tag{3.71}$$

We will return to the analysis of (3.71) after we consider the next order of expansions. To order ε^0 we only need the following equation for identification of the sharp interface limit.

$$W_0 = -\partial_{zz}\Phi_1 + \kappa_\Lambda \partial_z \Phi_0 - \Phi_1. \tag{3.72}$$

We can treat this equation the same as (3.27), multiplying by $\partial_z \Phi_0$ and integrating over the interfacial region using (3.61) and (3.62). This gives that

$$W_0(s,t) = S(\Phi_0)\kappa_\Lambda, \tag{3.73}$$

with the constant $S(U_0)$ independent of s and t and given by

$$S(\Phi_0) = \Big(\int_{-\pi/2}^{\pi/2} (\partial_z \Phi_0)^2 \Big) / (\beta - \alpha).$$

We may now analyse (3.71), integrating over the interfacial region we see that

$$(\beta - \alpha)\,(\boldsymbol{v} - \boldsymbol{v}_\Lambda) \cdot \boldsymbol{\mu}_\Lambda = \int_{-\pi/2}^{\pi/2} M(\Phi_0) \Delta_s W_0 \,\mathrm{d}z, \tag{3.74}$$

since the mobility is zero on the boundary. Using (3.73) we can replace W_0 to obtain

$$(\boldsymbol{v} - \boldsymbol{v}_\Lambda) \cdot \boldsymbol{\mu}_\Lambda = \tilde{S}(\Phi_0) \Delta_s \kappa_\Lambda, \tag{3.75}$$

where

$$\tilde{S}(\Phi_0) = S(\Phi_0) \int_{-\pi/2}^{\pi/2} M(\Phi_0).$$

Chapter 4

Numerics

4.1 Overview

Using numerical simulations, the aims of this section are: (1) to support the theoretical findings on the convergence as $\varepsilon \to 0$ stated in the previous chapters, and (2) to illustrate and display some of the possible effects due to the motion of the surface. The computational method is based on the evolving surface finite element method presented in Dziuk and Elliott [2007] which has been applied to the ESCH equation in Elliott and Ranner [2013].

This chapter is laid out as follows, we first describe the evolving surface finite element method, beginning with mesh generation and finite element spaces before discussing it's application to the ESCH equation. We postulate everything under the guise of an Arbitrary Lagrange Eulerian method (Elliott and Styles [2012]) and simplify where appropriate. We then test the chosen schemes and provide some examples of simulations before displaying the interesting results presented in the paper O'Connor and Stinner [2016].

4.2 The Surface Finite Element Method

4.2.1 Approximation of Geometry and Triangulations

As stated within Section 2.1 under our assumptions for the asymptotic analysis presented in the previous chapter; we restrict to smooth, connected, evolving compact hypersurfaces $\Gamma(t) \subset \boldsymbol{R}^{n+1}$, where $n = 1, 2$ is the dimension of the surface and $t \in [0, T]$, with $T > 0$, and such that $\partial\Gamma(t) = \emptyset$. We again assume that it is orientable and denote by $\boldsymbol{\nu}(\cdot, t) : \Gamma(t) \to \mathbb{R}^3$, $t \in [0, T]$, a spatial unit normal vector field. Recall the space time graph $\mathcal{G}_T$ comes with a material velocity $\boldsymbol{v}$. The evolving

surface finite element (ESFEM) can, in general, be applied to higher dimensions.

We approximate the evolving surface, $\{\Gamma(t)\}_t$, by an evolving polyhedral surface, $\{\Gamma_h(t)\}_t$. For the purpose of generating such an approximation we use a triangulation of the given hypersurface $\Gamma(t)$ at time $t = 0$. That is we approximate $\Gamma(0)$ by a polyhedral surface $\Gamma_h(0)$ which is formed by taking a given number, $N_h < \infty$, of nodes on the surface $\Gamma(0)$ and then using n-simplicies with these nodes as vertices to interpolate between them. The idea is visually represented in Figure 4.1.

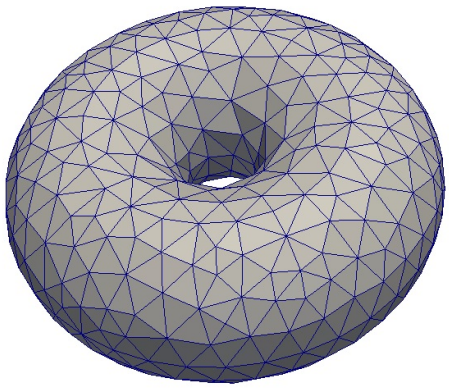

Figure 4.1: Approximation of a torus by a polygonal surface induced by a triangulation.

The discretely triangulated surface $\Gamma_h(0)$ is thus the union of a finite number of non-degenerate closed n-simplicies. We denote this set of simplicies $\mathcal{T}_h(0)$. We restrict to triangulations such that there is a bijection between $\Gamma(0)$ and $\Gamma_h(0)$, so that we have a simple covering. That is for $T_1, T_2 \in \mathcal{T}_h(0)$ either $T_1 \cap T_2 = \emptyset$ or $T_1 \cap T_2$ is an $(n-k)$-dimensional side simplex ($k \in \{1, ..., n\}$) common to both elements.

To obtain a triangulated surface for a given time $t > 0$, we advect the nodes used in the initial triangulation $\Gamma_h(0)$ in the following manner. We denote by $\{X_j(t)\}_j$, $j = 1, ..., N_h$ the set of vertices associated with the triangulation at each time, then the velocity of the nodes is given by $\dot{X}_j(t)$. It is natural to evolve the vertices with $\boldsymbol{v}$ as this keeps the nodes on the evolving surface $\Gamma(t)$ this requires at all times that

$$\dot{X}_j(t) = \boldsymbol{v}\left(X_j(t), t\right), \qquad X_j(0) = X_j^0 \quad \forall\, j = 1, ..., N_h. \tag{4.1}$$

The ESFEM is based on this procedure. However for the tangential components,

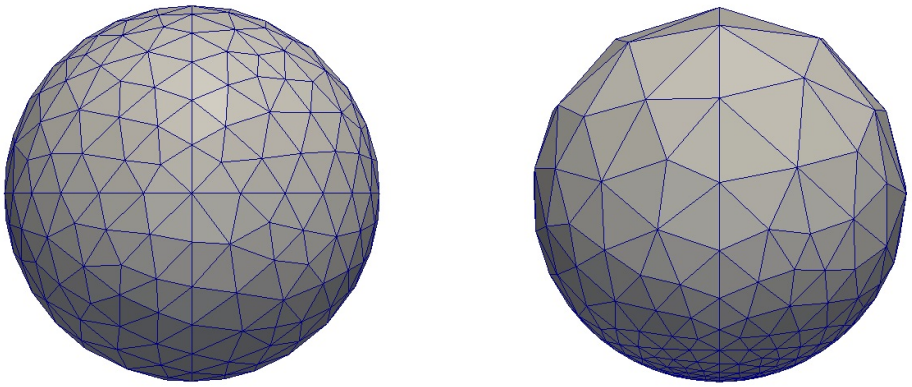

Figure 4.2: Example of mesh degeneration due to tangential velocity. Initial uniform triangulation on the left and at later time on right after advecting nodes by the material velocity which is given by $v(X(\theta,\phi)) = \sin(\theta)X_\theta$, where $X(\theta,\phi)$ is the standard parameterisation of a sphere.

although advection by the material velocity is natural, it is possible to see mesh degeneration. An example of this can be seen in Figure 4.2. To overcome this issue one may only require (4.1) to hold in the normal direction and leave the tangential motion arbitrary. Note that we will still have the property that $X_j(t) \in \Gamma(t)\ \forall j = 1, ..., N_h$ and $t \in [0, T]$. For our procedure we assume there is some intrinsic material tangential velocity, $\boldsymbol{v}_\tau := \boldsymbol{P}\boldsymbol{v}$, given as the tangential projection of the material velocity. We then assume in addition an arbitrary velocity, $\boldsymbol{a}_\tau$, satisfying $\boldsymbol{a}_\tau \cdot \boldsymbol{\nu} = 0$ such that nodes are transported according to

$$\boldsymbol{P}\dot{X}_j(t) = \boldsymbol{a}_\tau\left(X_j(t), t\right) + \boldsymbol{v}_\tau\left(X_j(t), t\right), \qquad X_j(0) = X_j^0 \quad \forall\, j = 1, ..., N_h. \tag{4.2}$$

For a surface PDE this leads naturally to an Arbitrary Lagrangian Eulerian (ALE) method, or in our case ALE-ESFEM. The ALE-ESFEM has been introduced in Elliott and Styles [2012] and more rigorously studied in Elliott and Venkataraman [2015]. In most cases we will use $\boldsymbol{a}_\tau = 0$ and evolve the nodes purely by the surface tangential velocity. However in some instances the ability to use an arbitrary velocity will enable us to ensure mesh regularity throughout a simulation and thus we will be able to avoid any complications due to re-meshing. In particular in the moving sphere example (Section 4.4.3), since the nodes are all transported towards the south pole, setting $\boldsymbol{a}_\tau = -\boldsymbol{v}_\tau$ avoids nodes bunching near the south pole and ensures an even spread of nodes near the north pole.

The subscript h refers to the time free, uniform bound on the maximum

diameter of an n-simplex's face. In addition to the above we assume that the evolution of the mesh is such that the ratio of the maximal simplex diameter and minimal simplex in-ball radius is uniformly bounded independently of both h and t.

Thus far the procedure for approximating the geometry does not change the topology of our mesh. Since we are interested in producing phase field simulations, the thin moving interfacial layers have to be resolved, this motivates the need for adaptive refinement and coarsening. In this work we only consider 'h'-refinements, as opposed to 'p'-refinements. In 'p'-refinements the polynomial degree of the simplex faces is increased, see Heine [2004], and in 'h'-refinements the maximal diameter is reduced. If we wish to refine the triangulation then we follow the practical point of view by introducing new nodal points on the current triangulation and project these points back onto the smooth surface. An example of the process is seen in Figure 4.3 and the details can be found in Dziuk and Elliott [2007] for a general refinement procedure and Demlow and Dziuk [2007] for adaptive refinement.

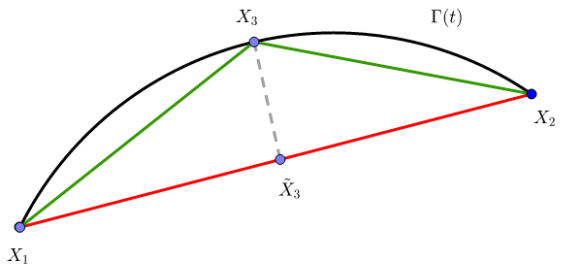

Figure 4.3: Example of h-refinement where h is reduced due to the introduction of the point $\tilde{X}_3$ which is then projected onto the surface $\Gamma(t)$ as the point X_3. The red line represents $\Gamma_h(t)$ for one particular h and the green line represents $\Gamma_h(t)$ for a smaller h.

4.2.2 Finite Element Spaces

Given an appropriate mesh generated by a triangulation, $\mathcal{T}_h(t)$, we define the following isoparametric finite element spaces at each time t, see Brenner and Scott [2007]:

$$S_h(t) = \left\{ \eta(\cdot,t) \in C^0(\Gamma_h(t)) \,\middle|\, \eta(\cdot,t)|_{T(t)} \in \mathbb{P} \;\forall\, T(t) \in \mathcal{T}_h(t) \right\} \tag{4.3}$$

where $\mathbb{P}$ is the polynomials of degree 1. These finite element spaces are isoparametric in that the polynomial degree of the faces used in the geometry approximation is

the same as the polynomial degree used for the approximating functions. We denote by $\eta_1(t), ..., \eta_{N_h}(t)$ the nodal basis of $S_h(t)$, which is characterised by the identity:

$$\eta_i(t, X_j(t)) = \delta_{ij}. \tag{4.4}$$

4.3 Function Spaces for Continuous Equations

Standard practice for parabolic problems is to use Bochner spaces of the form $L^p(0,T;X)$ with X some appropriate Banach space. The difficulty for this approach when combined with evolving surfaces is the time-dependence of the surface itself, i.e. we look to work with spaces such that $X = H^1(\Gamma(t))$. The natural setting for our solutions is in fact Sobolev spaces over the space time graph. These type of function spaces have been studied in some detail in Alphonse et al. [2014].

We can define Sobolev Spaces over the space-time surface as follows. Let $\nabla_{\mathcal{G}_T}$ be the space-time gradient and $\mathrm{d}\sigma_T$ the associated measure to the space-time surface.

$$\begin{aligned} L^2(\mathcal{G}_T) &:= \left\{ \eta \in L^1_{loc}(\mathcal{G}_T) \,:\, \int_{\mathcal{G}_T} \eta^2 \mathrm{d}\sigma_T < \infty \right\}, \\ H^1(\mathcal{G}_T) &:= \left\{ \eta \in L^2(\mathcal{G}_T) \,:\, \nabla_{\mathcal{G}_T}\eta \in L^2(\mathcal{G}_T) \right\}. \end{aligned}$$

The standard norms for the above spaces are

$$\begin{aligned} \|\eta\|_{L^2(\mathcal{G}_T)} &:= \left(\int_{\mathcal{G}_T} \eta^2 \mathrm{d}\sigma_T \right)^{1/2}, \\ \|\eta\|_{H^1(\mathcal{G}_T)} &:= \left(\|\eta\|^2_{L^2(\mathcal{G}_T)} + \|\nabla_{\mathcal{G}_T}\eta\|^2_{L^2(\mathcal{G}_T)} \right)^{1/2}. \end{aligned}$$

However using the following identity for splitting the integral into it's space and time components

$$\int_0^T \int_{\Gamma(T)} \eta \mathrm{d}\sigma \mathrm{d}t = \int_{\mathcal{G}_T} \frac{\eta}{\sqrt{1+|v_{\boldsymbol{\nu}}|^2}} \mathrm{d}\sigma_T,$$

alongside the characterisation of the space-time gradient

$$\nabla_{\mathcal{G}_T}\eta = \left(\nabla_\Gamma \eta + \frac{\partial^\bullet \eta v_{\boldsymbol{\nu}}}{1+|v_{\boldsymbol{\nu}}|^2}, \frac{\partial^\bullet \eta}{1+|v_{\boldsymbol{\nu}}|^2} \right),$$

then given a smooth velocity, $\boldsymbol{v}$, we can use the following equivalent norms

$$\|\eta\|'_{L^2(\mathcal{G}_T)} := \left(\int_0^T \int_{\Gamma(t)} \eta^2 \mathrm{d}\sigma\mathrm{d}t\right)^{1/2},$$
$$\|\eta\|'_{H^1(\mathcal{G}_T)} := \left(\int_0^T \int_{\Gamma(t)} \eta^2 + |\nabla_\Gamma \eta|^2 + (\partial^\bullet \eta)^2 \mathrm{d}\sigma\mathrm{d}t\right)^{1/2}.$$

These equivalent norms motivate us to define the necessary solution spaces for posing the ESCH equation in a weak form.

$$L^2_{L^2} := \left\{\eta \in L^1_{loc} : \int_0^T \int_{\Gamma(t)} \eta^2 \mathrm{d}\sigma\mathrm{d}t < \infty\right\}$$
$$L^2_{H^1} := \left\{\eta : \mathcal{G}_T \to \mathbb{R} : \eta \in L^2_{L^2} \text{ and } \nabla_\Gamma \eta \in (L^2_{L^2})^{n+1}\right\}$$
$$L^q_{H^1} := \left\{\eta \in L^q(\mathcal{G}_T) : \|\eta\|_{L^q_{H^1}} < \infty\right\}$$

We note that $L^\infty_{H^1} \subset L^2_{H^1}$ and that $\eta \in L^2_{H^1}$ with $\partial^\bullet \eta \in L^2_{L^2}$ if and only if $\eta \in H^1(\mathcal{G}_T)$. For more details see Elliott and Ranner [2013].

4.3.1 Weak Formulation

Denoting by $\boldsymbol{v}_a := \boldsymbol{v} + \boldsymbol{a}_\tau$ the sum of the surface velocity and the arbitrary tangential velocity, and using the notation $\partial^\bullet_{\boldsymbol{v}_a}$ and $\partial^\bullet_{\boldsymbol{v}}$ for the material derivatives with respect to the subscripted velocity, we may relate the two as follows. Let $\psi : \mathcal{G}_T \to \mathbb{R}$, and let $\tilde{\psi}$ be any sufficiently smooth extension to a neighbourhood of $\Gamma(t)$, then

$$\partial^\bullet_{\boldsymbol{v}_a} \psi = \partial_t \tilde{\psi} + \boldsymbol{v}_\nu \cdot \nabla \tilde{\psi} + (\boldsymbol{a}_\tau + \boldsymbol{v}_\tau) \cdot \nabla_{\Gamma(t)} \psi = \partial^\bullet_{\boldsymbol{v}} \psi + \boldsymbol{a}_\tau \cdot \nabla_{\Gamma(t)} \psi. \tag{4.5}$$

We generate the weak formulation of the ESCH equation through the standard method, multiplication by a test function in an appropriate test space, and integration over the whole domain.

Problem 4.3.1. *We say that the pair $(\phi, w) : \mathcal{G}_T \to \mathbb{R}^2$ with $\phi \in L^\infty_{H^1} \cap H^1(\mathcal{G}_T)$ and $w \in L^2_{H^1}$, are a weak solution of the evolving surface Cahn-Hilliard equation* (3.1), (3.2) *if, for almost every $t \in (0, T)$,*

$$\int_{\Gamma(t)} \partial^\bullet_t \phi \eta + \phi \eta \nabla_{\Gamma(t)} \cdot \boldsymbol{v} = -\int_{\Gamma(t)} M(\phi) \nabla_{\Gamma(t)} w \cdot \nabla_{\Gamma(t)} \eta \tag{4.6}$$
$$\int_{\Gamma(t)} w\psi = \int_{\Gamma(t)} \varepsilon \nabla_{\Gamma(t)} \cdot \phi \nabla_{\Gamma(t)} \psi + \int_{\Gamma(t)} \frac{1}{\varepsilon} f(\phi) \psi \tag{4.7}$$

for all $\eta, \psi \in L^2_{H^1}$ *with initial condition* $\phi(\cdot, 0) = \phi_0$ *with some* $\phi_0 : \Gamma(0) \to \boldsymbol{R}$.

By using the transport formula, (2.9), with $\boldsymbol{v}$ replaced by $\boldsymbol{v}_a$, we can remove the explicit dependence on the surface velocity $\boldsymbol{v}$ to obtain a variational formulation that we will use as the basis for our finite element approximation. In the variational formulation (4.6) is replaced by the following which differs from the standard variational formulation due to the movement of material points by the arbitrary tangential velocity $\boldsymbol{v}_a$.

$$\frac{d}{dt}\int_{\Gamma(t)} \phi\eta + \int_{\Gamma(t)} M(\phi)\nabla_{\Gamma(t)} w \cdot \nabla_{\Gamma(t)}\eta = \int_{\Gamma(t)} \phi\partial^{\bullet}_{\boldsymbol{v}_a}\eta - \phi\boldsymbol{a}_\tau \cdot \nabla_{\Gamma(t)}\eta. \tag{4.8}$$

where again $\eta \in L^2_{H^1}$

4.3.2 Spatial Discretisation

For the discretisation of time we employ the method of lines. Thus we require a spatial discretisation to exist first from which we then segment time into intervals. We denote the discrete space time graph by

$$\mathcal{G}^h_T = \bigcup_t \Gamma_h(t) \times \{t\}. \tag{4.9}$$

To define the spatial discretisation we must define several discrete analogues of quantities appearing in the variational formulation (4.8). First we define the discrete surface normal. Since $\Gamma(t)$ was assumed orientable, $\Gamma_h(t)$ as a linearly interpolated approximation is piecewise orientable. That is to say that on the face of each element, there exists a C^1 unit normal to the surface. We denote by $\boldsymbol{\nu}_h$ this piecewise unit normal. In the case that $\Gamma(t)$ (and hence $\Gamma_h(t)$) is a boundary we take the outward pointing unit normal to $\Gamma_h(t)$. Using this we define the tangential gradient, $\nabla_{\Gamma_h(t)}$, on $\Gamma_h(t)$ element-wise, let $\eta_h : \Gamma_h(t) \to \mathbb{R}$:

$$\nabla_{\Gamma_h(t)}\eta_h = \nabla\tilde{\eta}_h - (\nabla\tilde{\eta}_h \cdot \boldsymbol{\nu}_h)\boldsymbol{\nu}_h = \boldsymbol{P}_h\nabla\tilde{\eta}_h \tag{4.10}$$

where $\boldsymbol{P}_h = \boldsymbol{I} - \boldsymbol{\nu}_h \otimes \boldsymbol{\nu}_h$. Given $\eta \in H^{1+\delta}(\Gamma(t))$, the interpolation operator I_h onto $S_h(t)$ is given by

$$I_h(t)\eta(\boldsymbol{x}_h) = \sum_{i=1}^{N_h} \eta(X_j(t))\eta_j(\boldsymbol{x}_h, t), \quad \boldsymbol{x}_h(t) \in \Gamma_h(t). \tag{4.11}$$

We take functions in $H^{1+\delta}$ as a minimum so that they are continuous however H^2

would suffice, since $X_j(t) \in \Gamma_h(t)$ we can ensure that I_h is indeed well defined. In practice we will be applying the interpolation operator to surface velocities and initial conditions only, and will thus be using smooth functions.

We can characterise the velocity of the surface $\Gamma_h(t)$ using this interpolation operator. Material points in $\Gamma_h(t)$ move with a discrete material velocity $\boldsymbol{v}_{a,h}$ such that $\boldsymbol{v}_{a,h}(\boldsymbol{x}_h, t) := I_h \boldsymbol{v}_a$. The discrete velocity induces a discrete material derivative. For a scalar quantity, η_h, defined on $\mathcal{T}_h$, the discrete material derivative is given by

$$\partial^\bullet_{\boldsymbol{v}_{a,h}} \eta_h = \partial_t \tilde{\eta}_h + \nabla \tilde{\eta}_h \cdot \boldsymbol{v}_{a,h} \tag{4.12}$$

Note that η_h need not be in our finite element space $S_h(t)$ for this to be defined. The upshot of the discrete material velocity taking this form, and due to the characterisation of the basis functions in our choice of finite element space, it has been shown in Dziuk and Elliott [2007] that

$$\partial^\bullet_{\boldsymbol{v}_{a,h}} \eta_j = 0 \quad \text{for all } j \in \{1, ..., N_h\}. \tag{4.13}$$

Furthermore the transport identity 2.9 has also been shown in Dziuk and Elliott [2007] to hold in a discrete setting so that

$$\frac{d}{dt} \int_{\Gamma_h(t)} \eta_h = \int_{\Gamma_h(t)} \partial^\bullet_{\boldsymbol{v}_{a,h}} \eta_h + \eta_h \nabla_{\Gamma_h(t)} \cdot \boldsymbol{v}_{a,h}. \tag{4.14}$$

With these discrete analogues we can define the spatially discrete problem.

Problem 4.3.2. *We say that the pair $(\phi_h, w_h) : (\Gamma_h(t), t) \to \mathbb{R}^2$ with $\phi_h(t), w_h(t) \in S_h(t)$ for all t, are a discrete approximation to the solution of the evolving surface Cahn-Hilliard equation* (3.1), (3.2) *if, for almost every $t \in (0, T)$,*

$$\frac{d}{dt} \int_{\Gamma_h(t)} \phi_h \eta_h + \int_{\Gamma_h(t)} M(\phi_h) \nabla_{\Gamma_h(t)} w_h \cdot \nabla_{\Gamma_h(t)} \eta_h = \int_{\Gamma_h(t)} \phi_h \partial^\bullet_{\boldsymbol{v}_{a,h}} \eta_h - \phi_h I_h \boldsymbol{a}_\tau \cdot \nabla_{\Gamma_h(t)} \eta_h$$

$$\int_{\Gamma_h(t)} w_h \psi_h = \int_{\Gamma_h(t)} \varepsilon \nabla_{\Gamma_h(t)} \phi_h \cdot \nabla_{\Gamma_h(t)} \psi_h + \int_{\Gamma_h(t)} \frac{1}{\varepsilon} f(\phi_h) \psi_h$$

for all $\eta_h, \psi_h \in S_h(t)$ and $\phi_h(\cdot, 0) = I_h \phi(\cdot, 0)$ point-wise almost everywhere in $\Gamma_h(0)$.

Observe that $\eta_h \in S_h(t)$ can be any discrete function and is not necessarily a basis function and thus the term $\partial^\bullet_{\boldsymbol{v}_{a,h}} \eta_h$ does not necessarily vanish.

Since $\phi_h(t), w_h(t) \in S_h(t)$ we can write them as

$$\phi_h(\boldsymbol{x}_h, t) = \sum_{i=1}^{N_h} \Phi_i(t)\eta_i(\boldsymbol{x}_h, t), \qquad w_h(\boldsymbol{x}_h, t) = \sum_{i=1}^{N_h} W_i(t)\eta_i(\boldsymbol{x}_h, t) \quad \boldsymbol{x}_h \in \Gamma_h(t). \tag{4.15}$$

By restricting to the basis functions as test functions in the discrete problem 4.3.2, we can generate a matrix form of the problem where we use the basis transport property (4.13). We denote by $\Phi(t)$ the vector with coefficients $\Phi_i : (0, T) \to \mathbb{R}$ for $i = 1, ..., N_h$. Similarly we define $W(t)$. This matrix form reads as:

$$\frac{d}{dt}\left(\mathcal{M}(t)\Phi(t)\right) + \mathcal{S}_M(t)W(t) + \mathcal{A}(t)\Phi(t) = 0 \tag{4.16}$$

$$\mathcal{M}(t)W(t) = \varepsilon\mathcal{S}(t)\Phi(t) + \frac{1}{\varepsilon}\mathcal{F}(\Phi(t)). \tag{4.17}$$

where

$$\mathcal{M}(t)_{ij} = \int_{\Gamma_h(t)} \eta_i\eta_j \tag{4.18}$$

$$\mathcal{S}_M(t)_{ij} = \int_{\Gamma_h(t)} M(\phi_h)\nabla_{\Gamma_h(t)}\eta_i\nabla_{\Gamma_h(t)}\eta_j \tag{4.19}$$

$$\mathcal{S}(t)_{ij} = \int_{\Gamma_h(t)} \nabla_{\Gamma_h(t)}\eta_i\nabla_{\Gamma_h(t)}\eta_j \tag{4.20}$$

$$\mathcal{A}(t)_{ij} = \int_{\Gamma_h(t)} I_h(\boldsymbol{a}_\tau)\eta_i \cdot \nabla_{\Gamma_h(t)}\eta_j \tag{4.21}$$

$$\mathcal{F}(U(t))_i = \int_{\Gamma_h(t)} f(\phi_h)\eta_i. \tag{4.22}$$

4.3.3 Time Discretisations

As stated at the start of the previous section we employ the method of lines for our time discretisation. Although we could choose intervals of differing length, for the sake of convenience we choose to restrict to uniform intervals of length δt throughout our numerical experiments. We define $t_m = m\delta t$, $m = 0, ..., M = \frac{T}{\delta t}$, as the time nodes and with this discretisation of time we define

$$S_h^m = S_h(t_m) \tag{4.23}$$

thus obtaining a finite element space at each time step.

We will employ two different schemes throughout our simulations. The first is a fully implicit numerical scheme for use in 1D simulations. Letting $\Phi^m := \Phi(t_m)$

our fully implicit scheme reads:

$$\mathcal{M}^{m+1}\Phi^{m+1} + \delta t \mathcal{S}_M^{m+1} W^{m+1} + \mathcal{A}^{m+1}\Phi^{m+1} = \mathcal{M}^m \Phi^m \tag{4.24}$$

$$\mathcal{M}^{m+1} W^{m+1} = \varepsilon \mathcal{S}^{m+1}\Phi^{m+1} + \frac{1}{\varepsilon}\mathcal{F}(\Phi^{m+1}). \tag{4.25}$$

We use the Schur Complement method to create an expression involving Φ^{m+1} as the only unknown which is then solved for using a Newton method. The scheme has been implemented in MATLAB and tested by way of EOC tables which can be seen in Table 4.4 in Section 4.3.4.

For the $2D$ simulations we will use the following semi-implicit scheme

$$\mathcal{M}^{m+1}\Phi^{m+1} + \delta t \mathcal{S}_M^{m+1} W^{m+1} + \mathcal{A}^{m+1}\Phi^{m+1} = \mathcal{M}^m \Phi^m \tag{4.26}$$

$$\mathcal{M}^{m+1} W^{m+1} - \varepsilon \mathcal{S}^{m+1}\Phi^{m+1} - \frac{1}{\varepsilon} I_{\mathcal{F}}(\Phi^m)\Phi^{m+1} = \frac{1}{\varepsilon} E_{\mathcal{F}}(\Phi^m). \tag{4.27}$$

with $I_{\mathcal{F}}(\Phi^m)$ a diagonal matrix for the implicit part of the non-linear load vector and $E_{\mathcal{F}}$ a vector for the explicit part so that

$$I_{\mathcal{F}}(\Phi^m)_{ii} = \int_{\Gamma_h(t)} f'(\Phi^m)\eta_i \tag{4.28}$$

$$E_{\mathcal{F}}(\Phi^m) = \int_{\Gamma_h(t)} \left(f(\Phi^m) - \Phi^m f'(\Phi^m)\right)\eta_i \tag{4.29}$$

This system is written as a block matrix form and then solved using a conjugate gradient method. The method has been implemented with two separate software packages. The first is the Distributed and Unified Numerics Environment (DUNE Blatt and Bastian [2007]; Bastian et al. [2008a,b]; Dedner et al. [2010] the second is the Adaptive Multidimensional Simulations package (AMDiS) Vey and Voigt [2007], which has been used for the example in Section 4.4.3.

The one dimensional problems were solved with MATLAB, however when working in higher dimensions there is a need for greater efficiency and functionality, motivating the use of DUNE. A technical difficulty with the initial surface grid used together with the bisection refinement implemented in DUNE motivated the use of AMDiS.

4.3.4 Convergence Tests

We would like to test the implementation of the chosen numerical schemes, which we do by showing the theoretical orders of convergence. In line with Elliott and Venkataraman [2015] and Elliott and Ranner [2013] we expect order $\delta t + h^2$ for

the $L^{\infty}_{L^2}$ norm and $\delta t + h$ for the $L^2_{H^1}$ norm as the orders of convergence to the true solution. Since exact solutions for the ESCH equation cannot be written down analytically for a closed surface we include an additional forcing term in our test problem.

For the implicit scheme (4.26), we used the domain $\mathcal{G}_T = [0,1] \times [0,1]$ with surface velocity

$$v(x) = \sin(\pi x). \tag{4.30}$$

Starting from the *known* solution

$$\phi(x,t) = e^t \cos(2\pi x) + t \tag{4.31}$$

we solved the problem

$$\phi_t + (\phi v)_x - w_{xx} = g \tag{4.32}$$

$$w = -\varepsilon \phi_{xx} + \frac{1}{\varepsilon} f(\phi) \tag{4.33}$$

subject to the boundary conditions '$phi_x = w_x = 0$. The forcing term g was found by substituting the known solution into the differential operator. With $F(u)$ the standard quartic potential with minima at ± 1, g takes the form:

$$\begin{aligned} \varepsilon e^{-t} g(x,t) = &\left(\pi^2 \left(12t^2 + 3e^{2t} - 4\right) + 16\pi^4 \varepsilon^2 + \varepsilon\right) \cos(2\pi x) \\ &- \frac{1}{2}\pi \left(e^t - 2t\right) \varepsilon \cos(\pi x) + \frac{3}{2}\pi e^t \varepsilon \cos(3\pi x) + 24\pi^2 e^{2t} t \cos(4\pi x) \\ &+ 9\pi^2 e^{3t} \cos(6\pi x) + \varepsilon \end{aligned}$$

The solution is ε independent so we choose for our tests $\varepsilon = 0.1$.

To calculate the error in our approximation we have used a 3-point Gaussian quadrature rule on each element and approximated the error at each time step so that our $L^{\infty}_{L^2}$ error can be calculated from the formula

$$\|\phi_h - \phi\|^{\prime 2}_{L^2(\mathcal{G}_T)} = \max_{m \in \{1,\ldots,M\}} \sum_{E \in \mathcal{T}_h} \sum_{q=1}^{3} |E| \omega_g(q) |\phi_h(q, m\delta t) - \phi(q, m\delta t)|^2 \tag{4.34}$$

where q are the Gaussian quadrature points and $\omega_g(q)$ the corresponding quadrature weights. The error in $L^2_{H^1}$ norm is approximated using the H^1 semi-norm for the

$i = N_h$	$L^\infty(L^2)$	E.O.C.	$L^2(H^1)$	E.O.C
11	0.13489	-	1.73069	-
21	0.03027	2.31079	0.72473	1.34616
45	0.00641	2.03593	0.32363	1.05779
73	0.00242	2.00883	0.19812	1.01432
162	0.00049	2.00256	0.08898	1.00416
321	0.00012	2.00056	0.04487	1.00091

Figure 4.4: Error table for the solution of the forced ESCH equation using the implicit scheme (4.26), described around (4.32) analysing the spatial convergence rate. $h = \frac{1}{i}$, $\delta t = h^2$

spatial integral and we thus use

$$|\phi_h - \phi|^2_{H^1} = \frac{1}{T} \sum_{m=1,\dots,M} \sum_{E \in \mathcal{T}_h} \sum_{q=1}^{3} |E| \omega_g(q) |\partial_x \phi_h(q, m\delta t) - \partial_x(q, m\delta t)|^2. \tag{4.35}$$

Observe that since the problem is posed on $\Gamma(t) = [0, 1]$, ∂_x is the appropriate gradient for both functions.

In Table 4.4 we display the errors between the approximation and the exact solution as well as showing the experimental orders of convergence in the $L^\infty_{L^2}$ norm as well as the $L^2_{H^1}$ semi-norm. The experimental orders of convergence (eoc) are calculated from the formula

$$(eoc)_i = \frac{\log(E_i/E_{i-1})}{\log(h_i/h_{i-1})} \tag{4.36}$$

where E_i is the error associated with mesh size $h_i = \frac{1}{i}$. In order to see the individual orders of convergence in our spatial convergence test we have set $\delta t = h^2$. We can see from Figure 4.4 that we are obtaining the correct convergence orders of 2 and 1 respectively.

Similarly to be able to see the temporal orders of convergence we set $h = 1/321$ and vary the time step as $\delta t_i = 1/i$, so that the h error should be dominated by the error due to the temporal discretisation. We display these results in Table 4.5 and see that we obtain the order 1 convergence in the $L^\infty_{L^2}$ norm.

For testing the semi-implicit scheme (4.28) we use the surface $\mathcal{G}_T = \mathbb{S}^2 \times [0, 1]$ with the surface velocity

$$\boldsymbol{v}(x, y, z) = \left(xz, yz, z^2 - 1\right)^T. \tag{4.37}$$

which is a purely tangential motion allowing us to express $\boldsymbol{v} \cdot \nabla \tilde{\phi} = \boldsymbol{v} \cdot \nabla_{\Gamma(t)} \phi$. We

i	$L^\infty(L^2)$	E.O.C
10	0.13446	-
39	0.03412	1.00769
159	0.00832	1.00374
620	0.00211	1.00702
1289	0.00101	1.01322

Figure 4.5: Error table for the solution of the forced ESCH equation using the implicit scheme (4.26), described around (4.32) analysing the temporal convergence rate. $h = \frac{1}{321}$, $\delta t = \frac{1}{i}$

again start from a *known* solution, similar in idea to that used in the 1D setting however this time we use a steady state solution.

$$\phi(x, y, z) = z. \tag{4.38}$$

Observe that in spherical co-ordinates $\phi(X(\theta, \varphi)) = \cos(\theta)$ (note $\varphi is the polar angle co-ordinate$). We solve the problem

$$\partial_t^\bullet \phi + \nabla_{\Gamma(t)} \cdot (\phi \boldsymbol{v}) - \Delta_{\Gamma(t)} w = g \tag{4.39}$$

$$w = -\varepsilon \Delta_{\Gamma(t)} \phi + \frac{1}{\varepsilon} f(\phi) \tag{4.40}$$

where g is again found by substituting the known solution into the differential operator. With $F(\phi)$ the quartic potential with minima at ± 1, (3.5), g takes form

$$g(x, y, z) = 3z^2 - 1 + 4\varepsilon z - \frac{6z(1 - z^2) - 6z^3 + 2z}{\varepsilon}.$$

The mesh for this test is generated using an inscribed cube to the unit sphere which is then refined uniformly the appropriate number of times using the projection method discussed.

In Table 4.6 we display the errors between the approximation and the exact solution as well as showing the experimental orders of convergence in the $L^\infty_{L^2}$ norm as well as the $L^2_{H^1}$ semi-norm. These quantities were calculated using the in built expressions functionality of AMDiS. We can see that we do indeed obtain the correct orders of convergence as predicted by the theory.

4.3.5 Adaptive Refinements

As can be seen in the examples in Figure 4.9, solutions of the ESCH equation do indeed exhibit large domains where the gradient of the solution is relatively small.

h	$L^\infty(L^2)$	E.O.C.	$L^2(H^1)$	E.O.C
0.20853	0.04451	2.05665	0.08604	1.47755
0.10471	0.01101	2.01435	0.03752	1.19719
0.05241	0.00274	2.00439	0.01798	1.06110
0.02621	0.00068	2.00048	0.00889	1.01505

Figure 4.6: Error table for the solution of the forced ESCH equation described around (4.39).

This lends itself very well to an adaptive mesh refinement strategy, working on a coarse grid in the outer region and a more refined grid in the inner region so that we can drastically reduce the number of nodes for very little loss of accuracy. We discuss here how we have implemented an adaptive mesh strategy. Note a time adaptive strategy could also have been used as in Ratz [2016], however we used a uniform time step throughout.

The general strategy for adaptivity with parabolic problems can be summarised as

$$\textbf{SOLVE} \Rightarrow \textbf{ESTIMATE} \Rightarrow \textbf{MARK} \Rightarrow \textbf{REFINE}$$

Our strategy is a little more ad-hoc since the most sensible indicator function, for identifying elements for refinement, is the phase value or its gradient. Traditionally an estimator is used to test how well the approximate solution solves the problem on each element and the elements with the largest errors are refined. Our strategy uses the phase value instead and so we do not require an 'estimation' stage.

Using an initially uniform grid that is relatively coarse we identify the inner region as points for which the phase value lies in the interval $(-1+\delta\varepsilon, 1-\delta\varepsilon)$ and mark such elements for potential refinement. The quantity δ is a strict constant. If the phase value lies outside this interval then these elements are marked for potential coarsening. We say potential refinement and coarsening as elements may already be at the maximal/minimal level of refinement that we define at run time. An increase in level of refinement corresponds to a bisection of elements.

The process of adaptive mesh refinement has been considered for Poisson type problems on surfaces in Demlow and Dziuk [2007] and for parabolic problems in Kenneth and Claes [1991]. The difficulty for including adaptivity with evolving surfaces is in the choice of whether or not to refine and then evolve the mesh in time, or vice versa, evolving the grid to the next time step and then performing the refinement. In Figure 4.7 we graphically display the potential difference in the two strategies. As can be seen in 4.7c, if we evolve the mesh in time first and then refine

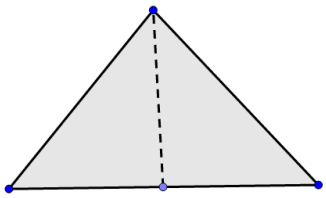

(a) Static Refinement

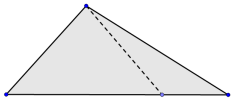

(b) Refine First

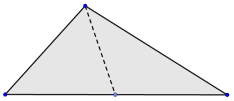

(c) Evolve First

Figure 4.7: Graphical display of the potential difference when refining before or after evolving the mesh. In 4.7a, we display the bisection method without an evolution. In 4.7b the element is refined by bisecting the longest edge and then evolved in time. In 4.7c the element is evolved in time and then refined by bisection.

we can maintain some control on the regularity of the mesh as the bisection still occurs at the midpoint of the longest length. We instead implement the alternative. We refine elements first, then evolve them, so that although we may lose some regularity on the mesh, the refinements should better follow the interface. We did not implement the post update refinement method and so cannot comment on any difference in any errors.

When using the adaptive method we wished to ensure that the chosen level for the outer region was sufficiently coarse so as to increase performance but sufficiently fine so that we were obtaining accurate results. The following tests for the moving sphere example in Section 4.4.3 were used to ensure this was the case. In Figure 4.8 we see the difference in the energy output for different levels in the outer region. In the inner region we used a level that ensured a minimum of 10 grid points across the interface. For a uniform grid (level 7 in Figure 4.8) there are approximately 1.1×10^5 degrees of freedom, compared with 3.0×10^4 for the coarsest outer grid (level 2). Thus for a reduction in degrees of freedom by a factor of 3 we maintain accuracy to well within 5×10^{-3}.

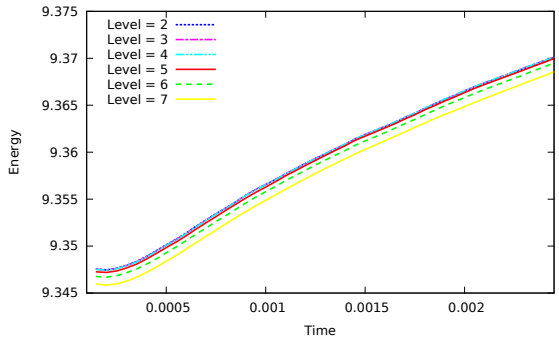

Figure 4.8: Comparison of energy profiles in Moving Sphere example presented in Section 4.4.3 for differing levels of refinement in the outer region. $\varepsilon = 0.025$, $\bar{v} = 10$, $\bar{M} = 5$.

4.4 Numerical Experiments

With regards to the 1D simulations, we have produced results on a bounded interval with Neumann type boundary conditions, that is $\phi_x = w_x = 0$, which contradicts the setting of the analysis where we assumed a closed surface in Chapter 3. However, we can double the (time dependent) interval and reflect the solution to make it symmetric with respect to the centre. The thus obtained setting can be further extended periodically to the whole real line so that we may think of a solution on an object which topologically is a circle.

We only carried out computations with the quartic potential (3.5) and the constant mobility (3.7). For the Cahn-Hilliard equation on the real line there exists an equilibrium profile given by

$$\frac{\phi_b + \phi_a}{2} + \frac{\phi_b - \phi_a}{2} \tanh\Big(\frac{\phi_b - \phi_a}{2\sqrt{2}} \frac{y}{\varepsilon}\Big), \qquad y \in \mathbb{R}. \tag{4.41}$$

We use this profile to specify initial conditions $\phi_{IC}(x) = \phi(x, 0)$, $x \in \Gamma(0)$, unless stated otherwise.

4.4.1 Stretching and Compression

We first pick $\phi_a = -1$ and $\phi_b = 1$ and consider a phase transition at the centre of an interval. Then the interval is homogeneously stretched or compressed for a while, i.e., $\nabla_{\Gamma(t)} \cdot \boldsymbol{v}(t)$ is constant in space. For the solution to (3.9), (3.10) one will expect that the interface position moves in the direction of the deformation and, in the long term, ends up in the centre of the deformed interval.

For our diffuse interface simulation we deform the domain as specified in

Parameter	Data for Figure 4.9	Data for Figure 4.10	Data for Figure 4.11
ϕ_a, ϕ_b; $\bar{M}$; T	-1, 1; 1; 10	-1, 1; 1; 10	0.2, 0.8; 1; 2
$\Gamma(t)$	$\begin{cases} (0, 1+t) & t \leq 2 \\ (0, 3) & t > 2 \end{cases}$	$\begin{cases} (0, 3-t) & t \leq 2 \\ (0, 1) & t > 2 \end{cases}$	$(0, 1+t)$
$v(x,t)$, $x \in \Gamma(t)$	$\begin{cases} \frac{x}{(t+1)} & t \leq 2 \\ 0 & t > 2 \end{cases}$	$\begin{cases} -\frac{x}{(t+1)} & t \leq 2 \\ 0 & t > 2 \end{cases}$	$\frac{x}{(t+1)}$
$\phi_{IC}(x)$	$0.9\tanh(10x - 5)$	$0.9\tanh(10x - 15)$	$0.3\tanh(\frac{x-0.5}{\varepsilon}) + 0.5$

Table 4.1: Simulation data for Section 4.4.1.

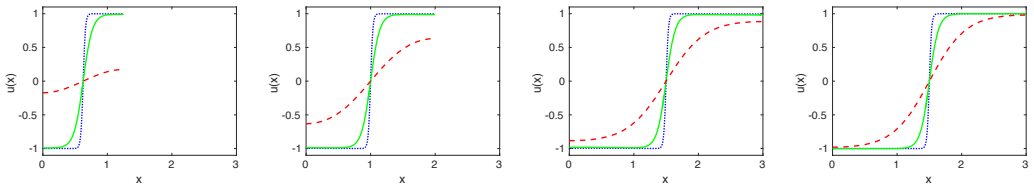

(a) $t = 0.25$ (b) $t = 1.0$ (c) $t = 2.0$ (d) $t = 10.0$

Figure 4.9: Stretching domain example as described in Section 4.4.1. Phase field for $\varepsilon = 0.4$ (red), $\varepsilon = 0.1$ (green), and $\varepsilon = 0.025$ (blue). Simulation data are in Table 4.1 on the left.

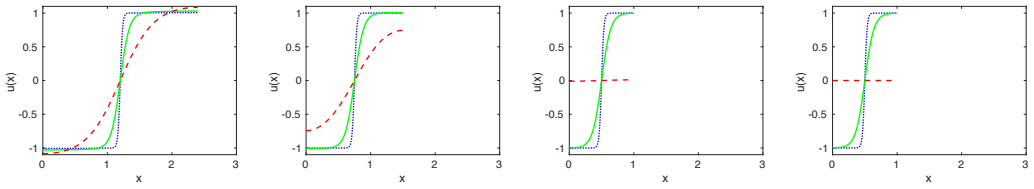

(a) $t = 0.25$ (b) $t = 1.0$ (c) $t = 2.0$ (d) $t = 10.0$

Figure 4.10: Compressing domain example as described in Section 4.4.1. Phase field for $\varepsilon = 0.4$ (red), $\varepsilon = 0.1$ (green), and $\varepsilon = 0.025$ (blue). Simulation data are in Table 4.1 in the middle.

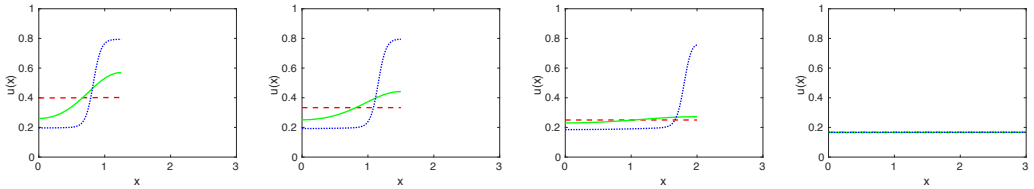

(a) $t = 0.25$ (b) $t = 0.5$ (c) $t = 1.0$ (d) $t = 2.0$

Figure 4.11: Stretching domain example with positive minima of F as described in Section 4.4.1. Phase field for $\varepsilon = 0.4$ (red), $\varepsilon = 0.1$ (green), and $\varepsilon = 0.025$ (blue). Simulation data are in Table 4.1 on the right.

Table 4.1 on the left and in the middle, respectively. At time $t = 2$ the interval has reached the final length and we then further relax the profile of ϕ on the then stationary domain.

In a first set of simulations we started with equilibrium tanh profiles defined in (4.41) and shifted them such that they were symmetric with respect to the centre of the interval. In the short term, the advection leads to stretched or compressed profiles, respectively, but the effect becomes smaller the smaller ε is. In the long term, the profiles relax back to equilibrium profiles at the expected position which they do the faster the smaller ε is.

In an attempt to investigate the robustness of the convergence behaviour we picked the profiles specified in Table 4.1 which are independent of ε for a second set of simulations. The results for different values of ε are displayed in Figure 4.9 and Figure 4.10, respectively, and indeed display the same long-term behaviour with one exception: for the largest $\varepsilon = 0.4$ in the compression case the advection effect (due to the surface evolution) is so strong that we observe mixing of the phases, i.e., $\phi = 0$, in the long term. We remark that as only the largest ε is affected this is a *finite* ε effect which does not contradict the asymptotic result.

We also examined the stretching example for a potential with minima at $\phi_a = 0.2$ and $\phi_b = 0.8$, see Table 4.1 on the right for the data and Figure 4.11 for the simulation results. In this case the expansion makes the phase transitions vanish and leads to flat profiles which takes the longer the smaller ε is. Note that at time $t = 2.0$ the (nearly) constant profiles of ϕ take value around 0.166, which is slightly lower than the minimum $\phi_a = 0.2$ of the double-well potential. It thus does not satisfy the setting for the asymptotic analysis as specified at the beginning of Section 3.2.1. Indeed, for the related sharp interface model the initial mass is

$$\mathcal{M}(0) = \int_{\Gamma^+(t=0)} \phi_b + \int_{\Gamma^-(t=0)} \phi_a = \int_0^{0.5} \phi_b + \int_{0.5}^1 \phi_a = 0.5.$$

If there was a solution to the sharp interface model which involves a phase transition its mass would satisfy

$$\mathcal{M}(2) = \int_{\Gamma^+(t=2)} \phi_b + \int_{\Gamma^-(t=2)} \phi_a \geq \int_0^3 \phi_a = 0.6 > \mathcal{M}(0),$$

which contradicts the mass conservation discussed around (3.29).

4.4.2 Bulk Effects

In the following examples we report on other effects due to velocity fields which do not have constant divergences and show some interesting behaviour.

First, recall that constant functions, different from ϕ_a and ϕ_b, are unstable stationary solutions to the Cahn-Hilliard equation which also holds true for the ESCH equation with $\boldsymbol{v} = 0$. In our first example we start from a constant initial condition, $\phi_{IC} = \frac{\phi_a+\phi_b}{2}$, with $\phi_a > 0$. We pick $\boldsymbol{v} \geq 0$ as specified in the left column of Table 4.2. Since mass is conserved, the advective effect of the velocity is expected to increase the mass where the domain is compressed and reduce the mass where the domain is stretched and, thus, is expected to induce a phase separation by perturbing the system away from the unstable constant solution. Note that the boundary points of the domain $[0, 1]$ do not move but internal movements take place, more precisely, stretching in $(0, 0.5)$ and compressing in $(0.5, 1)$.

In Figure 4.12 we see how the flat initial profile is perturbed by the advective effect of the velocity field such that a phase transition is obtained. Also note that when comparing with Figure 4.11 the gradient in the interface region appears to be less, however this is only appears to be the case due to the plotting of different length domains at the same physical size. The simulation data are given in Table 4.2 on the left. We remark that, in some cases, the velocity field from this example, has no destabilising effect. For instance, if $\phi_b = -\phi_a$ and $\phi_{IC} = 0$ then the solution remains constant at $\phi = 0$ for all times. This happens since the advective driving force of $\nabla_{\Gamma(t)} \cdot \boldsymbol{v}$ is scaled by the phase field value, thus $\phi = 0$ as a constant solution is still unstable however the mechanics by which a perturbation is introduced are negated.

In another example, initially, a phase interface is located at 0.25 within the initial domain $[0, 1]$. We then extend the interval but such that $\boldsymbol{v} = 0$ in $[0, 0.5]$ and $\boldsymbol{v}(x, t) \neq 0$ only if $x > 0.5$, see Table 4.2 on the right for the details.

Regarding the sharp interface model, (3.9) implies that w is no longer harmonic. Hence, the jump term $[M\nabla_\Gamma w] \cdot \boldsymbol{\mu}_\Lambda$ in (3.10) changes and is expected to be non-zero. We thus expect a motion of the phase interface, Λ, in the direction of the stretching despite the surface velocity, $\boldsymbol{v}$, being zero in the region containing the interface.

In Figure 4.13 we can see that there is indeed a motion induced by the non-trivial bulk problem. In addition, once the phase interface gets beyond the point 0.5, its velocity can be seen to increase. This is in accordance with the last equation in (3.10) as $\boldsymbol{v} \geq 0$ there.

Parameter	Data for Figures 4.12	Data for Figure 4.13
ϕ_a, ϕ_b; $\bar{M}$; T	0.2, 0.8; 1; 0.2	-1, 1; 1; 2
$\Gamma(t)$	$[0, 1]$	$[0, \cot^{-1}(1.83 - t) + 0.5]$
$v(x,t)$, $x \in \Gamma(t)$	$\sin(\pi x)$	$\begin{cases} \sin^2(x - \frac{1}{2}) & x \geq \frac{1}{2} \\ 0 & x < \frac{1}{2} \end{cases}$
$\phi_{IC}(x)$	0.5	$\tanh(\frac{x-0.25}{\varepsilon})$

Table 4.2: Simulation data for Section 4.4.2.

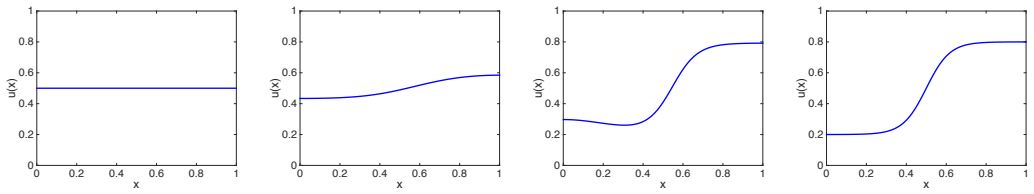

(a) $t = 0.0$ (b) $t = 0.03$ (c) $t = 0.075$ (d) $t = 0.15$

Figure 4.12: Generation of a phase interface by perturbing a flat initial profile as described in Section 4.4.2. $\varepsilon = 0.025$, other simulation data are in Table 4.2 on the left.

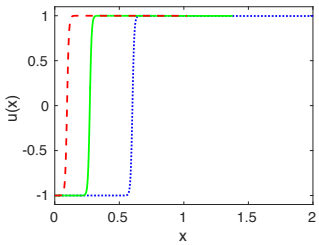

Figure 4.13: Phase interface motion induced by bulk effects away from the interface as described in Section 4.4.2. $\varepsilon = 0.01$, $t = 0.1$ (red), $t = 1.0$ (green), $t = 1.8$ (blue). Simulation data are in Table 4.2.

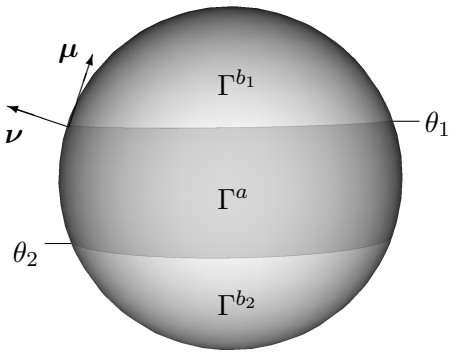

Figure 4.14: Setup for the example in Section 4.4.3.

4.4.3 A Solution on a Sphere with Tangential Mass Transport

Considering 2D hypersurfaces in 3D allows us to demonstrate the geometric behaviours of solutions to the ESCH equation and to discuss effects due to the geodesic curvature which appears in (3.10).

In this example we consider a sphere with a tangential velocity field $\boldsymbol{v}$ so that the shape doesn't change. As in Ratz [2016] we look for solutions to (3.9), (3.10) which are rotationally symmetric and, thus, are constant in the azimuthal angle $\phi \in (0, 2\pi)$ and only depend on the polar angle $\theta \in (0, \pi)$, i.e.,

$$w(x(\theta,\phi),t) = W(\theta,t) \quad \text{where } x(\theta,\phi) = (\sin\theta\cos\phi,\, \sin\theta\sin\phi,\, \cos\phi)^T . \tag{4.42}$$

The difference to Ratz [2016] is the presence of the velocity field $\boldsymbol{v}$. We pick a velocity field which transports mass from the north to the south pole, $\boldsymbol{v}(x(\theta,\phi),t) = \bar{v}\sin(\theta)x_\theta(\theta,\phi)$ with some $\bar{v} > 0$. One can easily show that $\nabla_\Gamma \cdot \boldsymbol{v} = 2\bar{v}\cos(\theta)$.

We then consider two distinct regions around the poles, where $\phi = \phi_b$, which are separated by a band where $\phi = \phi_a$, see Figure 4.14. We will refer to the inner region as $\Gamma^a(t)$ and and the two caps as $\Gamma^{b_{1,2}}(t)$. We denote by $\theta_{1,2}(t)$ the polar angle of the boundaries between $\Gamma^{b_{1,2}}(t)$ and $\Gamma^a(t)$, respectively.

With the ansatz (4.42) the Laplace-Beltrami operator applied to w becomes

$$\Delta_\Gamma w = \frac{1}{\sin\theta}\frac{\partial}{\partial\theta}\left(\sin\theta\frac{\partial W}{\partial\theta}\right).$$

The general solution $W^{(i)}(\theta,t)$ to (3.9) in $\Gamma^i(t)$, $i \in \{b_1, b_2, a\}$, then is

$$W^{(i)}(\theta,t) = c_1^{(i)}(t)\log\left[\tan\left(\frac{\theta}{2}\right)\right] - \frac{\phi_i \bar{v}}{\bar{M}}\cos(\theta) + c_2^{(i)}(t), \quad \theta \in \begin{cases} (0,\theta_1(t)), & i = b_1, \\ (\theta_1(t),\theta_2(t)), & i = a, \\ (\theta_2(t),\pi), & i = b_2, \end{cases} \tag{4.43}$$

with functions $c_k^{(i)}(t)$, $k = 1, 2$, which will be determined by the interface conditions.

Assuming a smooth solution in $\Gamma^{b_{1,2}}(t)$ the gradient has to be zero at the poles which implies that $c_1^{(b_1)}(t) = c_1^{(b_2)}(t) = 0$. We now use the second equation of (3.10) and that the geodesic curvature of the phase interface is equal to $(-1)^{k+1}\cot(\theta_k(t))$, $k = 1, 2$:

$$c_2^{(b_k)}(t) = (-1)^{k+1} S\cot(\theta_k(t)) + \frac{\bar{v}}{\bar{M}}\phi_b \cos(\theta_k(t)), \quad k = 1, 2.$$

We can use the same boundary condition on each boundary of $\Gamma^a(t)$ in order to determine $c_1^{(a)}(t)$ and $c_2^{(a)}(t)$. We only include $c_1^{(a)}(t)$ below as the formula for $c_2^{(a)}(t)$ is not needed to progress:

$$c_1^{(a)}(t) = \frac{S\left[\cot\left((\theta_1(t)\right) + \cot\left(\theta_2(t)\right)\right] + \frac{\bar{v}}{\bar{M}}\phi_a(\cos(\theta_1(t)) - \cos(\theta_2(t)))}{\log\left[\tan(\theta_1(t)/2)\right] - \log\left[\tan(\theta_2(t)/2)\right]}$$

Having expressed the solution (4.43) in terms of the $\theta_k(t)$ we can use the third equation of (3.10) in order to derive a system of ODEs for the $\theta_k(t)$, k=1,2 (note that $v_\Lambda(\theta_k(t)) \cdot \mu(\theta_k(t)) = (-1)^k \theta_k'(t)$):

$$\theta_1'(t) = \frac{\bar{M}\tilde{c}_1^{(a)}(\theta_1(t),\theta_2(t))}{(\phi_b - \phi_a)\sin(\theta_1(t))}, \quad \theta_2'(t) = \frac{\bar{M}\tilde{c}_1^{(a)}(\theta_1(t),\theta_2(t))}{(\phi_b - \phi_a)\sin(\theta_2(t))}.$$

where $\tilde{c}_1^{(a)}(\theta_1(t),\theta_2(t)) = c_1^{(a)}(t)$.

We choose the quartic potential $F(\phi) = \frac{1}{4}(\phi^2 - 1)^2$, i.e., $\phi_a = -1$, $\phi_b = 1$, for which $S = \frac{\sqrt{2}}{3}$ in (3.10) and for the initial condition of the sharp interface problem set $\theta_1(0) = 0.8$ and $\theta_2(0) = 2.1$ so that $\Gamma^{b_2}(0)$ is slightly bigger than $\Gamma^{b_1}(0)$.

For the initial condition of the Cahn-Hilliard equation we use

$$\phi_{IC}(\theta) = \begin{cases} \tanh\left(\frac{0.8-\theta}{\varepsilon\sqrt{2}}\right), & \theta < 1.45, \\ \tanh\left(\frac{\theta-2.1}{\varepsilon\sqrt{2}}\right), & \theta \geq 1.45. \end{cases}$$

In the case $\bar{v} = 0$, i.e., without any mass transport, we expect the solution to coarsen to a two region solution with the area around the southern pole, $\theta = \pi$,

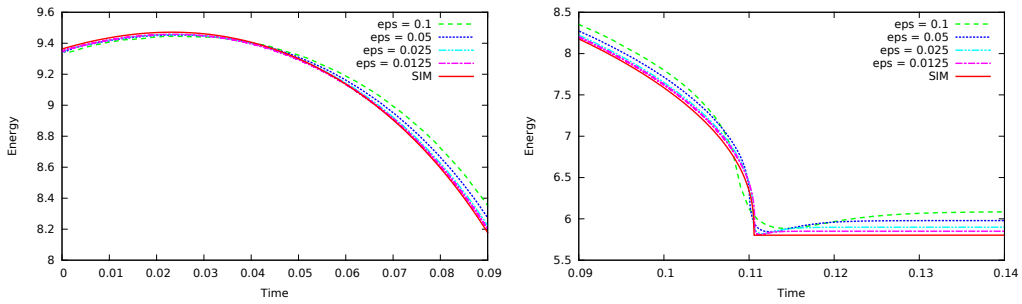

Figure 4.15: Energy plots for the example in Section 4.4.3 with $\bar{v} = 10$, $\bar{M} = 5$. We compare the Ginzburg-Landau energy, (3.3), with the sharp interface energy, (4.44).

taking the phase value ϕ_b. This is indeed what we observe, see Figure 4.16. In turn, if the mass transport towards the south pole with a tangential velocity field is strong enough we expect that again a two region solution emerges but with the domain of the phase $\{\phi = \phi_b\}$ around the northern pole, $\theta = 0$. For $\bar{v} = 10$, Figure 4.17 displays that solutions indeed exhibit this behaviour.

We want to compare our solution to the sharp interface model with solutions of the Cahn-Hilliard equation by considering the energy of the system. The Ginzburg-Landau energy (3.3) is the energy for the diffuse interface model and, as shown in Le [2008], converges to the energy of the sharp interface model which is proportional to the length of the phase interface:

$$\mathcal{E}_\varepsilon \to 2S \text{ length}(\Lambda) =: \mathcal{E}_0$$

which here amounts to

$$\mathcal{E}_0(t) = \frac{4\sqrt{2}\pi}{3} \left[\sin(\theta_1(t)) + \sin(\theta_2(t))\right]. \tag{4.44}$$

In Figure 4.15 we display the evolution of the energies (3.3) for several values of ε as well as the limiting energy (4.44). Around the time 0.11 the solution to the sharp interface model becomes singular as then $\theta_2(t) \to \pi$. The asymptotic analysis is not valid around such events but we see that even then the approximation gets more accurate as $\varepsilon \to 0$.

4.4.4 Scaling Effects

In our analysis we saw that different scalings of $\bar{M}$ lead to different limiting free boundary problems, namely (3.9), (3.10) for $\bar{M} \sim \varepsilon^0$ and (3.42), (3.43) for $\bar{M} \sim \varepsilon^{-1}$. In this example we present a pair of simulations to demonstrate the differing

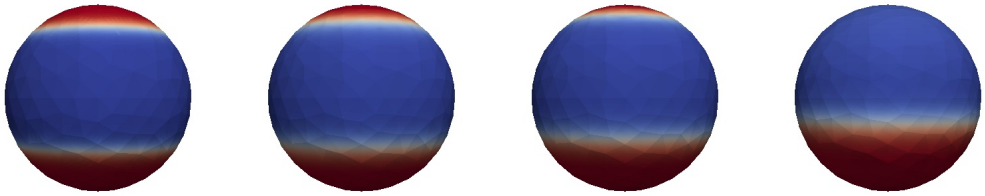

(a) $t = 0$ (b) $t = 0.05$, (c) $t = 0.1$ (d) $t = 0.15$

Figure 4.16: Coarsening example on the sphere as described in Section 4.4.3, $\varepsilon = 0.1$, $\bar{v} = 0$, $\bar{M} = 5$.

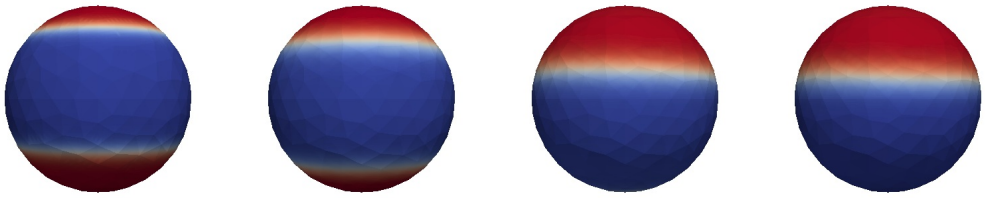

(a) $t = 0$ (b) $t = 0.05$ (c) $t = 0.1$ (d) $t = 0.15$

Figure 4.17: Example with tangential mass transport on the sphere as described in Section 4.4.3, $\varepsilon = 0.1$, $\bar{v} = 10$, $\bar{M} = 5$.

Parameter	Data for Figure 4.18		Data for Figure 4.20
ϕ_a, ϕ_b; $\bar{M}; T$	-1, 1; 5 or 50; 0.2		-1, 1; 10; 0.5
$\phi_{IC}(x)$	$\tanh\left(\frac{1-\arccos(x)}{\varepsilon\sqrt{2}}\right)$	$\arccos(x) < 1.55$	$\tanh\left(\frac{0.7-x_1}{\varepsilon\sqrt{2}}\right)$
	$\tanh\left(\frac{\arccos(x)-2.1}{\varepsilon\sqrt{2}}\right)$	$\arccos(x) \geq 1.55$	

Table 4.3: Simulation data for Sections 4.4.4 and 4.4.5.

behaviour of solutions to the ESCH equation in dependence of the scaling of $\bar{M}$ in ε.

We begin with the unit sphere with two regions of phase ϕ_b at opposite sides of the sphere separated by a band of phase ϕ_a, as displayed in Figure 4.18a. As with the previous example, the two regions are of different size so that we can expect to see the coarsening of the phase ϕ_b if the surface velocity is zero (rotating Figure 4.16 through 90 degrees would produce this solution). We choose a surface velocity to deform the sphere so as to introduce obstacles by increasing the radius of (y, z)-circles. More specifically, the surface $\mathcal{G}_T$ is given as the image of $Q : \boldsymbol{S}^2 \times [0, 0.2] \to \boldsymbol{R}^3$ by

$$Q(x, y, z, t) = (1 - \tilde{t})(x, y, z) + \tilde{t}(x, \rho(x)y, \rho(x)z), \quad \tilde{t} = \min(0.05, t)$$

where $\rho(x) = 1 - \frac{1}{2}\cos^2(2\pi x)$. For a fixed interfacial thickness parameter $\varepsilon = 0.1$ we use two different values for the mobility, namely $\bar{M} = 5$ and, dividing by ε, $\bar{M} = 50$. The other parameters are in Table 4.3 on the left.

Based on the observations in the previous example, the slightly larger domain of phase ϕ_b is expected to attempt to grow at the expense of the smaller domain until the latter vanishes. This phenomenon is driven by the different values of the geodesic curvature of the phase interfaces. By altering the radii of (y, z)-circles over time as given above the curvature of the underlying surface is varied. If a phase interface moves into the affected area, then its geodesic curvature is changed in such a way that further movement towards the equator is damped. In the case $\bar{M} = 5$ we observe (see Figure 4.18b) that coarsening indeed is prevented and two domains of phase b persist. In turn, by scaling the mobility with $\frac{1}{\varepsilon}$ we increase the Cahn-Hilliard dynamics and, thus, the velocity of the phase interface. Indeed, $\bar{M} = 50$ is big enough such that the system can coarsen before the deformation can impact on the dynamics (see Figure 4.18c).

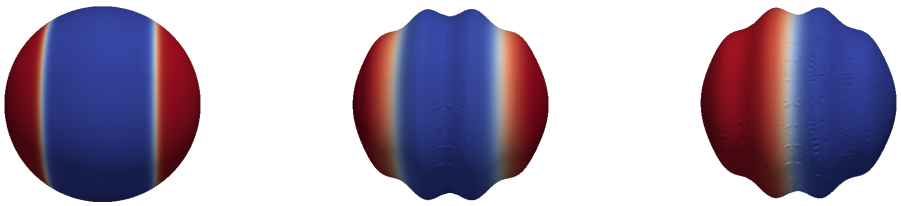

(a) $t = 0$ (b) $t = 0.2$, $\bar{M} = 5$ (c) $t = 0.2$, $\bar{M} = 50$

Figure 4.18: Initial configuration (left) and different states (middle, right) achieved by varying the mobility, $\varepsilon = 0.1$. See Section 4.4.4 for other parameters and details.

4.4.5 Topological Changes

Topological changes can be particularly difficult to simulate for free boundary problems. In this example we display a topological change of the interface induced by the motion of the surface that would not happen in a stationary setting. Although our asymptotic analysis from Chapter 3 precludes topological changes, we include this example to show that the presence of a surface velocity does indeed remove the gradient flow structure from the ESCH equation.

The surface is a torus which we denote by $\mathbb{T}(R, r)$ where R is the major radius and r is the minor radius. We deform the torus by making R and r time dependent functions, specifically, $R(t) = \sqrt{2} + 1.2\sin(2\pi t)$ and $r(t) = 1 - 0.65\sin(2\pi t)$, thus increasing the overall surface area in the interval $0 < t < 0.25$, decreasing the surface area in the interval $0.25 < t < 0.5$, and obtaining the same surface at final time $T = 0.5$ as at $t = 0$.

We consider an initial phase distribution which contains a single connected interface using the profile function as described in Table 4.3 on the right. Note that this function is only dependent on the spatial co-ordinate x_1, rather than any tangential co-ordinate. This creates a relatively large initial energy, however the interfacial layers quickly relax to energetically more favourable profiles. Thus when reporting the energy of the system we start shortly after initialisation.

On the stationary torus $\mathbb{T}(R(0), r(0))$ the described phase interface would evolve only so as to reduce its length but without any topological change as seen in Figure 4.21 (note that the level of relaxation required is minimal). However, by changing the ratio of the two radii, the phase interface can be driven to self intersect and even to induce a topological change. In Figure 4.20 we display the latter solution at 4 time steps for one specific value of $\varepsilon = 0.71$. We observe that the interfacial

layer self intersects and splits up into two independent interfacial layers through the hole of the torus. These remain stable when the surface relaxes back to its original shape and the solution as seen in Figure 4.20d, persists for all times.

In Figure 4.19 we also include a plot showing the energy evolution of solutions for the two discussed cases. For the stationary surface we see a small drop in the energy due to relaxation and then it remains constant. In contrast the energy in the evolving setting increases initially before the rapid transition through the topological change. Although two interfaces is energetically more favourable at the time of the topological change, we can see that when the surface returns to its original proportions the total energy has increased in comparison with that of the final resting energy in a stationary setting.

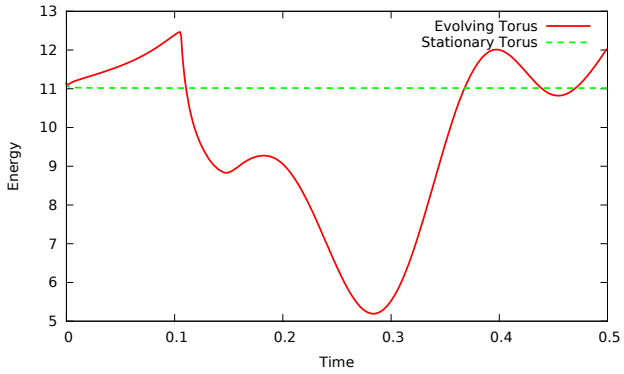

Figure 4.19: Comparison of energy profiles in case of stationary torus and moving torus as discussed in Section 4.4.5 and displayed in Figures 4.20 and 4.21.

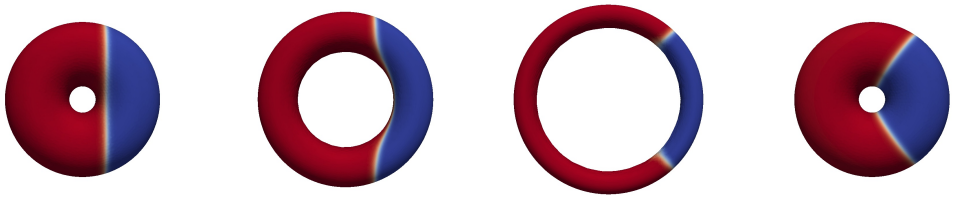

(a) $M = 10$, $t = 0.0$ (b) $M = 10$, $t = 0.1$ (c) $M = 10$, $t = 0.25$ (d) $M = 10$, $t = 0.5$

Figure 4.20: Topological change of the interface as discussed in Section 4.4.5. $\varepsilon = 0.71$ $\bar{M} = 10$.

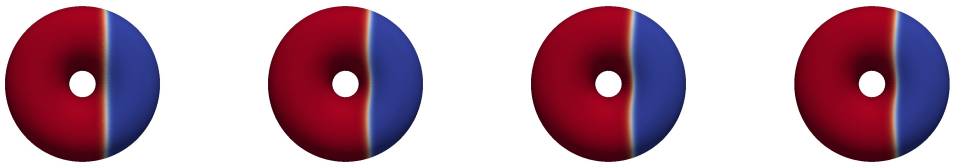

(a) $M = 10$, $t = 0.0$ (b) $M = 10$, $t = 0.1$ (c) $M = 10$, $t = 0.25$ (d) $M = 10$, $t = 0.5$

Figure 4.21: Relaxation of singular interface in case of stationary surface as discussed in Section 4.4.5. $\varepsilon = 0.71$ $\bar{M} = 10$.

Chapter 5

Application: Cell Adhesion

5.1 Overview

In this chapter we look at an application of phase field modelling, in particular we derive a model for focal cell adhesion that aims to extend a previously known model derived by Freund and Lin [2004]. We study the asymptotic limit of our newly derived model for the purpose of comparing with free boundary models in the literature. Note that the surface in this chapter is an unknown and the method of formally matched asymptotic expansions must be extended to account for this.

This chapter is laid out as follows, we first provide some background to the physically setting that we wish to model. We wish to use an energetic framework and use variations of proposed energy functionals. Thus, following the introduction to the problem we carefully consider the process by which we take variations and carry out the calculations required for our model. We then complete the model derivation before analysing it's sharp interface limit. We conclude the analysis with some short remarks on comparisons with known literature results. Finally we provide some simulations of a reduced version of our model produced using a scheme based on the work of Barrett et al. [2008].

Observe that although in Chapter 3 we predominantly studied the conservative form of the Cahn-Hilliard equation, (3.1)-(3.2), in this chapter we will be studying a phase field equation that is not conservative and thus will not have a term of the form $\phi \nabla_{\Gamma(t)} \cdot \boldsymbol{v}$. This is motivated by the type of free boundary problem that we would like to recover. For similar reasons we will also be studying a phase field equation corresponding to the fast scaling of the mobility.

5.2 Introduction

Adhesion of cells to other cellular organism or biological substrata such as collagen plays an important role in a number of processes, for example, embryo growth, cancer metastasis, tissue regeneration and inflammatory response Bao and Suresh [2003]; Wolgemuth [2005]. The standard view of cellular adhesion is as a competition between a reduction in free energy arising from changes in a bonding potential and an increase in free energy due to elastic deformation required for the membrane to conform to the extra-cellular surface. Early works Bell et al. [1978, 1984] have developed quantitative models for cell adhesion based on equilibrium thermodynamics, demonstrating this competitive nature of adhesion.

In many instances cell adhesion is based on a set of bridging molecules, or binders, confined to the cell membrane, but mobile within the cell wall, these binders can attach to specific ligands on the opposite surface. Experimental evidence has shown that when a surface consists of a large concentration of receptor ligands, complementary to the binders in the membrane, adhesion results from the formation of localised regions of tight adhesion. These patches are often called focal adhesion zones. Examples include spreading of blood platelets Park et al. [1990], vesicles Boulbitch et al. [2001]; Guttenberg et al. [2001], and different types of cells including fibroblasts, melanocytes, osteoblasts, lymphoblasts and red blood cells Dustin et al. [1996]; Smilenov et al. [1999]; Cuvelier et al. [2003]; Arnold et al. [2004] on substrates functionalised with receptors.

These focal patches arise due to a relatively low equilibrium density in comparison to the numbers required for adhesion. As a result of the low equilibrium density of binders, after nucleation, local recruitment is necessary for the growth of an adhesion patch.

The authors of Freund and Lin [2004] proposed a one-dimensional model of an infinite length membrane adhering to a flat substrate. They restricted to a single adhesion patch and derived a one sided free boundary problem describing the propagation of the adhesion patches front. It is our aim to generalize this work to an intrinsic model on the cell membrane, taking account of the higher dimension of the cell wall as well as allowing for diffusion in the adhered region, resulting in a two sided model. Our model is also representative of the post nucleation regime but is more robust in that it allows for multiple adhesion patches and is capable of modelling topological changes.

We represent the cell membrane by an n-dimensional evolving hypersurface, $\Gamma(t) \subset \mathbb{R}^{n+1}$. Associated with this hypersurface is the material velocity, $\boldsymbol{v} = \boldsymbol{v}_\tau +$

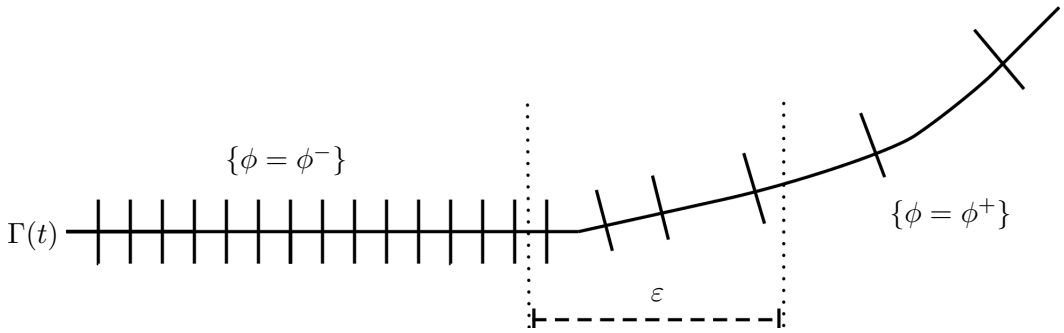

Figure 5.1: Qualitative sketch of a focal cell adhesion front with individual binders represented by the vertical bars.

$v_{\boldsymbol{\nu}}\boldsymbol{\nu}$, consisting of a tangential component $\boldsymbol{v}_\tau$ and a normal component $v_{\boldsymbol{\nu}}$, by which material points belonging to $\Gamma(t)$, are transported. We wish to employ the phase field methodology and will denote by ϕ the phase field variable that will be used to differentiate between adhered regions, approximated by $\{\phi = \phi^-\}$, and free regions, approximated by $\{\phi = \phi^+\}$, where $\phi^- < \phi^+$ are constants. These regions will be separated by thin layers proportional in width to the length scale ε. The phase field variable changes value smoothly but quickly within these layers. We denote by c the binder density in the cell membrane and postulate an energetic framework for the governing system.

For the phase field variable we postulate a standard gradient flow structure given by

$$\varepsilon\omega\partial_t^\bullet\phi = -\delta_\phi E(\Gamma, \phi, c), \tag{5.1}$$

where E is some free energy for the system which will be defined below and $\delta_\phi E$ is it's variation with respect to the phase field variable which we will carefully define in a later section. The constant ω is a scaling coefficient. For the binder density we postulate the following balance law which ensures conservation of the total binder density.

$$\partial_t^\bullet c + c\nabla_{\Gamma(t)} \cdot \boldsymbol{v} = \nabla_{\Gamma(t)} \cdot \left(M_c(\phi, c)\nabla_{\Gamma(t)}\delta_c E(\Gamma, \phi, c)\right). \tag{5.2}$$

The quantity $\delta_c E$ is the variation with respect c of the free energy. The phase and density dependent binder mobility is denoted by M_c and is assumed non-negative in general and strictly positive whenever $\phi \in (\phi^-, \phi^+)$.

We account for the visco-elastic properties of the membrane in a similar fashion to that in Rodrigues et al. [2015]; Rahimi et al. [2013] postulating a virtual work principle. We propose that the governing equations for the membrane evolution be the result of balancing applied forces. The motion of the membrane under the action of surface elastic forces and surface adhesion forces gives the virtual work

principle as:

$$\int_{\Gamma(t)} \boldsymbol{\sigma} : D_\Gamma \boldsymbol{w} = -\langle \delta_\Gamma E, \boldsymbol{w} \rangle \quad \forall \boldsymbol{w} \in V. \tag{5.3}$$

The tensor $\boldsymbol{\sigma}$ represents the tangential stresses and V is a set of admissible virtual velocities. The operator $D_\Gamma \boldsymbol{w} := \frac{1}{2}\boldsymbol{P}(\nabla_\Gamma \boldsymbol{w} + \nabla_\Gamma \boldsymbol{w}^T)\boldsymbol{P}$ is the surface analogue of the symmetric gradient, with $\boldsymbol{P}$ the projection operator to the tangent space, so that $D_\Gamma \boldsymbol{w}$ gives the surface virtual strain rate. The quantity $\delta_\Gamma E$ is the variation of the proposed free energy with respect to surface deformations. This is also carefully considered in a later section.

We have assumed in our virtual work principle that fluids adjacent to the membrane can be neglected. This is valid in the setting of a low Reynolds number so that the equations of slow viscous motion apply. The authors of Saffman and Delbrück [1975], considered how to define a translational mobility in an anisotropic setting where the viscosity of the embedding fluid is much lower than that of the viscosity of the fluid membrane.

When considering the tangential stresses, $\boldsymbol{\sigma}$, we postulate the same form as in Rodrigues et al. [2015], assuming the standard Boussinesq-Scriven model so that

$$\boldsymbol{\sigma} = -\pi \boldsymbol{P} + 2\mu(\phi) D_\Gamma \boldsymbol{v}. \tag{5.4}$$

The phase dependent coefficient of the membrane velocity term, $\mu(\phi)$, is the surface viscosity, and is allowed to differ in each phase but should be strictly positive. The surface pressure, π is the Lagrange multiplier resulting from an assumption of an inextensible membrane, expressed by the constraint

$$\nabla_{\Gamma(t)} \cdot \boldsymbol{v} = 0, \tag{5.5}$$

which can also be written as $\operatorname{tr} D_\Gamma(\boldsymbol{v}) = 0$.

As stated around Equation (5.1) we wish to utilise an energetic framework for our model. Our postulated surface energy is a combination of several different components and can be expressed as follows

$$E = E_{MC} + E_{GC} + E_{GL} + E_{AD} + E_B. \tag{5.6}$$

The term E_{GL} is a Ginzburg-Landau energy functional and is a phase field form of a line energy given by

$$E_{GL} = \sigma \int_{\Gamma(t)} \frac{\varepsilon}{2} |\nabla_\Gamma \phi|^2 + \frac{1}{\varepsilon}\theta(\phi) = \sigma \int_{\Gamma(t)} \delta(\phi, \nabla_\Gamma \phi). \tag{5.7}$$

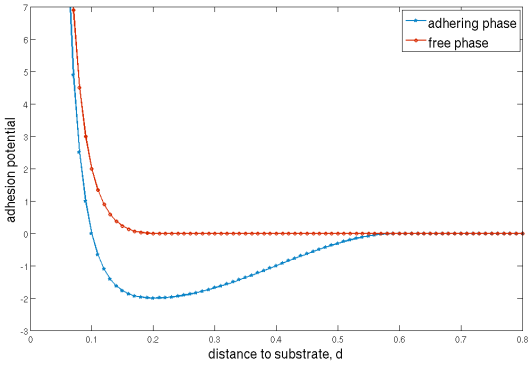

Figure 5.2: Qualitative forms of the adhesion potentials in each phase as used in (5.8) and simulations in Sections 5.6.2 and 5.6.3.

We choose a double well type potential with minima at $\phi = \phi^{\pm}$ such that $\theta(\phi) = \frac{1}{4k_\theta}(\phi^- - \phi)^2(\phi^+ - \phi)^2$. The constant k_θ is chosen so that certain coefficients scale to 1 in our asymptotic analysis. We postulate abstract potential functions for the adhesion energy, E_{AD}, and the binder energy, E_B such that

$$E_{AD} = \int_{\Gamma(t)} p(\phi, c, d_{\mathcal{S}}) \tag{5.8}$$

$$E_B = \int_{\Gamma(t)} f(\phi, c), \tag{5.9}$$

The adhesion potentials should depend on the distance, $d_{\mathcal{S}}$, between the membrane and the substrate. Qualitatively we expect them to take forms as seen in Figure 5.2 in each phase so that in the case of a free region the unspecified repulsive forces dominate and increase exponentially as $d_{\mathcal{S}} \to 0$ and decay to zero as $d_{\mathcal{S}} \to \infty$. Similar behaviour is expected in an adhered region with the exception that there exists a unique stable minimiser of the energy at some finite distance. We denote by $\boldsymbol{\nu}_{\mathcal{S}}$ the normal to the substrate.

Biomembrances are bilayers of lipid molecules and established models treat them as deformable inextensible fluid surfaces of infinitesimal thickness, unable to sustain shear stress, and governed by bending energy functionals with the membrane strain energy depending on the curvature of the surface. As an extension of the work of Freund and Lin [2004] we wish to account for membrane dynamics due to bending, rather than considering a static adhesion patch. A classical model for the elastic components of the bending energy is the Canham-Helfrich-Evans energy functional Canham [1970]; Evans [1974]; Helfrich [1973]. This consists of a mean curvature

component and a Gaussian curvature component:

$$E_{MC} + E_{GC} = \int_{\Gamma(t)} \frac{1}{2} b_k(\phi, c)|\kappa_m - \kappa_s(\phi, c)|^2 + \int_{\Gamma(t)} b_g(\phi, c)\kappa_g. \tag{5.10}$$

The mean curvature of the surface is denoted by κ_m and the Gaussian curvature by κ_g, κ_s represents a preferred curvature of the cell membrane which is called the spontaneous curvature. The quantities b_k and b_g are bending rigidities.

Writing our problem in a strong form gives the stress terms as $\nabla_{\Gamma(t)} \cdot \boldsymbol{\sigma}(t)$. This is related to the surface velocity by way of the differential operator known as the Boussinesq-Scriven operator, $\mathcal{S}_{\Gamma(t)}\boldsymbol{v}(t) = 2\nabla_{\Gamma(t)} \cdot D_{\Gamma(t)}\boldsymbol{v}(t)$, via the following relation.

$$\nabla_{\Gamma(t)} \cdot \boldsymbol{\sigma}(t) = -\mu(\phi)\mathcal{S}_{\Gamma(t)}\boldsymbol{v}(t) + \nabla_{\Gamma(t)}\pi + \pi\kappa_m\boldsymbol{\nu}. \tag{5.11}$$

Our strong problem, which we derive through the subsequent sections, thus reads as follows.

Problem 5.2.1. *Given an initial hypersurface $\Gamma(0) \subset \mathbb{R}^3$, and initial conditions for the binder density, $c(0) : \Gamma(0) \to \mathbb{R}$ and phase field variable, $\phi(0) : \Gamma(0) \to \mathbb{R}$, find $(\Gamma(t), \pi(t), \phi(t), c(t))$ such that at each time $t \in [0, T]$:*

$$\begin{aligned}
\boldsymbol{\nu} \cdot \left(\nabla_{\Gamma(t)} \cdot \boldsymbol{\sigma}(t)\right) &= \Delta_{\Gamma(t)} \left(b_k(\phi, c)(\kappa_m - \kappa_s(\phi, c))\right) + |\nabla_{\Gamma(t)}\boldsymbol{\nu}|^2 b_k(\phi, c)(\kappa_m - \kappa_s(\phi, c)) \\
&\quad + \nabla_{\Gamma(t)} \cdot \left((\kappa_m \mathbb{I} + \nabla_{\Gamma(t)}\boldsymbol{\nu})(b_{g,\phi}(\phi, c)\nabla_{\Gamma(t)}\phi + b_{g,c}(\phi, c)\nabla_{\Gamma(t)}c)\right) \\
&\quad + \sigma \left(\kappa_m \delta(\phi, \nabla_\Gamma \phi) + \boldsymbol{\nu}\nabla_\Gamma \cdot \left(\varepsilon \nabla_{\Gamma(t)}\phi \otimes \nabla_{\Gamma(t)}\phi\right)\right) + p_{,d_\mathcal{S}}\boldsymbol{\nu}_\mathcal{S} \cdot \boldsymbol{\nu}
\end{aligned} \tag{5.12}$$

$$\begin{aligned}
\boldsymbol{P}\nabla_{\Gamma(t)} \cdot \boldsymbol{\sigma}(t) &= b_k(\phi, c)(\kappa_m - \kappa_s(\phi, c))\nabla_{\Gamma(t)}\kappa_m + \kappa_g \nabla_{\Gamma(t)} b_g(\phi, c) \\
&\quad + \sigma \boldsymbol{P}\nabla_\Gamma \cdot \left(\varepsilon \nabla_{\Gamma(t)}\phi \otimes \nabla_{\Gamma(t)}\phi - \delta(\phi, \nabla_\Gamma \phi)\mathbb{I}\right) + p_{,d_\mathcal{S}}\boldsymbol{P}\boldsymbol{\nu}_\mathcal{S}
\end{aligned} \tag{5.13}$$

$$\boldsymbol{\sigma}(t) = -\pi \boldsymbol{P} + 2\mu(\phi) D_\Gamma \boldsymbol{v} \tag{5.14}$$

$$\nabla_{\Gamma(t)} \cdot \boldsymbol{v} = 0 \tag{5.15}$$

$$\begin{aligned}
-\varepsilon\omega\partial_t^\bullet \phi &= \frac{1}{2} b_{k,\phi}(\phi, c)|\kappa_m - \kappa_s(\phi, c)|^2 - b_k(\phi, c)(\kappa_m - \kappa_s(\phi, c))k_{s,\phi}(\phi, c) \\
&\quad + \sigma \left(-\varepsilon \Delta_{\Gamma(t)}\phi + \frac{1}{\varepsilon}\theta'(\phi)\right) + b_{g,\phi}\kappa_g + p_{,\phi} + f_{,\phi}
\end{aligned} \tag{5.16}$$

$$\partial_t^\bullet c = \nabla_{\Gamma(t)} \cdot \left(M_c(\phi, c)\nabla_{\Gamma(t)}\chi\right) \tag{5.17}$$

$$\begin{aligned}
\chi &= \frac{1}{2} b_{k,c}(\phi, c)|\kappa_m - \kappa_s(\phi, c)|^2 - b_k(\phi, c)(\kappa_m - \kappa_s(\phi, c))k_{s,c}(\phi, c) \\
&\quad + b_{g,c}\kappa_g + f_{,c} + p_{,c}.
\end{aligned} \tag{5.18}$$

We have in mind identifying a free boundary problem associated to the sharp

interface limit of Problem 5.2.1 and are thus searching for a 2-phase surface. To be able to do this, it is convenient to define certain quantities in each phase. Given a ϕ dependent function b, which may depend on other variables, we define $b^{\pm} := b(\phi^{\pm})$ and denote by $[b] = b^{+} - b^{-}$. Using this additional notation the free boundary problem, in the limit $\varepsilon \to 0$, reads as follows.

Problem 5.2.2. *Given an initial hypersurface $\Gamma(0) \subset \mathbb{R}^3$, decomposed as $\Gamma(0) = \Gamma^{-}(0) \cup \Lambda(0) \cup \Gamma^{+}(0)$ and initial condition for the binder density, $c(0) : \Gamma(0) \to \mathbb{R}$, find $(\Gamma(t), \pi(t), c(t))$ such that at each time $t \in [0, T]$:*

$$
\left.
\begin{aligned}
\nabla_{\Gamma(t)} \cdot \boldsymbol{\sigma}^{\pm}(t) &= \Delta_{\Gamma(t)} \left(b_k^{\pm}(c)(\kappa_m - \kappa_s^{\pm}(c)) \right) \boldsymbol{\nu} \\
&\quad + \left(|\nabla_{\Gamma(t)} \boldsymbol{\nu}|^2 \boldsymbol{\nu} + \nabla_{\Gamma(t)} \kappa_m \right) b_k^{\pm}(c)(\kappa_m - \kappa_s^{\pm}(c)) \\
&\quad + \boldsymbol{\nu} \nabla_{\Gamma(t)} \cdot \left((\kappa_m \mathbb{I} + \nabla_{\Gamma(t)} \boldsymbol{\nu}) b_{g,c}^{\pm}(c) \nabla_{\Gamma(t)} c \right) \\
&\quad + \kappa_g \nabla_{\Gamma(t)} b_g^{\pm}(c) + p_{,d_{\mathcal{S}}}^{\pm} \boldsymbol{\nu}_{\mathcal{S}} \\
\boldsymbol{\sigma}^{\pm}(t) &= -\pi \boldsymbol{P} + 2\mu^{\pm} D_{\Gamma} \boldsymbol{v} \\
\nabla_{\Gamma(t)} \cdot \boldsymbol{v} &= 0 \\
\partial_t^{\bullet} c &= \nabla_{\Gamma(t)} \cdot \left(M_c^{\pm}(c) \nabla_{\Gamma(t)} \chi \right) \\
\chi &= \tfrac{1}{2} b_{k,c}^{\pm}(c) |\kappa_m - \kappa_s^{\pm}(c)|^2 + b_k^{\pm}(c)(\kappa_m - \kappa_s^{\pm}(c)) k_{s,c}^{\pm}(c) \\
&\quad + b_{g,c}^{\pm}(c) \kappa_g + f_{,c}^{\pm} + p_{,c}^{\pm}
\end{aligned}
\right\} \text{ in } \Gamma^{\pm}(t)
$$

$$
\left.
\begin{aligned}
[\chi] &= 0 \\
[\boldsymbol{v}] &= 0 \\
[b_k(\kappa_m - \kappa_s) + \kappa_{\boldsymbol{\nu}} b_g] &= 0 \\
-(\boldsymbol{v} - \boldsymbol{v}_{\Lambda}) \cdot \boldsymbol{\mu}_{\Lambda} [c] &= [M_c \nabla_{\Gamma(t)} \chi] \cdot \boldsymbol{\mu}_{\Lambda} \\
-\omega \, (\boldsymbol{v} - \boldsymbol{v}_{\Lambda}) \cdot \boldsymbol{\mu}_{\Lambda} + [c] \chi &= \sigma \kappa_{\Lambda} + \left[\tfrac{1}{2} b_k |\kappa_m - \kappa_s|^2 + b_g \kappa_g \right] \\
&\quad - \left[(b_k(\kappa_m - \kappa_s) + b_g \kappa_{\boldsymbol{\nu}}) \kappa_p \right] + [p + f] \\
\boldsymbol{\mu}_{\Lambda} \cdot [\boldsymbol{\sigma}(t)] \, \boldsymbol{\mu}_{\Lambda} &= [b_g \kappa_g] + \left[(b_k(\kappa_m - \kappa_s) - b_g \kappa_{\boldsymbol{\nu}}) \kappa_p \right] - \sigma \kappa_{\Lambda}
\end{aligned}
\right\} \text{ on } \Lambda(t).
$$

The identification of this free boundary problem comes from the method of matched asymptotics as in Fife and Penrose [1995]. The major difficulty arises from the underlying dependence on ε of the unknown surface velocity. Thus we have extended the technique, similarly to Elliott and Stinner [2010c], parameterising over an assumed limiting surface but also accounting for the time dependence of the surface similarly to the work appearing in the preprint O'Connor and Stinner [2016].

5.3 The Membrane Energy

Following the lines of Elliott and Stinner [2010c], in this section we will discuss in detail the membrane energy and how we mean to take variations for the model

derivation.

Definition 5.3.1. *An **admissible (phase field adhesion) surface** is the smooth boundary Γ of a bounded simply connected open set $\Omega \subset \mathbb{R}^3$ together with a smooth field $\phi : \Gamma \to \mathbb{R}$ which is called the **phase field variable** and a secondary smooth field $c : \Gamma \to \mathbb{R}$ which is called the **binder density**.*

Since the phase field variable, $\phi : \Gamma \to \mathbb{R}$, and the binder density, $c : \Gamma \to \mathbb{R}$, depend on the underlying surface we must be careful by what we mean when discussing the variation of the surface energy. We use the following notion of an admissible deformation to an admissible surface.

Definition 5.3.2. *Given an admissible surface (Γ, ϕ, c), a smooth vector field $\boldsymbol{w} : \Gamma \to \mathbb{R}^3$ and smooth functions $\psi, \zeta : \Gamma \to \mathbb{R}$, the deformed admissible surface $\left(\tilde{\Gamma}[\tau], \tilde{\phi}[\tau], \tilde{c}[\tau]\right)$ in direction $(\boldsymbol{w}, \psi, \zeta)$ for small $\tau \in \mathbb{R}$ is defined by*

$$\begin{aligned}
\tilde{\Gamma}[\tau] &:= \{\tilde{\boldsymbol{x}}[\tau] := \boldsymbol{x} + \tau \boldsymbol{w}(\boldsymbol{x}) \mid \boldsymbol{x} \in \Gamma\}, \\
\tilde{\phi}[\tau] : \tilde{\Gamma}[\tau] \to \mathbb{R}, &\quad \tilde{\phi}[\tau, \tilde{\boldsymbol{x}}[\tau]] := \phi(\boldsymbol{x}) + \tau\psi(\boldsymbol{x}), \\
\tilde{c}[0, \tau] : \tilde{\Gamma}[\tau] \to \mathbb{R} &\text{ satisfies } \tilde{c}[\tilde{\boldsymbol{x}}[0]] = c(\boldsymbol{x}), \\
\text{and } \frac{d}{d\tau}\tilde{c}[\tau, \tilde{\boldsymbol{x}}[\tau]] &+ \tilde{c}[\tau, \tilde{\boldsymbol{x}}[\tau]]\nabla_\Gamma \cdot \boldsymbol{w}(\boldsymbol{x}) = \zeta(\boldsymbol{x}).
\end{aligned}$$

*Such a triple $(\boldsymbol{w}, \psi, \zeta)$ is called an **admissible deformation (field)** for an admissible surface.*

Remark 5.3.3. *The solution to the ODE in this definition exists thanks to the smoothness of Γ and $\boldsymbol{w}$.*

To allow us to calculate the variations of the energy it is convenient to define

$$\partial_\tau^\bullet \tilde{c}(0, x) := \frac{d}{d\tau}\tilde{c}[\tau, \tilde{x}[\tau]]\Big|_{\tau=0}, \tag{5.19}$$

with similar definitions for the other fields. Thus for an admissible surface we have analogues of (2.9), (2.10) and (2.11) valid with the following replacements $t \to \tau$, $V(t) \to \tilde{\Gamma}[\tau]$, $\boldsymbol{v} \to \boldsymbol{w}$ and at the point $\tau = 0$. In addition there is a analogous decomposition of the material derivative as discussed after (2.3), so that we may write $\partial_\tau^\bullet \kappa_m = \partial_\tau^\circ \kappa_m + \boldsymbol{w} \cdot \nabla_\Gamma \kappa_m$.

The definition for an admissible deformation of the binder density may seem out of line with the definition used for the other fields. However, if we consider the mass functional $E'(c) = \int_\Gamma c$, for the binder density, then with the above definition, in the case of no deformation to the density, $\zeta = 0$, mass conservation holds

regardless of the deformations made to the other components. Observe that mass conservation of the binder density is implied by the balance law (5.2).

As discussed in the introduction we propose the following system energy which is defined on the space of admissible surfaces.

$$E(\Gamma,\phi,c) = E_{MC}(\Gamma,\phi,c) + E_{GC}(\Gamma,\phi,c) + E_{GL}(\Gamma,\phi) + E_{AD}(\Gamma,\phi,c) + E_B(\Gamma,\phi,c). \tag{5.20}$$

With the notion of an admissible deformation we can properly define a variation of the energy functional.

Definition 5.3.4. *Let $E = E(\Gamma,\phi,c)$ be a functional defined on admissible phase field adhesion surfaces. Let (Γ,ϕ,c) be an admissible surface and let $(\boldsymbol{w},\psi,\zeta)$ be an admissible deformation. The variation of E in (Γ,ϕ,c) in direction $(\boldsymbol{w},\psi,\zeta)$ is defined by*

$$\langle \delta E(\Gamma,\phi,c), (\boldsymbol{w},\psi,\zeta)\rangle = \frac{d}{d\tau} E(\tilde{\Gamma}[\tau],\tilde{\phi}[\tau],\tilde{c}[\tau])\Big|_{\tau=0}. \tag{5.21}$$

Using this definition we consider the variation of each component of the diffuse interface energy. Observe that in Elliott and Stinner [2013], the variation of many of these quantities was considered for a purely normal surface velocity field however since that work was in a stationary setting and was interested in the shape of the membrane, the tangential variations of the membrane could be determined via variations in the phase field variable only. In our setting since the binder density is dependent upon the surface velocity, tangential mass transport can have an effect and thus must be accounted for.

Lemma 5.3.5. ***Variation of the Mean Curvature bending Energy.*** *For an admissible surface (Γ,ϕ,c) with an admissible deformation $(\boldsymbol{w},\psi,\zeta)$ we have that:*

$$\begin{aligned}
&\langle \delta E_{MC}(\Gamma,\phi,c), (\boldsymbol{w},\psi,\zeta)\rangle \\
&= \int_\Gamma \left[\frac{1}{2} b_{k,\phi}(\phi,c)|\kappa_m - \kappa_s(\phi,c)|^2 - b_k(\phi,c)(\kappa_m - \kappa_s(\phi,c))\kappa_{s,\phi}(\phi,c)\right]\psi \\
&+ \int_\Gamma \left[\frac{1}{2} b_{k,c}(\phi,c)|\kappa_m - \kappa_s(\phi,c)|^2 - b_k(\phi,c)(\kappa_m - \kappa_s(\phi,c))\kappa_{s,c}(\phi,c)\right]\zeta \\
&+ \int_\Gamma \left[\Delta_\Gamma\left(b_k(\phi,c)(\kappa_m - \kappa_s(\phi,c))\right)\boldsymbol{\nu} + \left(|\nabla_\Gamma \boldsymbol{\nu}|^2 \boldsymbol{\nu} + \nabla_\Gamma \kappa_m\right) b_k(\phi,c)(\kappa_m - \kappa_s(\phi,c))\right]\cdot \boldsymbol{w} \\
&+ \int_\Gamma \left[\frac{1}{2}(b_k(\phi,c) - c b_{k,c}(\phi,c))|\kappa_m - \kappa_s(\phi,c)|^2 + b_k(\phi,c)(\kappa_m - \kappa_s(\phi,c))\kappa_{s,c}(\phi,c)c\right]\nabla_\Gamma \cdot \boldsymbol{w}
\end{aligned}$$

Proof. Using (2.10) and then (2.23) and (5.3.2) we obtain

$$
\begin{aligned}
&\frac{d}{d\tau} E_{MC}\big(\tilde{\Gamma}[\tau], \tilde{\phi}[\tau], \tilde{c}[\tau]\big)\Big|_{\tau=0} \\
&= \int_\Gamma \frac{1}{2}[b_{\kappa,\phi}(\phi,c)\partial_\tau^\bullet \phi + b_{\kappa,c}\partial_\tau^\bullet c]\big|\kappa_m - \kappa_s(\phi,c)\big|^2 + \frac{1}{2} b_\kappa(\phi,c)\big|\kappa_m - \kappa_s(\phi,c)\big|^2 \nabla_\Gamma \cdot \boldsymbol{w} \\
&\quad + \int_\Gamma b_\kappa(\phi,c)\big(\kappa_m - \kappa_s(c)\big)\big(\partial_\tau^\circ \kappa_m + \boldsymbol{w}\nabla_\Gamma \kappa_m - [\kappa_{s,\phi}(\phi,c)\partial_\tau^\bullet \phi + \kappa_{s,c}(\phi,c)\partial_\tau^\bullet c]\big) \\
&= \int_\Gamma \left[\frac{1}{2} b_{k,\phi}(\phi,c)|\kappa_m - \kappa_s(\phi,c)|^2 - b_k(\phi,c)(\kappa_m - \kappa_s(\phi,c))k_{s,\phi}(\phi,c)\right]\psi \\
&\quad + \int_\Gamma \left[\frac{1}{2} b_{k,c}(\phi,c)|\kappa_m - \kappa_s(\phi,c)|^2 - b_k(\phi,c)(\kappa_m - \kappa_s(\phi,c))k_{s,c}(\phi,c)\right]\zeta \\
&\quad + \int_\Gamma b_k(\phi,c)(\kappa_m - \kappa_s(\phi,c))\Delta_\Gamma(\boldsymbol{w}\cdot\boldsymbol{\nu}) + \left[\left(|\nabla_\Gamma \boldsymbol{\nu}|^2 \boldsymbol{\nu} + \nabla_\Gamma \kappa_m\right) b_k(\phi,c)(\kappa_m - \kappa_s(\phi,c))\right]\cdot \boldsymbol{w} \\
&\quad + \int_{\Gamma(t)} \left[\frac{1}{2}(b_k(\phi,c) - c b_{k,c}(\phi,c))|\kappa_m - \kappa_s(\phi,c)|^2 + b_k(\phi,c)(\kappa_m - \kappa_s(\phi,c))\kappa_{s,c}(\phi,c)c\right]\nabla_\Gamma \cdot \boldsymbol{w}
\end{aligned}
$$

Twice integrating by parts in the term with $\Delta_\Gamma(\boldsymbol{w}\cdot\boldsymbol{\nu})$ yields the assertion. □

This is similar to the result obtained in Elliott and Stinner [2013] but has some additional terms due to allowing for tangential variations as well as quantities depending on the binder density. The additional term due to tangential variations is represented by the $\nabla_\Gamma \kappa_m$ term.

Lemma 5.3.6. ***Variation of the Gaussian Curvature bending energy****. For an admissible surface $(\Gamma(t), \phi, c)$ with an admissible deformation $(\boldsymbol{w}, \psi, \zeta)$ we have that:*

$$
\begin{aligned}
&\langle \delta E_{GC}(\Gamma,\phi,c), (\boldsymbol{w},\psi,\zeta)\rangle \\
&= \int_\Gamma [b_{g,\phi}(\phi,c)]\,\psi \\
&+ \int_\Gamma [b_{g,c}(\phi,c)]\,\zeta \\
&+ \int_\Gamma [(\nabla_\Gamma \cdot ((\kappa_m \mathbb{I} + \nabla_\Gamma \boldsymbol{\nu})(b_{g,\phi}(\phi,c)\nabla_\Gamma \phi + b_{g,c}(\phi,c)\nabla_\Gamma c)))\,\boldsymbol{\nu} + \kappa_g \nabla_\Gamma b_g(\phi,c)]\cdot \boldsymbol{w} \\
&- \int_\Gamma [b_{g,c}(\phi,c)c]\,\nabla_\Gamma \cdot \boldsymbol{w}
\end{aligned}
$$

Proof. We use formula (2.6) for the Gaussian curvature. With (5.3.2), (2.9), (2.11),

(2.22)

$$
\begin{aligned}
&\frac{d}{d\tau}\int_{\Gamma[\tau]}\frac{1}{2}b_g(\tilde{\phi}[\tau],\tilde{c}[\tau])|\nabla_{\tilde{\Gamma}[\tau]}\tilde{\boldsymbol{\nu}}[\tau]|^2\Big|_{\tau=0}\\
&=\int_\Gamma\frac{1}{2}\partial_\tau^\bullet\big(b_g(\phi,c)|\nabla_\Gamma\boldsymbol{\nu}|^2\big)+\frac{1}{2}b_g(\phi,c)|\nabla_\Gamma\boldsymbol{\nu}|^2\nabla_\Gamma\cdot\boldsymbol{w}\\
&=\sum_i\int_\Gamma\frac{1}{2}[b_{g,\phi}(\phi,c)\partial_\tau^\bullet\phi+b_{g,c}(\phi,c)\partial_\tau^\bullet c]|\nabla_\Gamma\boldsymbol{\nu}_i|^2+\frac{1}{2}b_g(\phi,c)|\nabla_\Gamma\boldsymbol{\nu}_i|^2\nabla_\Gamma\cdot\boldsymbol{w}\\
&\quad+\sum_i\int_\Gamma b_g(\phi,c)\nabla_\Gamma\boldsymbol{\nu}_i\cdot\nabla_\Gamma\partial_\tau^\circ\boldsymbol{\nu}_i-b_g(\phi,c)\nabla_\Gamma\boldsymbol{\nu}_i\cdot D_\Gamma(\boldsymbol{w}\cdot\boldsymbol{\nu}\boldsymbol{\nu})\nabla_\Gamma\boldsymbol{\nu}_i\\
&\quad+\sum_i\int_\Gamma\frac{1}{2}b_g(\phi,c)\nabla_\Gamma|\nabla_\Gamma\boldsymbol{\nu}_i|^2\cdot\boldsymbol{w}\\
&=\sum_i\int_\Gamma\frac{1}{2}[b_{g,\phi}(\phi,c)\psi+b_{g,c}(\phi,c)(\zeta-c\nabla_\Gamma\cdot\boldsymbol{w})]|\nabla_\Gamma\boldsymbol{\nu}_i|^2+\frac{1}{2}b_g(\phi,c)|\nabla_\Gamma\boldsymbol{\nu}_i|^2\nabla_\Gamma\cdot\boldsymbol{w}\\
&\quad+\sum_i\int_\Gamma b_g(\phi,c)\sum_i\nabla_\Gamma\boldsymbol{\nu}_i\cdot\nabla_\Gamma(-\underline{D}_i(\boldsymbol{w}\cdot\boldsymbol{\nu}))-b_g(\phi,c)\Big(\sum_i\nabla_\Gamma\boldsymbol{\nu}_i\otimes\nabla_\Gamma\boldsymbol{\nu}_i:\nabla_\Gamma\boldsymbol{\nu}\Big)\boldsymbol{\nu}\cdot\boldsymbol{w}\\
&\quad+\sum_i\int_\Gamma\frac{1}{2}b_g(\phi,c)\nabla_\Gamma|\nabla_\Gamma\boldsymbol{\nu}_i|^2\cdot\boldsymbol{w}
\end{aligned}
$$

Using (2.7) we obtain that

$$
\begin{aligned}
&\int_\Gamma b_g(\phi,c)\sum_i\nabla_\Gamma\boldsymbol{\nu}_i\cdot\nabla_\Gamma(-\underline{D}_i(\boldsymbol{w}\cdot\boldsymbol{\nu}))\\
&\quad=\int_\Gamma\sum_i\nabla_\Gamma\cdot\big(b_g(\phi,c)\nabla_\Gamma\boldsymbol{\nu}_i\big)\underline{D}_i(\boldsymbol{w}\cdot\boldsymbol{\nu})\\
&\quad=\int_\Gamma\sum_i[b_{g,\phi}(\phi,c)\nabla_\Gamma\phi+b_{g,c}(\phi,c)\nabla_\Gamma c]\cdot\nabla_\Gamma\boldsymbol{\nu}_i\underline{D}_i(\boldsymbol{w}\cdot\boldsymbol{\nu})\\
&\quad+b_g(\phi,c)\Delta_\Gamma\boldsymbol{\nu}_i\underline{D}_i(\boldsymbol{w}\cdot\boldsymbol{\nu})\\
&\quad=\int_\Gamma\nabla_\Gamma\boldsymbol{\nu}[b_{g,\phi}(\phi,c)\nabla_\Gamma\phi+b_{g,c}(\phi,c)\nabla_\Gamma c]\cdot\nabla_\Gamma(\boldsymbol{w}\cdot\boldsymbol{\nu})\\
&\quad-\int_\Gamma b_g(\phi,c)\nabla_\Gamma\kappa_m\cdot\nabla_\Gamma(\boldsymbol{w}\cdot\boldsymbol{\nu})\\
&\quad=\int_\Gamma\nabla_\Gamma\cdot\big(-\nabla_\Gamma\boldsymbol{\nu}[b_{g,\phi}(\phi,c)\nabla_\Gamma\phi+b_{g,c}(\phi,c)\nabla_\Gamma c]+b_g(\phi,c)\nabla_\Gamma\kappa_m\big)\boldsymbol{\nu}\cdot\boldsymbol{w}.
\end{aligned}
$$

Considering Lemma 5.3.5 with $b_\kappa = b_g$ and $\kappa_s = 0$ we get

$$\begin{aligned}\frac{d}{d\tau}\int_{\Gamma(\cdot)} \frac{1}{2} b_g(\tilde{c}[\tau])\kappa_m^2\Big|_{\tau=0} &= \int_\Gamma \frac{1}{2} b_{g,\phi}(\phi,c)\kappa_m^2\psi + \frac{1}{2} b_{g,c}(\phi,c)\kappa_m^2\zeta \\ &+ \int_\Gamma \left[\Delta_\Gamma\left(b_g(\phi,c)\kappa_m\right)\boldsymbol{\nu} + \left(|\nabla_\Gamma \boldsymbol{\nu}|^2\boldsymbol{\nu} + \nabla_\Gamma \kappa_m\right) b_g(\phi,c)\kappa_m\right]\cdot \boldsymbol{w} \\ &+ \int_\Gamma \left(\frac{1}{2}(b_g(\phi,c) - c b_{g,c}(\phi,c))\kappa_m^2\right)\nabla_\Gamma \cdot \boldsymbol{w}\end{aligned}$$

Altogether

$$\begin{aligned}&\frac{d}{d\tau}\int_{\Gamma(\cdot)} \frac{1}{2} b_g(\tilde{\phi}[\tau],\tilde{c}[\tau])\left(\kappa_m^2 - |\nabla_{\tilde{\Gamma}[\tau]}\boldsymbol{\nu}|^2\right)\Big|_{\tau=0} \qquad (5.22)\\ =&\int_{\Gamma(t)} [b_{g,\phi}(\phi,c)\psi + b_{g,c}(\phi,c)(\zeta - c\nabla_\Gamma\cdot\boldsymbol{w})]\kappa_g + b_g(\phi,c)\boldsymbol{w}\cdot\nabla_\Gamma\kappa_g + b_g(\phi,c)\kappa_g\nabla_\Gamma\cdot\boldsymbol{w} \\ &+\int_\Gamma \nabla_\Gamma\cdot\left(\nabla_\Gamma(b_g(\phi,c)\kappa_m) - b_g(\phi,c)\nabla_\Gamma\kappa_m + \nabla_\Gamma\boldsymbol{\nu}\left[b_{g,\phi}(\phi,c)\nabla_\Gamma\phi + b_{g,c}(\phi,c)\nabla_\Gamma c\right]\right)\boldsymbol{\nu}\cdot\boldsymbol{w} \\ &+\int_\Gamma b_g(\phi,c)\left(\kappa_m|\nabla_\Gamma\boldsymbol{\nu}|^2 + \sum_i \nabla_\Gamma\boldsymbol{\nu}_i\otimes\nabla_\Gamma\boldsymbol{\nu}_i : \nabla_\Gamma\boldsymbol{\nu}\right)\boldsymbol{\nu}\cdot\boldsymbol{w}.\end{aligned}$$

Observe that $\nabla_\Gamma(b_g(\phi,c)\kappa_m) - b_g(c)\nabla_\Gamma\kappa_m = \kappa_m[b_{g,\phi}\nabla_\Gamma\phi + b_{g,c}\nabla_\Gamma c]$. Furthermore we may decompose the term $b_g\kappa_g\nabla_\Gamma\cdot\boldsymbol{w}$ using integration by parts to $-\nabla_\Gamma(b_g\kappa_g)\cdot\boldsymbol{w} + \boldsymbol{w}\cdot\boldsymbol{\nu}\kappa_m b_g\kappa_g$. We can combine the second term of this decomposition with the last line of (5.22), to obtain a term with the following coefficient which vanishes.

$$|\nabla_\Gamma\boldsymbol{\nu}|^2\kappa_m + \sum_i \nabla_\Gamma\boldsymbol{\nu}_i\otimes\nabla_\Gamma\boldsymbol{\nu}_i : \nabla_\Gamma\boldsymbol{\nu} - \kappa_g\kappa_m = 0. \qquad (5.23)$$

To see that this term vanishes, consider an orthogonal matrix $Q\in\mathbb{R}^{3\times 3}$, such that

$$Q^{-1}\nabla_\Gamma\boldsymbol{\nu}Q = \begin{pmatrix} -\kappa_1 & 0 & 0\\ 0 & -\kappa_2 & 0\\ 0 & 0 & 0\end{pmatrix}. \qquad (5.24)$$

Recall that κ_1 and κ_2 are the principal curvatures. Each of the summands in (5.23) is invariant under such a transformation and so we have the following three identities

from which the result follows.

$$|\nabla_\Gamma \boldsymbol{\nu}|^2 \kappa_m = (\kappa_1^2 + \kappa_2^2)(\kappa_1 + \kappa_2),$$
$$\sum_i \nabla_\Gamma \boldsymbol{\nu}_i \otimes \nabla_\Gamma \boldsymbol{\nu}_i : \nabla_\Gamma \boldsymbol{\nu} = -\kappa_1^3 - \kappa_2^3,$$
$$\kappa_g \kappa_m = \kappa_1 \kappa_2 (\kappa_1 + \kappa_2).$$

Finally, expanding $\nabla_\Gamma(b_g \kappa_g) \cdot \boldsymbol{w}$ as $b_g \boldsymbol{w} \cdot \nabla_\Gamma \kappa_g + \kappa_g \boldsymbol{w} \cdot \nabla_\Gamma b_g$, upon cancelling with the like term in (5.22) the result follows. □

Again there are the additions resulting from allowing quantities to depend on the binder density and the novelty arising from tangential motion is the term $\kappa_g \nabla_\Gamma b_g$. This can be further expanded using $\nabla_\Gamma b_g = b_{g,\phi} \nabla_\Gamma \phi + b_{g,c} \nabla_\Gamma c$ but is written in the more concise form for ease of reading. Observe that in the case of a constant Gaussian bending rigidity then the energy due to Gaussian curvature is still a topological invariant.

Lemma 5.3.7. ***Variation of the Ginzburg-Landau energy****. For an admissible surface* (Γ, ϕ, c) *with an admissible deformation* $(\boldsymbol{w}, \psi, \zeta)$ *we have that:*

$$\begin{aligned}\langle \delta E_{GL}(\Gamma, \phi), (\boldsymbol{w}, \psi) \rangle =& \sigma \int_\Gamma \left[-\varepsilon \Delta_\Gamma \phi + \frac{1}{\varepsilon} \theta'(\phi) \right] \psi \\ &+ \sigma \int_\Gamma \left[\kappa_m \delta(\phi, \nabla_\Gamma \phi) \boldsymbol{\nu} + \nabla_\Gamma \cdot \left(\varepsilon \nabla_\Gamma \phi \otimes \nabla_\Gamma \phi - \delta(\phi, \nabla_\Gamma \phi) \boldsymbol{I} \right) \right] \cdot \boldsymbol{w}\end{aligned}$$

Proof. We use (2.9), (2.11) and (5.3.2) to obtain

$$\begin{aligned}\frac{d}{d\tau} E_{GL}\big(\tilde{\Gamma}[\tau], \tilde{\phi}[\tau]\big)\Big|_{\tau=0} =& \sigma \int_\Gamma \varepsilon \nabla_\Gamma \phi \cdot \nabla_\Gamma \partial_\tau^\bullet \phi - \varepsilon \nabla_\Gamma \phi \otimes \nabla_\Gamma \phi : D_\Gamma(\boldsymbol{w}) + \frac{1}{\varepsilon} \theta'(\phi) \partial_\tau^\bullet \phi \\ &+ \sigma \int_\Gamma \delta(\phi, \nabla_\Gamma \phi) \nabla_\Gamma \cdot \boldsymbol{w} \\ =& \sigma \int_\Gamma -\varepsilon \Delta_\Gamma \phi \, \psi + \frac{1}{\varepsilon} \theta'(\phi) \psi - \varepsilon \nabla_\Gamma \phi \otimes \nabla_\Gamma \phi : D_\Gamma(\boldsymbol{w}) \\ &+ \sigma \int_\Gamma \kappa_m \delta(\phi, \nabla_\Gamma \phi) \boldsymbol{\nu} \cdot \boldsymbol{w} - \nabla_\Gamma \cdot \big(\delta(\phi, \nabla_\Gamma \phi) \boldsymbol{I} \big) \cdot \boldsymbol{w}.\end{aligned}$$

Observe that:

$$\begin{aligned}\int_\Gamma \nabla_\Gamma\phi\otimes\nabla_\Gamma\phi : D_G(\boldsymbol{w}) =& \frac{1}{2}\int_\Gamma \sum_{i,j} \underline{D}_i\phi\underline{D}_j\phi(\underline{D}_i\boldsymbol{w}_j + \underline{D}_j\boldsymbol{w}_i)\\ =& \sum_{i,j}\int_\Gamma \underline{D}_i\left(\underline{D}_i\phi\underline{D}_j\phi\boldsymbol{w}_j\right) - \underline{D}_i\left(\underline{D}_i\phi\underline{D}_j\phi\right)\boldsymbol{w}_j\\ =& -\sum_{i,j}\int_\Gamma \underline{D}_i\left(\underline{D}_i\phi\underline{D}_j\phi\right)\boldsymbol{w}_j = -\int_\Gamma \nabla_\Gamma\cdot(\nabla_\Gamma\phi\otimes\nabla_\Gamma\phi)\cdot\boldsymbol{w}\end{aligned}$$

From which the result follows. Note we have used that the projection operators in D_Γ act as the identity on the tangential gradients.

□

Lemma 5.3.8. ***Variation of the adhesion energy and binder density energy***. *For an admissible surface* (Γ,ϕ,c) *with an admissible deformation* $(\boldsymbol{w},\psi,\zeta)$ *we have that:*

$$\langle\delta E_{AD}(\Gamma,\phi,c),(\boldsymbol{w},\psi,\zeta)\rangle = \int_\Gamma \left[p_{,c}\zeta + p_{,\phi}\psi + p_{,d_\mathcal{S}}\boldsymbol{\nu}_\mathcal{S}\cdot\boldsymbol{w} + (p - cp_{,c})\,\nabla_\Gamma\cdot\boldsymbol{w}\right] \tag{5.25}$$

$$\langle\delta E_B(\Gamma,\phi,c),(\boldsymbol{w},\psi,\zeta)\rangle = \int_\Gamma \left[f_{,c}\zeta + f_{,\phi}\psi + (f - cf_{,c})\,\nabla_\Gamma\cdot\boldsymbol{w}\right] \tag{5.26}$$

Proof. We use (2.9) and (5.3.2) to obtain

$$\begin{aligned}\frac{d}{d\tau}E_{AD}(\tilde{\Gamma}[\tau],\tilde{\phi}[\tau],\tilde{c}[\tau])\Big|_{\tau=0} &= \int_\Gamma \partial_\tau^\bullet p + p\nabla_\Gamma\cdot\boldsymbol{w}\\ &= \int_\Gamma p_{,c}\partial_\tau^\bullet c + p_{,d_\mathcal{S}}\partial_\tau^\bullet d_\mathcal{S} + p_{,\phi}\partial_\tau^\bullet\phi + p\nabla_\Gamma\cdot\boldsymbol{w}\\ &= \int_\Gamma p_{,c}\zeta + (p - cp_{,c})\,\nabla_\Gamma\cdot\boldsymbol{w} + p_{,d_\mathcal{S}}\boldsymbol{\nu}_\mathcal{S}\cdot\boldsymbol{w} + p_{,\phi}\psi.\end{aligned}$$

Here we have used that the distance function can be expressed as

$$d_\mathcal{S}(\tilde{\boldsymbol{x}}[\tau]) = \|\tilde{\boldsymbol{x}}[\tau] - \tilde{\boldsymbol{x}}_\mathcal{S}[\tau]\|_2 \tag{5.27}$$

where $\tilde{\boldsymbol{x}}_{\mathcal{S}}[\tau]$ is the closest point in the substrate to the point $\tilde{\boldsymbol{x}}[\tau]$. Thus we have

$$\partial_\tau^\bullet d_{\mathcal{S}}(\tilde{\boldsymbol{x}}[\tau]) = \frac{d}{d\tau} d_{\mathcal{S}}(\tilde{\boldsymbol{x}}[\tau])\bigg|_{\tau=0} = \frac{\tilde{\boldsymbol{x}}[\tau] - \tilde{\boldsymbol{x}}_{\mathcal{S}}[\tau]}{\|\tilde{\boldsymbol{x}}[\tau] - \tilde{\boldsymbol{x}}_{\mathcal{S}}[\tau]\|_2} (\tilde{\boldsymbol{x}}'[\tau] - \tilde{\boldsymbol{x}}'_{\mathcal{S}}[\tau])\bigg|_{\tau=0}$$

We have that $\tilde{\boldsymbol{x}}'[\tau]|_{\tau=0} = \boldsymbol{w}(t)$ and upon noting that

$$\frac{\tilde{\boldsymbol{x}}[\tau] - \tilde{\boldsymbol{x}}_{\mathcal{S}}[\tau]}{\|\tilde{\boldsymbol{x}}[\tau] - \tilde{\boldsymbol{x}}_{\mathcal{S}}[\tau]\|_2}\bigg|_{\tau=0} = \boldsymbol{\nu}_{\mathcal{S}}(\boldsymbol{x}_{\mathcal{S}}(t)) \tag{5.28}$$

is the normal to the substrate, and that $\tilde{\boldsymbol{x}}'_{\mathcal{S}}[\tau]$ is tangential to the substrate the result for the variation of the adhesion potential follows. The other result, for the variation of the binder potential, follows by replacing p with f and noting that the derivative with respect to the distance, $d_{\mathcal{S}}$, is zero. □

5.4 Model Derivation

In this section we will use the variations calculated in the previous section to derive a system of evolving surface partial differential equations to model focal cell adhesion.

Firstly, by setting any two components of an admissible deformation to zero gives rise to the notion of a variation with respect to an individual component. We will denote these quantities as follows:

$$\langle \delta_\Gamma E(\Gamma, \phi, c), \boldsymbol{w} \rangle := \langle \delta E(\Gamma, \phi, c)(\boldsymbol{w}, 0, 0) \rangle \tag{5.29}$$

$$\langle \delta_\phi E(\Gamma, \phi, c), \psi \rangle := \langle \delta E(\Gamma, \phi, c)(0, \psi, 0) \rangle \tag{5.30}$$

$$\langle \delta_c E(\Gamma, \phi, c), \zeta \rangle := \langle \delta E(\Gamma, \phi, c)(0, 0, \zeta) \rangle \tag{5.31}$$

In the previous section we saw that when calculating the variations of the different energy functionals, that there were many terms associated with the Lagrange multiplier of the incompressibility constraint, that is coefficients of the term $\nabla_\Gamma \cdot \boldsymbol{w}$. The majority of these terms scaled at an order of ε^0 or higher. The terms of importance are those that scale as $\frac{1}{\varepsilon}$. Although we will identify these terms that scale as $\frac{1}{\varepsilon}$ in our model, we do not identify higher order terms. Instead we absorb the higher order terms back into the pressure and reuse the variable π .

Associated with the virtual work principle, (5.3), there is a bilinear form for expressing the virtual power along a virtual velocity field $\boldsymbol{w}$ performed by the stresses $\boldsymbol{\sigma}$ with associated actual velocity field $\boldsymbol{v}$ and surface pressure π, given by

$$\mathcal{W}((\boldsymbol{v}, \pi), \boldsymbol{w}) = \int_{\Gamma(t)} 2\mu(\phi) D_{\Gamma(t)} \boldsymbol{v} : D_{\Gamma(t)} \boldsymbol{w} - \int_{\Gamma(t)} \pi \nabla_{\Gamma(t)} \cdot \boldsymbol{w}. \tag{5.32}$$

Associated with this bilinear form is a surface differential operator which can be denoted $\nabla_{\Gamma(t)} \cdot \boldsymbol{\sigma} = -\mu(\phi)\mathcal{S}_{\Gamma(t)}\boldsymbol{v} + \nabla_{\Gamma(t)}\pi + \pi\kappa_m\boldsymbol{\nu}$. Here $\mathcal{S}_{\Gamma(t)}$ is what is often referred to as the Boussinesq-Scriven operator and in an incompressible planar setting would be the Laplacian. The difficulty with forming an analogues expression for surfaces is that there is not a unique form for the Laplacian of a vector field.

For a vector field there is the intuitive definition of the Laplacian, known as the Bochner or rough Laplacian and denoted $\Delta_{\Gamma(t)}\boldsymbol{v}$ which is defined in terms of the covariant derivative and its adjoint and is equivalent to the Laplace-Beltrami operator acting on each component:

$$\left(\Delta_{\Gamma(t)}\boldsymbol{v}\right)_i = \Delta_{\Gamma(t)}\left(\boldsymbol{v}_i\right). \tag{5.33}$$

On the other hand there is the Laplace-de Rham operator (or Hodge-de Rham Laplacian) which acts on differential forms and is defined as $\Delta^R = -\boldsymbol{\delta}\boldsymbol{d} - \boldsymbol{d}\boldsymbol{\delta}$ where $\boldsymbol{d}$ is the exterior derivative and $\boldsymbol{\delta}$ is the co-differential operator, formally the adjoint operator of the exterior derivative. This can be extended to act on vector fields through the process of raising and lower indices. In the notation of surface calculus we can express the Laplace-de Rham operator, $\Delta^R_{\Gamma(t)}$ as:

$$\Delta^R_{\Gamma(t)}\boldsymbol{v} = -\nabla_{\Gamma(t)} \times \nabla_{\Gamma(t)} \times \boldsymbol{v} + \nabla_{\Gamma(t)}\left(\nabla_{\Gamma(t)} \cdot \boldsymbol{v}\right). \tag{5.34}$$

For scalar fields on surfaces the two forms coincide, as they do in a planar setting, although for vectorial quantities on a surface they differ. Using the Bochner formula, Rosenberg [1997] the two different Laplacians can be related:

$$\Delta_{\Gamma(t)}\boldsymbol{v} = \Delta^R_{\Gamma(t)}\boldsymbol{v} + \kappa_g\boldsymbol{v} \tag{5.35}$$

We quote the following result from Arroyo and DeSimone [2009] which gives the Boussinesq-Scriven operator in its strong form.

Lemma 5.4.1. *The strong form, $\mathcal{S}_{\Gamma(t)}$, of the Boussinesq-Scriven operator which is such that*

$$\int_{\Gamma(t)} \boldsymbol{\sigma} : D_{\Gamma(t)}\boldsymbol{w} = \int_{\Gamma(t)} \left(-\mu(\phi)\mathcal{S}_{\Gamma(t)}\boldsymbol{v} + \nabla_{\Gamma(t)}\pi + \pi\kappa_m\boldsymbol{\nu}\right) \cdot \boldsymbol{w} \tag{5.36}$$

has explicit form:

$$\begin{aligned}\mathcal{S}_{\Gamma(t)}\boldsymbol{v} &= 2\nabla_{\Gamma(t)}\cdot D_{\Gamma(t)}\boldsymbol{v}\\ &= -\nabla_{\Gamma(t)}\times\nabla_{\Gamma(t)}\times\boldsymbol{v}_\tau + 2\nabla_{\Gamma(t)}\left(\nabla_{\Gamma(t)}\cdot\boldsymbol{v}\right) - 2\left(\nabla_{\Gamma(t)}\boldsymbol{\nu} - \kappa_m\mathbb{I}\right)\nabla_{\Gamma(t)}(v_{\boldsymbol{\nu}}) + 2\kappa_g\boldsymbol{v}_\tau\\ &= \Delta^R_{\Gamma(t)}\boldsymbol{v}_\tau + \nabla_{\Gamma(t)}\left(\nabla_{\Gamma(t)}\cdot\boldsymbol{v}\right) - 2\left(\nabla_{\Gamma(t)}\boldsymbol{\nu} - \kappa_m\mathbb{I}\right)\nabla_{\Gamma(t)}(v_{\boldsymbol{\nu}}) + 2\kappa_g\boldsymbol{v}_\tau\\ &= \Delta_{\Gamma(t)}\boldsymbol{v}_\tau + \nabla_{\Gamma(t)}\left(\nabla_{\Gamma(t)}\cdot\boldsymbol{v}\right) - 2\left(\nabla_{\Gamma(t)}\boldsymbol{\nu} - \kappa_m\mathbb{I}\right)\nabla_{\Gamma(t)}(v_{\boldsymbol{\nu}}) + \kappa_g\boldsymbol{v}_\tau.\end{aligned}$$

Using the derived variations in Section 5.3 with the above discussions we may write the motivated virtual work principle in a strong form. Although we could express the evolution law in terms of the Boussinesq-Scriven operator, we have chosen to present the model in the split form using the stress tensor, $\boldsymbol{\sigma}$, as this makes the asymptotic analysis easier and is in keeping with common practices of continuum mechanics. This gives our proposed surface evolution law, which can be written as a normal component (5.12) and the tangential component (5.13). Combining this with the postulated evolution laws (5.1) and (5.2) we obtain (5.16)-(5.18).

Note that the dynamics of the diffuse interface model 5.2.1 are dissipative with respect to the system energy (5.20).

$$\begin{aligned}\frac{d}{dt}E(\Gamma(t),\phi,c) =& \langle\delta E(\Gamma(t),\phi,c),(\boldsymbol{w},\psi,\zeta)\rangle\Big|_{\boldsymbol{w}=\boldsymbol{v},\,\psi=\partial_t^\bullet\phi,\,\zeta=\partial_t^\bullet c+c\nabla_{\Gamma(t)}\cdot\boldsymbol{v}}\\ =& \langle\delta_\Gamma E,\boldsymbol{v}\rangle + \langle\delta_\phi E,\partial_t^\bullet\phi\rangle + \langle\delta_c E,\partial_t^\bullet c + c\nabla_{\Gamma(t)}\cdot\boldsymbol{v}\rangle\\ =& \int_{\Gamma(t)}\delta_\Gamma E\cdot\boldsymbol{v} + \int_{\Gamma(t)}\delta_\phi E\partial_t^\bullet\phi + \int_{\Gamma(t)}\delta_c E(\partial_t^\bullet c + c\nabla_{\Gamma(t)}\cdot\boldsymbol{v})\\ =& -\int_{\Gamma(t)}\boldsymbol{\sigma}:D_\Gamma\boldsymbol{v} + \int_{\Gamma(t)}\delta_\phi E\partial_t^\bullet\phi + \int_{\Gamma(t)}\delta_c E\nabla_{\Gamma(t)}\cdot(M_c\nabla_{\Gamma(t)}(\delta_c E))\\ =& \int_{\Gamma(t)}(\pi\boldsymbol{P}-\mu(\phi)D_\Gamma\boldsymbol{v}):D_\Gamma\boldsymbol{v} - \int_{\Gamma(t)}\frac{1}{\varepsilon\omega}|\delta_\phi E|^2\\ &- \int_{\Gamma(t)}M_c\nabla_{\Gamma(t)}(\delta_c E)\cdot\nabla_{\Gamma(t)}(\delta_c E)\\ =& \int_{\Gamma(t)}-\mu(\phi)|D_\Gamma\boldsymbol{v})|^2 - \int_{\Gamma(t)}\frac{1}{\varepsilon\omega}|\delta_\phi E|^2\\ &- \int_{\Gamma(t)}M_c\nabla_{\Gamma(t)}(\delta_c E)\cdot\nabla_{\Gamma(t)}(\delta_c E)\le 0\end{aligned}$$

In the last line we have used, with $\mathbf{1}$ the identity matrix, that $\boldsymbol{P}:D_\Gamma\boldsymbol{v}=\mathbf{1}:\boldsymbol{P}D_\Gamma\boldsymbol{v}=\mathrm{tr}D_\Gamma\boldsymbol{v}=\nabla_{\Gamma(t)}\cdot\boldsymbol{v}=0$ to eliminate the term involving the surface pressure.

5.5 Asymptotic Analysis

The aim of this section is now to analyse the diffuse interface model under the sharp interface limit $\varepsilon \to 0$. We do this by matching appropriate asymptotic expansions in the interface variable ε. The technique has been previously extended to unknown surfaces in Elliott and Stinner [2013]. Time dependence of the underlying space, in the case of a given surface, has been discussed in Chapter 3. The major novelty here, now being that we must take account of time dependence of an unknown underlying surface. Some of the machinery used here, for example the matching conditions (5.69a)-(5.69e), are similar to that used in Chapter 3, (3.20a)-(3.20e), however, we have included them again in their current form so as to clarify certain dependencies, such as which surface the differential operators are acting over.

5.5.1 Assumptions

We suppose we have a family of solutions $\Gamma_\varepsilon(t)$, π_ε, ϕ_ε, c_ε, with velocity field, $\boldsymbol{v}_\varepsilon$, to the diffuse interface Problem 5.2.1 and assume that there is a piecewise smooth limiting surface $\Gamma_0(t)$ and limiting fields π_0, ϕ_0, c_0, $\boldsymbol{v}_0$ to which the surface $\Gamma_\varepsilon(t)$ and solution fields converge to as $\varepsilon \to 0$. It is thus our goal to identify equations that these limiting fields should satisfy as well as limiting equations describing the evolution of the surface. We will refer to these equations as the sharp interface problem.

We assume that the level sets

$$\Lambda_\varepsilon(t) := \left\{ \boldsymbol{x}_\varepsilon \in \Gamma_\varepsilon(t) \middle| \phi_\varepsilon(\boldsymbol{x}_\varepsilon) = 0 \right\} \tag{5.37}$$

converge to a finite number of smooth time dependent curves $\Lambda_0(t)$ on $\Gamma_0(t)$, which evolve with a velocity $\boldsymbol{v}_{\Lambda_0}$. This velocity field should coincide with the surface velocity, $\boldsymbol{v}_0$, in the normal direction to ensure that the curve remains within the surface, however the two velocities can differ in a tangential direction to Γ_0. Using the limiting interfacial curve we may decompose the limiting surface as $\Gamma_0(t) = \Gamma_0^\pm(t) \cup \Lambda_0(t)$ with the domains $\Gamma_0^\pm(t)$ the limits of the sets $\Gamma_\varepsilon^\pm(t) := \left\{ \phi_\varepsilon \gtrless \frac{\phi^+ + \phi^-}{2} \right\}$. Furthermore, we assume that the limiting surface, $\Gamma_0(t)$, is C^1 across $\Lambda_0(t)$ with the normal evolution, $\boldsymbol{v}_0 \cdot \boldsymbol{\nu}_0$, continuous across the limiting interface, $\Lambda_0(t)$.

We suppose that there exists a parameterisation of the surface $\Gamma_\varepsilon(t)$ over $\Gamma_0(t)$ of the form $\left\{ \boldsymbol{p}_\varepsilon(\boldsymbol{x}, t) \middle| \boldsymbol{x} \in \Gamma_0(t)\,,\ t \in [0,T] \right\}$. We make the assumption that we may make a Taylor series expansion in ε for this parameterisation such that:

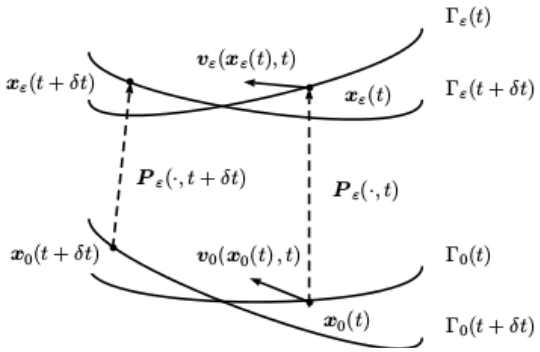

Figure 5.3: Graphical display of setup for asymptotic analysis. The surface $\Gamma_\varepsilon(t)$ is parameterised over $\Gamma_0(t)$ using $\boldsymbol{p}_\varepsilon$. Although the parameterisation maintains trajectories the two velocities $\boldsymbol{v}_\varepsilon$ and $\boldsymbol{v}_0$ can differ.

$$\boldsymbol{p}_\varepsilon(\boldsymbol{x},t) = \boldsymbol{x} + \varepsilon \boldsymbol{p}_1(\boldsymbol{x},t) + \mathcal{O}(\varepsilon^2), \tag{5.38}$$

with $\boldsymbol{p}_1\big|_t \in C^1(\Gamma_0(t))$. We further make the simplifying assumption that the parameterisation preserves the trajectories of material points: given any trajectory $t \mapsto \boldsymbol{x}_0(t) \in \Gamma_0(t)$, i.e. a solution to $\boldsymbol{x}_0'(t) = \boldsymbol{v}_0(\boldsymbol{x}_0(t),t)$, then $\boldsymbol{x}_\varepsilon(t) := \boldsymbol{p}_\varepsilon(\boldsymbol{x}_0(t),t)$ is a trajectory, too, and satisfies $\boldsymbol{x}_\varepsilon'(t) = \boldsymbol{v}_\varepsilon(\boldsymbol{x}_\varepsilon(t),t)$. Note that this assumption defines the map $\boldsymbol{p}_\varepsilon(\cdot,t)$ given some initial map $\boldsymbol{p}_\varepsilon(\cdot,0) : \Gamma_0(0) \to \Gamma_\varepsilon(0)$.

As a result of the assumptions on the parameterisation over the underlying unknown surface, the unit normal to Γ_ε can be expanded in the form

$$\boldsymbol{\nu}_\varepsilon(\boldsymbol{x}_\varepsilon(t),t) = \boldsymbol{\nu}_0(\boldsymbol{x}_0(t),t) + \varepsilon \boldsymbol{\nu}_1(\boldsymbol{x}_0(t),t) + \mathcal{O}(\varepsilon^2) \tag{5.39}$$

where $\boldsymbol{\nu}_1$ is a vector field tangential to Γ_0 and $\boldsymbol{\nu}_0$ is its unit normal. This implies that the projection operator to the tangent space of Γ_ε given by $\boldsymbol{P}_\varepsilon$ also has an ε-series expansion. Furthermore, the velocity $\boldsymbol{v}_\varepsilon$ can be expanded as an ε-expansion over the underlying surface:

$$\begin{aligned}
\boldsymbol{v}_\varepsilon(\boldsymbol{x}_\varepsilon(t),t) &= \frac{d}{dt}\boldsymbol{x}_\varepsilon(t) && (5.40)\\
&= \frac{d}{dt}\left(\boldsymbol{x}_0(t) + \varepsilon \boldsymbol{p}_1(\boldsymbol{x}_0(t),t) + \mathcal{O}(\varepsilon^2)\right) && (5.41)\\
&= \boldsymbol{v}_0(\boldsymbol{x}_0(t),t) + \varepsilon \partial^\bullet_{\Gamma_0(t)} \boldsymbol{p}_1(\boldsymbol{x}_0(t),t) + \mathcal{O}(\varepsilon^2) && (5.42)
\end{aligned}$$

where $\partial^\bullet_{\Gamma_0(t)}$ is the material derivative on the surface $\Gamma_0(t)$, we denote by $\partial^\bullet_{\Gamma_\varepsilon(t)}$ the material derivative on $\Gamma_\varepsilon(t)$ and in the following section we show how the two can be related.

Observe that in (5.12) and (5.13), the distance $d_{\mathcal{S}}$ is the distance from a point $\boldsymbol{x}_\varepsilon \in \Gamma_\varepsilon(t)$. Denoting by d_{Γ_ε} the distance for points in $\Gamma_\varepsilon(t)$ and d_{Γ_0} for points in $\Gamma_0(t)$, we may express the distance in an alternative form from (5.27).

$$d_{\Gamma_\varepsilon}(\boldsymbol{x}_\varepsilon) = \inf_{y\in\mathcal{S}} \|\boldsymbol{x}_\varepsilon - y\|. \tag{5.43}$$

In this form it should be clearer that for ε small enough

$$|d_{\Gamma_\varepsilon}(\boldsymbol{x}_\varepsilon(t)) - d_{\Gamma_0}(\boldsymbol{x}_0(t))| \leq \|\boldsymbol{p}_\varepsilon(\boldsymbol{x}_0(t),t) - \boldsymbol{x}_0(t)\|. \tag{5.44}$$

Thus we may conclude that

$$d_{\Gamma_\varepsilon}(\boldsymbol{x}_\varepsilon) = d_{\Gamma_0}(\boldsymbol{x}_0) + \mathcal{O}(\varepsilon) \tag{5.45}$$

We will assume a Taylor series expansion is possible for the following fields

$$\phi_\varepsilon(\boldsymbol{x}_\varepsilon(t),t) = \phi_0(\boldsymbol{x}_0(t),t) + \varepsilon\phi_1(\boldsymbol{x}_0(t),t) + \varepsilon^2\phi_2(\boldsymbol{x}_0(t),t) + ... \tag{5.46}$$

$$\pi_\varepsilon(\boldsymbol{x}_\varepsilon(t),t) = \pi_0(\boldsymbol{x}_0(t),t) + \varepsilon\pi_1(\boldsymbol{x}_0(t),t) + \varepsilon^2\pi_2(\boldsymbol{x}_0(t),t) + ... \tag{5.47}$$

$$c_\varepsilon(\boldsymbol{x}_\varepsilon(t),t) = c_0(\boldsymbol{x}_0(t),t) + \varepsilon c_1(\boldsymbol{x}_0(t),t) + \varepsilon^2 c_2(\boldsymbol{x}_0(t),t) + ... \tag{5.48}$$

$$\chi_\varepsilon(\boldsymbol{x}_\varepsilon(t),t) = \chi_0(\boldsymbol{x}_0(t),t) + \varepsilon\chi_1(\boldsymbol{x}_0(t),t) + \varepsilon^2\chi_2(\boldsymbol{x}_0(t),t) + ... \tag{5.49}$$

$$\boldsymbol{\sigma}_\varepsilon(\boldsymbol{x}_\varepsilon(t),t) = \boldsymbol{\sigma}_0(\boldsymbol{x}_0(t),t) + \varepsilon\boldsymbol{\sigma}_1(\boldsymbol{x}_0(t),t) + \varepsilon^2\boldsymbol{\sigma}_2(\boldsymbol{x}_0(t),t) + ... \tag{5.50}$$

Similar ε expansions of the Weingarten map, $\nabla_{\Gamma_\varepsilon}\boldsymbol{\nu}_\varepsilon$, the mean curvature $\kappa_{m,\varepsilon}$ and the Gaussian curvature, $\kappa_{g,\varepsilon}$, will follow as a result of expanding the differential operators.

5.5.2 Expanding Gradient Operators

With the above set up in mind we aim to express the differential operators expressed on Γ_ε in terms of differential operators expressed on Γ_0 with corrections written to each order in ε. For the spatial operators we have suppressed the t dependence for ease of reading.

Proposition 5.5.1. *For a function $f : \Gamma_\varepsilon(t) \to \mathbb{R}$ and a vector $\boldsymbol{f} : \Gamma_\varepsilon(t) \to \mathbb{R}^{n+1}$, with $\boldsymbol{x}_\varepsilon(t) = \boldsymbol{p}_\varepsilon(\boldsymbol{x}_0(t),t)$ and $x_0(t) \in \Gamma_0(t)$, we may express the following differential*

operators on $\Gamma_\varepsilon(t)$ in terms of operators on $\Gamma_0(t)$.

$$\nabla_{\Gamma_\varepsilon} f(\boldsymbol{x}_\varepsilon) = \nabla_{\Gamma_0}(f\circ\boldsymbol{p}_\varepsilon)(\boldsymbol{x}_0) - \varepsilon\nabla_{\Gamma_0}\boldsymbol{p}_1^T(\boldsymbol{x}_0)\nabla_{\Gamma_0}(f\circ\boldsymbol{p}_\varepsilon)(\boldsymbol{x}_0) + \mathcal{O}(\varepsilon^2) \tag{5.51}$$

$$\nabla_{\Gamma_\varepsilon}\cdot\boldsymbol{f}(\boldsymbol{x}_\varepsilon) = \nabla_{\Gamma_0}\cdot(\boldsymbol{f}\circ\boldsymbol{p}_\varepsilon)(\boldsymbol{x}_0) - \varepsilon\nabla_{\Gamma_0}\boldsymbol{p}_1(\boldsymbol{x}_0) : \nabla_{\Gamma_0}(\boldsymbol{f}\circ\boldsymbol{p}_\varepsilon)(\boldsymbol{x}_0) + \mathcal{O}(\varepsilon^2) \tag{5.52}$$

$$\Delta_{\Gamma_\varepsilon} f(\boldsymbol{x}_\varepsilon) = \Delta_{\Gamma_0}(f\circ\boldsymbol{p}_\varepsilon)(\boldsymbol{x}_0) - \varepsilon\Delta_{\Gamma_0}\boldsymbol{p}_1(\boldsymbol{x}_0)\cdot\nabla_{\Gamma_0}(f\circ\boldsymbol{p}_\varepsilon)(\boldsymbol{x}_0) \tag{5.53}$$

$$-2\varepsilon\nabla_{\Gamma_0}\boldsymbol{p}_1(\boldsymbol{x}_0) : \nabla^2_{\Gamma_0}(f\circ\boldsymbol{p}_\varepsilon)(\boldsymbol{x}_0) + \mathcal{O}(\varepsilon^2) \tag{5.54}$$

$$\partial^\bullet_{\Gamma_\varepsilon(t)} f(\boldsymbol{x}_\varepsilon(t),t) = \partial^\bullet_{\Gamma_0(t)}(f\circ\boldsymbol{p}_\varepsilon)(\boldsymbol{x}_0(t),t) \tag{5.55}$$

$$+\varepsilon\nabla\tilde{f}(\boldsymbol{x}_0(t),t)\cdot\Big(\partial^\bullet_{\Gamma_0(t)}\boldsymbol{p}_1(\boldsymbol{x}_0(t),t) - \nabla\tilde{\boldsymbol{p}}_1^T(\boldsymbol{x}_0(t),t)\boldsymbol{v}_0(\boldsymbol{x}_0(t))\Big) + \mathcal{O}(\varepsilon^2) \tag{5.56}$$

Proof:

1. Let $\boldsymbol{\tau}\in T_{\boldsymbol{x}_0}\Gamma_0$ then by the chain rule

$$\nabla_{\Gamma_0}(f\circ\boldsymbol{p}_\varepsilon)(\boldsymbol{x}_0)\cdot\boldsymbol{\tau} = \nabla_{\Gamma_\varepsilon} f(\boldsymbol{x}_\varepsilon)\cdot\nabla_{\Gamma_0}\boldsymbol{p}_\varepsilon(\boldsymbol{x}_0)\boldsymbol{\tau}$$

since $\boldsymbol{p}_\varepsilon:\Gamma_0\to\Gamma_\varepsilon$, it is the case that $\nabla_{\Gamma_0}\boldsymbol{p}_\varepsilon : T_{\boldsymbol{x}_0}\Gamma_0\to T_{\boldsymbol{p}_\varepsilon(\boldsymbol{x}_0)}\Gamma_\varepsilon$. Furthermore since the parameterisation is a regular map we can conclude that for any $\boldsymbol{\tau}_\varepsilon\in T_{\boldsymbol{p}_\varepsilon(\boldsymbol{x}_0)}\Gamma_\varepsilon$ that

$$\begin{aligned}\nabla_{\Gamma_\varepsilon} f(\boldsymbol{x}_\varepsilon)\cdot\boldsymbol{\tau}_\varepsilon &= \nabla_{\Gamma_0}(f\circ\boldsymbol{p}_\varepsilon)(\boldsymbol{x}_0)\cdot(\nabla_{\Gamma_0}\boldsymbol{p}_\varepsilon(\boldsymbol{x}_0))^{-1}\boldsymbol{\tau}_\varepsilon\\ &= ((\nabla_{\Gamma_0}\boldsymbol{p}_\varepsilon(\boldsymbol{x}_0))^{-1})^T\nabla_{\Gamma_0}(f\circ\boldsymbol{p}_\varepsilon)(\boldsymbol{x}_0)\cdot\boldsymbol{\tau}_\varepsilon.\end{aligned}$$

Using the identity $(\boldsymbol{I}-\boldsymbol{A})^{-1}=\sum_{i=0}^\infty\boldsymbol{A}^i$ for every matrix $\boldsymbol{A}$ with $\|\boldsymbol{A}\|<1$ we obtain (5.51).

2. Observing that for any surface, Γ, that $\nabla_\Gamma\cdot\boldsymbol{f} := \text{tr}\,(\nabla_\Gamma\boldsymbol{f})$ we may use (5.51) to see that

$$\begin{aligned}\nabla_{\Gamma_\varepsilon}\cdot\boldsymbol{f}(\boldsymbol{x}_\varepsilon) &= \text{tr}\,(\nabla_{\Gamma_\varepsilon}\boldsymbol{f}(\boldsymbol{x}_\varepsilon))\\ &= \text{tr}\,\left(\nabla_{\Gamma_0}(\boldsymbol{f}\circ\boldsymbol{p}_\varepsilon)(\boldsymbol{x}_0) - \varepsilon\nabla_{\Gamma_0}\boldsymbol{p}_1(\boldsymbol{x}_0)^T\nabla_{\Gamma_0}(\boldsymbol{f}\circ\boldsymbol{p}_\varepsilon)(\boldsymbol{x}_0) + \mathcal{O}(\varepsilon^2)\right)\end{aligned}$$

It is clear that

$$\text{tr}\,(\nabla_{\Gamma_0}(\boldsymbol{f}\circ\boldsymbol{p}_\varepsilon)(\boldsymbol{x}_0)) = \nabla_{\Gamma_0}\cdot(\boldsymbol{f}\circ\boldsymbol{p}_\varepsilon)(\boldsymbol{x}_0)$$

Then using that for any matrix, $\boldsymbol{A}$, that tr $\boldsymbol{A} = \mathbf{1} : \boldsymbol{A}$ we see

$$\text{tr } \left(\nabla_{\Gamma_0} \boldsymbol{p}_1(\boldsymbol{x}_0)^T \nabla_{\Gamma_0} (\boldsymbol{f} \circ \boldsymbol{p}_\varepsilon)(\boldsymbol{x}_0)\right) = \mathbf{1} : \nabla_{\Gamma_0} \boldsymbol{p}_1(\boldsymbol{x}_0)^T \nabla_{\Gamma_0} (\boldsymbol{f} \circ \boldsymbol{p}_\varepsilon)(\boldsymbol{x}_0)$$

from which the result follows using the cyclic permutation property of the tensor scalar product.

3. We obtain this result using the identity $\Delta_{\Gamma_\varepsilon} f(\boldsymbol{x}_\varepsilon) = \text{tr } (\nabla_{\Gamma_\varepsilon} \nabla_{\Gamma_\varepsilon} f(\boldsymbol{x}_\varepsilon))$ applying (5.51) twice and rearranging. In detail

$$\begin{aligned}
\text{tr } (\nabla_{\Gamma_\varepsilon} \nabla_{\Gamma_\varepsilon} f(\boldsymbol{x}_\varepsilon)) &= \text{tr } \left(\nabla_{\Gamma_\varepsilon} \left[\nabla_{\Gamma_0} (f \circ \boldsymbol{p}_\varepsilon)(\boldsymbol{x}_0) - \varepsilon \nabla_{\Gamma_0} \boldsymbol{p}_1(\boldsymbol{x}_0)^T \nabla_{\Gamma_0} (f \circ \boldsymbol{p}_\varepsilon)(\boldsymbol{x}_0)\right]\right) \\
&= \text{tr } \left(\nabla^2_{\Gamma_0} (f \circ \boldsymbol{p}_\varepsilon)(\boldsymbol{x}_0) - \varepsilon \nabla_{\Gamma_0} (\nabla_{\Gamma_0} \boldsymbol{p}_1(\boldsymbol{x}_0)^T \nabla_{\Gamma_0} (f \circ \boldsymbol{p}_\varepsilon)(\boldsymbol{x}_0))\right. \\
&\quad \left. - \varepsilon \nabla_{\Gamma_0} \boldsymbol{p}_1(\boldsymbol{x}_0)^T \nabla^2_{\Gamma_0} (f \circ \boldsymbol{p}_\varepsilon)(\boldsymbol{x}_0)\right) + \mathcal{O}(\varepsilon^2) \\
&= \Delta_{\Gamma_0} (f \circ \boldsymbol{p}_\varepsilon)(\boldsymbol{x}_0) - \nabla_{\Gamma_0} \cdot \left(\nabla_{\Gamma_0} \boldsymbol{p}_1(\boldsymbol{x}_0)^T \nabla_{\Gamma_0} (f \circ \boldsymbol{p}_\varepsilon)(\boldsymbol{x}_0)\right) \\
&\quad - \varepsilon \text{ tr } \left(\nabla_{\Gamma_0} \boldsymbol{p}_1(\boldsymbol{x}_0)^T \nabla^2_{\Gamma_0} (f \circ \boldsymbol{p}_\varepsilon)(\boldsymbol{x}_0)\right) + \mathcal{O}(\varepsilon^2).
\end{aligned}$$

Applying the divergence product rule gives the result.

4. We start by expressing the material derivative on $\Gamma_\varepsilon(t)$ as the total time derivative for the trajectory of a material point, so that

$$\partial^\bullet_{\Gamma_\varepsilon(t)} f(\boldsymbol{x}_\varepsilon, t) = \frac{d}{dt} f(\boldsymbol{x}_\varepsilon(t), t) = \partial_t \tilde{f}(\boldsymbol{x}_\varepsilon(t), t) + \nabla \tilde{f}(\boldsymbol{x}_\varepsilon(t), t) \frac{d}{dt} \boldsymbol{p}_\varepsilon(\boldsymbol{x}_0(t), t)$$

using (5.40)-(5.42) we can expand the term $\frac{d}{dt} \boldsymbol{p}_\varepsilon(\boldsymbol{x}(t), t)$ as a power series in ε. Thus it remains to identify an expansion for the gradient operator. We consider the natural identity extension of $\boldsymbol{x}_\varepsilon$ and $\boldsymbol{x}_0$ off $\Gamma_\varepsilon(t)$ and $\Gamma_0(t)$ respectively. We assume an extension, $\tilde{\boldsymbol{p}}_\varepsilon$ of $\boldsymbol{p}_\varepsilon$ off Γ_0 with individual extensions of its expansion terms, $\tilde{\boldsymbol{p}}_i$, that maintains a local bijection between the identity maps. Under this set up, as an application of the chain rule it can be shown that

$$\nabla_{\boldsymbol{x}_\varepsilon} f(\boldsymbol{x}_\varepsilon(t), t) = \nabla_{\boldsymbol{x}_0} (f \circ \boldsymbol{p}_\varepsilon)(\boldsymbol{x}_0, t) - \varepsilon \nabla_{\boldsymbol{x}_0} \tilde{\boldsymbol{p}}_1(\boldsymbol{x}_0, t)^T \nabla_{\boldsymbol{x}_0} (f \circ \boldsymbol{p}_\varepsilon)(\boldsymbol{x}_0, t) + \mathcal{O}(\varepsilon^2). \tag{5.57}$$

With the expansion of the gradient identified we have

$$\begin{aligned}
&\nabla \tilde{f}(\boldsymbol{x}_\varepsilon(t), t) \frac{d}{dt} \boldsymbol{p}_\varepsilon(\boldsymbol{x}_0(t), t) && (5.58) \\
&\quad = \boldsymbol{v}_0(\boldsymbol{x}_0(t), t) \nabla (f \circ \boldsymbol{p}_\varepsilon)(\boldsymbol{x}_0(t), t) && (5.59) \\
&\quad + \varepsilon \nabla \tilde{f}(\boldsymbol{x}_0(t), t) \cdot \left(\partial^\bullet_{\Gamma_0(t)} \boldsymbol{p}_1(\boldsymbol{x}_0(t), t) - \nabla \tilde{\boldsymbol{p}}_1(\boldsymbol{x}_0(t), t)^T \boldsymbol{v}_0(\boldsymbol{x}_0(t), t)\right) + \mathcal{O}(\varepsilon^2) && (5.60)
\end{aligned}$$

Adding the partial time derivative and grouping the resulting terms which are independent of ε into the material derivative, $\partial^{\bullet}_{\Gamma_0(t)}(f \circ \boldsymbol{p}_\varepsilon)(\boldsymbol{x}_0(t), t)$, the result follows.

□

5.5.3 Outer Solutions

Inserting the expansions (5.46)-(5.49), as well as the expansion of the velocity, (5.40)-(5.42) into equations (5.12)-(5.18) and combined with the gradient expansions of Prop. 5.5.1 we expand all terms in ε and match by powers.

To the lowest order ε^{-1}, from equation (5.16) we obtain

$$\theta'(\phi_0) = 0. \tag{5.61}$$

There are 3 solutions to this equation, namely $\phi_0 = \phi^{\pm}$ and $\phi_0 = \frac{\phi^+ + \phi^-}{2}$. The later is an unstable steady state solution and in line with our assumptions on the decomposition of the domain we must conclude that in the outer region we have $\phi_0 = \phi^{\pm}$. To the next order, ε^0, we obtain the following set of equations:

$$\begin{aligned}
\nabla_{\Gamma_0(t)} \cdot \boldsymbol{\sigma}_0 &= \Delta_{\Gamma_0(t)} \left(b_k(\phi_0, c_0)(\kappa_{m,0} - \kappa_s(\phi_0, c_0)) \right) \boldsymbol{\nu}_0 + \\
&+ \left(|\nabla_{\Gamma_0(t)} \boldsymbol{\nu}_0|^2 \boldsymbol{\nu}_0 + \nabla_{\Gamma_0(t)} \kappa_{m,0} \right) b_k(\phi_0, c_0)(\kappa_{m,0} - \kappa_s(\phi_0, c_0)) \\
&+ \boldsymbol{\nu}_0 \nabla_{\Gamma_0(t)} \cdot \left((\kappa_{m,0} \mathbb{I} + \nabla_{\Gamma_0(t)} \boldsymbol{\nu}_0) b_{g,c}(\phi_0, c_0) \nabla_{\Gamma_0(t)} c_0 \right) \\
&+ p_{0,d_{\Gamma_0}}(\phi_0, c_0, d_{\mathcal{S}}) \boldsymbol{\nu}_{\mathcal{S}} + \kappa_{g,0} \nabla_{\Gamma_0(t)} b_g(\phi_0, c_0) \\
\boldsymbol{\sigma}_0 &= -\pi_0 \boldsymbol{P}_0 + 2\mu(\phi_0) D_{\Gamma_0} \boldsymbol{v}_0 \\
\nabla_{\Gamma_0(t)} \cdot \boldsymbol{v}_0 &= 0 \\
0 &= \theta'(\phi_0)\phi_1 \\
\partial^{\bullet}_{\Gamma_0(t)} c_0 + c_0 \nabla_{\Gamma_0(t)} \cdot \boldsymbol{v}_0 &= \nabla_{\Gamma_0(t)} \cdot \left(M_c(\phi_0, c_0) \nabla_{\Gamma_0(t)} \chi_0 \right) \\
\chi_0 &= \frac{1}{2} b_{k,c}(\phi_0, c_0) |\kappa_{m,0} - \kappa_s(\phi_0, c_0)|^2 \\
&+ b_k(\phi_0, c_0)(\kappa_{m,0} - \kappa_s(\phi_0, c_0)) k_{s,c}(\phi_0, c_0) \\
&+ b_{g,c}(\phi_0, c_0) \kappa_{g,0} + f_{0,c} + p_{0,c}
\end{aligned}$$

Using the information derived from (5.61) with the equation $\theta'(\phi_0)\phi_1 = 0$ we can first conclude that the first order correction to the phase field variable is zero and thus that $\delta(\phi, \nabla_\Gamma \phi) = \mathcal{O}(\varepsilon)$. Recalling that for an arbitrary ϕ dependent function that $b^{\pm} := b(\phi^{\pm})$, we recover the bulk equations from Problem 5.2.1 if we drop the subscript 0.

5.5.4 Interface Coordinates

Since the thickness of the layer between phases scales with ε, we want to blow it up to unit length in order to be able to study the limit of fields and functions as $\varepsilon \to 0$ in a sensible manner. We therefore introduce the scaled (geodesic) distance on $\Gamma_0(t)$ to the interface $\Lambda_0(t)$ by

$$z := \frac{r}{\varepsilon}. \tag{5.62}$$

It is with respect to the new coordinates (s, z, t) we choose to work with in the interfacial layer. But before we state the (inner) expansions of the fields in these coordinates and state the matching conditions with the outer expansions in the adjacent domains we need to discuss how the differential operators transform by the change of coordinates.

With regards to the spatial differential operators we may proceed as in Elliott and Stinner [2010a]. For fixed t consider the inversion of the map $R_\Lambda(t)S^1 \times [-\bar{\varepsilon}, \bar{\varepsilon}] \ni (s, r) \to \boldsymbol{x}_{\Gamma_0(t)}(s, r, t) \in \Gamma(t)$ and let $\boldsymbol{x} \in \Gamma_0(t)$ be a point with a distance to $\Lambda_0(t)$ which is $\mathcal{O}(\varepsilon)$. The identity (2.16) implies that $\varepsilon \nabla_{\Gamma_0(t)} z(\boldsymbol{x}, t) = \nabla_{\Gamma_0(t)} r(\boldsymbol{x}, t) = \boldsymbol{\mu}(\boldsymbol{x}, t)$. Taylor expanding in $\boldsymbol{x}_{\Lambda_0} := \lambda(s, t)$ then yields

$$\nabla_{\Gamma_0(t)} z(\boldsymbol{x}, t) = \frac{1}{\varepsilon} \boldsymbol{\mu}_{\Lambda_0}(\boldsymbol{x}_{\Lambda_0}, t) + \nabla_{\Gamma_0(t)} \boldsymbol{\mu}(\boldsymbol{x}_{\Lambda_0}, t) \boldsymbol{\mu}_{\Lambda_0}(\boldsymbol{x}_{\Lambda_0}, t) z(\boldsymbol{x}, t) + \mathcal{O}(\varepsilon).$$

Similarly we see that

$$\nabla_{\Gamma_0(t)} s(\boldsymbol{x}, t) = \boldsymbol{\tau}_{\Lambda_0}(\boldsymbol{x}_{\Lambda_0}, t) + \mathcal{O}(\varepsilon), \tag{5.63}$$

$$\boldsymbol{\nu}(\boldsymbol{x}, t) = \boldsymbol{\nu}_{\Lambda_0}(\boldsymbol{x}_{\Lambda_0}, t) + \varepsilon z(\boldsymbol{x}, t) \nabla_{\Gamma_0(t)} \boldsymbol{\nu}(\boldsymbol{x}_{\Lambda_0}, t) \boldsymbol{\mu}_{\Lambda_0}(\boldsymbol{x}_{\Lambda_0}, t) + \mathcal{O}(\varepsilon^2). \tag{5.64}$$

For a scalar field $f : \Gamma_0(t) \to \mathbb{R}$ and a vector field $\boldsymbol{f} : \Gamma_0(t) \to \mathbb{R}$ define $f(\boldsymbol{x}, t) = F(s, z, t)$ and $\boldsymbol{f}(\boldsymbol{x}, t) = \boldsymbol{F}(s, z, t)$ close to $\Lambda_0(t)$. Then we obtain for the surface gradient and the surface divergence in the new coordinates

$$\begin{aligned}
\nabla_{\Gamma_0(t)} f(\boldsymbol{x}, t) &= F_s(s, z, t) \nabla_{\Gamma_0(t)} s + F_z(s, z, t) \nabla_{\Gamma_0(t)} z \\
&= \tfrac{1}{\varepsilon} F_z(s, z, t) \boldsymbol{\mu}_{\Lambda_0}(\boldsymbol{x}_{\Lambda_0}, t) + \Phi_s(s, z, t) \boldsymbol{\tau}_{\Lambda_0}(\boldsymbol{x}_{\Lambda_0}, t) \\
&+ F_z(s, z, t) \nabla_{\Gamma_0(t)} \boldsymbol{\mu}(\boldsymbol{x}_{\Lambda_0}, t)\, \boldsymbol{\mu}_{\Lambda_0}(\boldsymbol{x}_{\Lambda_0}, t) z + \mathcal{O}(\varepsilon), \qquad (5.65a) \\
\nabla_{\Gamma_0(t)} \cdot \boldsymbol{f}(\boldsymbol{x}, t) &= \boldsymbol{F}_s(s, z, t) \cdot \nabla_{\Gamma_0(t)} s + \boldsymbol{F}_z(s, z, t) \cdot \nabla_{\Gamma_0(t)} z \\
&= \tfrac{1}{\varepsilon} \boldsymbol{F}_z(s, z, t) \cdot \boldsymbol{\mu}_{\Lambda_0}(\boldsymbol{x}_{\Lambda_0}, t) \boldsymbol{F}_s(s, z, t) \cdot \boldsymbol{\tau}_{\Lambda_0}(\boldsymbol{x}_{\Lambda_0}, t) \\
&+ \boldsymbol{F}_z(s, z, t) \cdot \nabla_{\Gamma_0(t)} \boldsymbol{\mu}(\boldsymbol{x}_{\Lambda_0}, t) \boldsymbol{\mu}_{\Lambda_0}(\boldsymbol{x}_{\Lambda_0}, t) z + \mathcal{O}(\varepsilon). \qquad (5.65b)
\end{aligned}$$

Using these identities, (2.14), and (2.15), a short calculation shows that we can write

for the Laplace-Beltrami operator

$$\Delta_{\Gamma_0(t)} f(\boldsymbol{x},t) = \frac{1}{\varepsilon^2} F_{zz}(s,z,t) - \frac{1}{\varepsilon}\kappa_{\Lambda_0}(\boldsymbol{x}_{\Lambda_0},t) F_z(s,z,t) + \mathcal{O}(\varepsilon^0). \tag{5.66}$$

With regards to the operator $\partial^\bullet_{\Gamma_0(t)}$, we may follow the procedure as in Chapter 3 to see

$$\partial^\bullet_{\Gamma_0(t)} f(\boldsymbol{x},t) = F_s(s,z,t)\partial^\bullet_{\Gamma_0(t)} s(\boldsymbol{x},t) + F_z(s,z,t)\partial^\bullet_{\Gamma_0(t)} z(\boldsymbol{x},t)$$

and $\partial^\bullet_{\Gamma_0(t)} z = \frac{1}{\varepsilon}\partial^\bullet_{\Gamma_0(t)} r$ with

$$\partial^\bullet_{\Gamma_0(t)} r(\boldsymbol{x},t) = (\boldsymbol{v}(\boldsymbol{x}_{\Lambda_0},t) - \boldsymbol{v}_{\Lambda_0}(\boldsymbol{x}_{\Lambda_0},t)) \cdot \boldsymbol{\mu}_{\Lambda_0}(\boldsymbol{x}_{\Lambda_0},t) + \mathcal{O}(\varepsilon)$$

so that

$$\partial^\bullet_{\Gamma_0(t)} f(\boldsymbol{x},t) = \frac{1}{\varepsilon} F_z(s,z,t)(\boldsymbol{v}(\boldsymbol{x}_{\Lambda_0},t) - \boldsymbol{v}_{\Lambda_0}(\boldsymbol{x}_{\Lambda_0},t)) \cdot \boldsymbol{\mu}_{\Lambda_0}(\boldsymbol{x}_{\Lambda_0},t) + \mathcal{O}(\varepsilon^0). \tag{5.67}$$

As with the outer region we then suppose a power series expansion in ε for the inner field such that

$$F(s,z,t) = F_0(s,z,t) + \varepsilon F_1(s,z,t) + \mathcal{O}(\varepsilon^2). \tag{5.68}$$

5.5.5 Matching conditions

In light of the two expansions for a field, f_ε, one valid away from the interface and the other, expressed in rescaled coordinates, valid close to the interface. There should be some intermediary region for which the two expansions match. Given the two sets of expansions functions, $\{f_i\}$ and $\{F_i\}$, there are a set of matching conditions that these functions should satisfy. These conditions are related to the spatial coordinates only and, thus, are independent of the movement of the domain. Therefore and because a full derivation can be found in the literature (for instance, see Garke and Stinner [2006b]) we only state them here: In the limit as $z \to \pm\infty$

$$\begin{aligned}
F_0(s,z,t) &\sim f_0^\pm(\boldsymbol{x}_{\Lambda_0},t), && (5.69a)\\
\partial_z F_0(s,z,t) &\sim 0, && (5.69b)\\
F_1(s,z,t) &\sim f_1^\pm(\boldsymbol{x}_{\Lambda_0},t) \pm \nabla_{\Gamma_0(t)} f_0^\pm(\boldsymbol{x}_{\Lambda_0},t) \cdot \boldsymbol{\mu}_{\Lambda_0}(\boldsymbol{x}_{\Lambda_0},t) z, && (5.69c)\\
\partial_z F_1(s,z,t) &\sim \pm\nabla_{\Gamma_0(t)} f_0^\pm(\boldsymbol{x}_{\Lambda_0},t) \cdot \boldsymbol{\mu}_{\Lambda_0}(\boldsymbol{x}_{\Lambda_0},t), && (5.69d)\\
\partial_z F_2(s,z,t) &\sim \pm\nabla_{\Gamma_0(t)} f_1^\pm(\boldsymbol{x}_{\Lambda_0},t) \cdot \boldsymbol{\mu}_{\Lambda_0}(\boldsymbol{x}_{\Lambda_0},t) && (5.69e)\\
&\quad + \big(\boldsymbol{\mu}_{\Lambda_0}(\boldsymbol{x}_{\Lambda_0},t) \cdot \nabla_{\Gamma_0(t)}\big)^2 f_0^\pm(\boldsymbol{x}_{\Lambda_0},t) z.
\end{aligned}$$

Recalling (2.21) we assume that in the inner region we have expansions of the decomposed curvature functions such that

$$\kappa_{\boldsymbol{\nu},\varepsilon}(\boldsymbol{p}_\varepsilon(\boldsymbol{x})) = K_{\boldsymbol{\nu},0}(s) + \varepsilon K_{\boldsymbol{\nu},1}(s,z) + \mathcal{O}(\varepsilon^2) \tag{5.70}$$

$$\kappa_{d,\varepsilon}(\boldsymbol{p}_\varepsilon(\boldsymbol{x})) = K_{d,0}(s) + \varepsilon K_{d,1}(s,z) + \mathcal{O}(\varepsilon^2) \tag{5.71}$$

$$\kappa_{p,\varepsilon}(\boldsymbol{p}_\varepsilon(\boldsymbol{x})) = K_{p,0}(s,z) + \varepsilon K_{p,1}(s,z) + \mathcal{O}(\varepsilon^2). \tag{5.72}$$

Recall our assumption that $\Gamma_0(t)$ be C^1 across $\Lambda_0(t)$. Thus the quantities $\kappa_{\boldsymbol{\nu}}$ and κ_d are continuous in the limit. The matching condition (5.69a) motivates the assumption that $K_{\boldsymbol{\nu},0}$ and $K_{d,0}$ are independent of z.

5.5.6 Inner Solutions

Employing inner expansions of the form (5.68) for the additional fields, combined with the change of variable formulae (5.65), (5.66) and (5.67) we insert all of these expansions into the governing equations (5.12)-(5.18), expand and match powers of ε.

We begin our analysis by considering the result of (5.16) at the order ε^{-1}.

$$0 = \partial_{zz}\Phi_0 + \theta'(\Phi_0). \tag{5.73}$$

Using the matching conditions (5.69a) this gives the standard phase profile which is independent of the interface parametrisation variable, s:

$$\Phi_0(z) = \frac{\phi^+ - \phi^-}{2}\tanh\left(\frac{z}{\sqrt{k_\theta}}\right) + \frac{\phi^+ + \phi^-}{2}. \tag{5.74}$$

Multiplying (5.73) by $\partial_z\Phi_0$ and integrating with respect to z from $-\infty$ to $\tilde{z}$ we obtain the equation often referred to as equipartition of energy

$$\theta(\Phi_0(\tilde{z})) = \frac{1}{2}|\partial_z\Phi_0(\tilde{z})|^2. \tag{5.75}$$

At the same order from (5.15) we have

$$\boldsymbol{\mu}_{\Lambda_0} \cdot \partial_z \boldsymbol{V}_0 = 0. \tag{5.76}$$

Integrating this over the interfacial region gives continuity of the surface velocity in the direction of the co-normal. If we remain at the same order again and consider

(5.14) we obtain

$$0 = \mu(\Phi_0)\boldsymbol{P}_0 \left(\partial_z \boldsymbol{V}_0 \otimes \boldsymbol{\mu}_{\Lambda_0} + \boldsymbol{\mu}_{\Lambda_0} \otimes \partial_z \boldsymbol{V}_0\right) \boldsymbol{P}_0. \tag{5.77}$$

Applying this tensor to $\boldsymbol{\mu}_{\Lambda_0}$ we obtain, using that $\mu(\Phi_0)$ is strictly positive, that

$$\boldsymbol{P_0}\partial_z \boldsymbol{V}_0 = 0. \tag{5.78}$$

From (5.78) we have that the tangential portion of the velocity is continuous. Recall by assumption the normal component of the surface velocity is continuous across the interface, thus from (5.78) we may conclude that each component of the velocity is continuous across the interface, that is

$$[\boldsymbol{v}_0] = 0. \tag{5.79}$$

We now turn to (5.12) and it's order ε^{-2} terms, from which we see

$$0 = \left(b_k(\Phi_0, C_0)(K_{\boldsymbol{\nu},0} + K_{p,0} - \kappa_s(\Phi_0, C_0))\right)_{zz} + \left(K_{v,0} b_g(\Phi_0, C_0)\right)_{zz} \tag{5.80}$$

Let us define the zero order term

$$Q_0 := b_k(\Phi_0, C_0)\left(K_{\boldsymbol{\nu},0} + K_{p,0} - \kappa_s(\Phi_0, C_0)\right) + K_{v,0} b_g(\Phi_0, C_0). \tag{5.81}$$

then (5.80) can be expressed as $0 = \partial_{zz} Q_0$. Thus Q_0 is a degree 1 polynomial in z and since Q_0 is a composition of zero order terms, the matching conditions (5.69b), imply that $\partial_z Q_0 = 0$. Hence we may integrate over the interfacial region to conclude that

$$0 = \left[b_k(\kappa_{\boldsymbol{\nu},0} + \kappa_{p,0} - \kappa_s) + \kappa_{\boldsymbol{\nu},0} b_g\right]. \tag{5.82}$$

Now consider the function

$$\gamma(\kappa_p, \phi, c, \kappa_{\boldsymbol{\nu}}, \kappa_d) := \frac{1}{2} b_k(\phi, c)|\kappa_{\boldsymbol{\nu}} + \kappa_p - \kappa_s(\phi, c)|^2 + b_g(\phi, c)(\kappa_{\boldsymbol{\nu}}\kappa_p - \kappa_d^2). \tag{5.83}$$

We denote the partial derivative of this function with respect to κ_p by

$$q(\kappa_p, \phi, \kappa_{\boldsymbol{\nu}}, \kappa_d) := \partial_{\kappa_p}\gamma(\kappa_p, \phi, c, \kappa_{\boldsymbol{\nu}}, \kappa_d) = b_k(\phi, c)(\kappa_{\boldsymbol{\nu}} + \kappa_p - \kappa_s(\phi, c)) + b_g(\phi, c)\kappa_{\boldsymbol{\nu}} \tag{5.84}$$

and we may invert this relationship and thus write

$$\kappa_p = \kappa_p(q, \phi, c, \kappa_{\boldsymbol{\nu}}, \kappa_d) = \frac{1}{b_k(\phi, c)}(q - b_g(\phi, c)\kappa_{\boldsymbol{\nu}}) - \kappa_{\boldsymbol{\nu}} + \kappa_s(\phi, c).$$

The Legendre transform of (5.83) in the variable κ_p is given by

$$l(q,\phi,c,\kappa_{\boldsymbol{\nu}},\kappa_d) := \gamma(\kappa_p(q,\phi,c,\kappa_{\boldsymbol{\nu}},\kappa_d),\phi,\kappa_{\boldsymbol{\nu}},\kappa_d) - q\kappa_p(q,\phi,c,\kappa_{\boldsymbol{\nu}},\kappa_d) \tag{5.85}$$

which satisfies $\partial_\phi l = \partial_\phi \gamma$ and $\partial_c l = \partial_c \gamma$. The exact form of the Legendre transform of γ is given as

$$\begin{aligned} l(q(\kappa_p,\phi,c,\kappa_{\boldsymbol{\nu}},\kappa_d),\phi,\kappa_{\boldsymbol{\nu}},\kappa_d) =& \frac{1}{2}b_k(\phi,c)|\kappa_{\boldsymbol{\nu}}+\kappa_p-\kappa_s(\phi,c)|^2 + b_g(\phi,c)(\kappa_{\boldsymbol{\nu}}\kappa_p-\kappa_d^2) \\ &- b_k(\phi,c)(\kappa_{\boldsymbol{\nu}}+\kappa_p-\kappa_s(\phi,c))\kappa_p - b_g(\phi,c)\kappa_{\boldsymbol{\nu}}\kappa_p. \end{aligned} \tag{5.86}$$

Observe that $Q_0 = q(K_{p,0},\Phi_0,C_0,K_{\boldsymbol{\nu},0},K_{d,0})$ and using that $\partial_z Q_0 = 0$ with the matching condition (5.69a) we see that

$$\begin{aligned} &\int_{-\infty}^{\infty} \partial_\phi\gamma(K_{p,0},\Phi_0,K_{\boldsymbol{\nu},0},K_{d,0})\partial_z\Phi_0 + \partial_c\gamma(K_{p,0},\Phi_0,K_{\boldsymbol{\nu},0},K_{d,0})\partial_z C_0 \\ =&\int_{-\infty}^{\infty} \partial_\phi l(Q_0,\Phi_0,K_{\boldsymbol{\nu},0},K_{d,0})\partial_z\Phi_0 + \partial_c l(K_{p,0},\Phi_0,K_{\boldsymbol{\nu},0},K_{d,0})\partial_z C_0 + \partial_q l(Q_0,\Phi_0,K_{\boldsymbol{\nu},0},K_{d,0})\partial_z Q_0 \\ =&\int_{-\infty}^{\infty} \partial_z l(Q_0,\Phi_0,K_{\boldsymbol{\nu},0},K_{d,0}) = [l(Q_0,\phi_0,\kappa_{\boldsymbol{\nu},0},\kappa_{d,0})]. \end{aligned}$$

For the third line we have used that $K_{\boldsymbol{\nu},0}$ and $K_{d,0}$ are independent of z.

Looking to order ε^0 from (5.16) we obtain

$$-\omega(\boldsymbol{v}_0-\boldsymbol{v}_{\Lambda_0})\cdot\boldsymbol{\mu}_{\Lambda_0}\partial_z\Phi_0 = \frac{1}{2}b_{k,\phi}(\Phi_0,C_0)|K_{\boldsymbol{\nu},0}+K_{p,0}-\kappa_s(\Phi_0,C_0)|^2 \tag{5.87}$$

$$\begin{aligned} &- b_k(\Phi_0,C_0)(K_{\boldsymbol{\nu},0}+K_{p,0}-\kappa_s(\Phi_0,C_0))\kappa_{s,\phi}(\Phi_0,C_0) \\ &- \sigma\left(\partial_{zz}\Phi_1 - \kappa_{\Lambda_0}\partial_z\Phi_0 - 2\boldsymbol{\mu}_{\Lambda_0}\cdot\nabla_{\Gamma(t)}\boldsymbol{p}_1\boldsymbol{\mu}_{\Lambda_0}\partial_{zz}\Phi_0 - \theta'(\Phi_0)\Phi_1\right) \\ &+ p_{,\phi}(\Phi_0,C_0,d_{\Gamma_0}) + f_{,\phi}(\Phi_0,C_0) + b_{g,\phi}(\Phi_0,C_0)(K_{\boldsymbol{\nu},0}K_{p,0}-K_{d,0}^2). \end{aligned} \tag{5.88}$$

The right hand side of which is equal to $\partial_\phi l$. At the same order from (5.18) we get

$$\begin{aligned} X_0 = &\frac{1}{2}b_{k,c}(\Phi_0,C_0)|K_{\boldsymbol{\nu},0}+K_{p,0}-\kappa_s(\Phi_0,C_0)|^2 \\ &- b_k(\Phi_0,C_0)(K_{\boldsymbol{\nu},0}+K_{p,0}-\kappa_s(\Phi_0,C_0))\kappa_{s,c}(\Phi_0,C_0) \\ &+ (K_{\boldsymbol{\nu},0}K_{p,0}-K_{d,0}^2)b_{g,c}(\Phi_0,C_0) + f_{,c}(\Phi_0,C_0) + p_{,c}(\Phi_0,C_0,d_{\Gamma_0}). \end{aligned} \tag{5.89}$$

which has right hand side equal to $\partial_c l$. Thus if we multiply (5.87) by $\partial_z\Phi_0$, multiply (5.89) by $\partial_z C_0$, add the two resultant expressions and integrate over the interfacial

region we obtain a Gibbs-Thomson type relation

$$-\omega\left(\boldsymbol{v}_0-\boldsymbol{v}_{\Lambda_0}\right)\cdot\boldsymbol{\mu}_{\Lambda_0}+[c]\chi_0=\sigma\kappa_{\Lambda_0}+\left[\frac{1}{2}b_k|\kappa_{\boldsymbol{\nu},0}+\kappa_{p,0}-\kappa_s|^2+b_g(\kappa_{\boldsymbol{\nu},0}\kappa_{p,0}-\kappa_{d,0}^2)\right] \tag{5.90}$$
$$-\left[(b_k(\kappa_{\boldsymbol{\nu},0}+\kappa_{p,0}-\kappa_s)+b_g\kappa_{\boldsymbol{\nu},0})\kappa_{p,0}\right]+[p+f]\,,$$

Note also that we have used that $\partial_z\Phi_0$ lies in the kernel of the operator $\partial_{zz}-\theta'(\Phi_0)$ to eliminate the terms involving Φ_1.

At order ε^{-1}, the resultant equation from (5.13) reads:

$$\begin{aligned}\boldsymbol{\mu}_{\Lambda_0}^T\partial_z\boldsymbol{\Sigma}_0 &= b_k(\Phi_0,C_0)(K_{\boldsymbol{\nu},0}+K_{p,0}-\kappa_s(\Phi_0,C_0))\boldsymbol{\mu}_{\Lambda_0}\partial_z K_{p,0} \\ &+(K_{\boldsymbol{\nu},0}K_{p,0}-K_{d,0}^2)\boldsymbol{\mu}_{\Lambda_0}(b_{g,\phi}(\Phi_0,C_0)\partial_z\Phi_0+b_{g,c}(\Phi_0,C_0)\partial_z C_0) \\ &+\sigma\boldsymbol{\mu}_{\Lambda_0}\left(\partial_z\Phi_0\partial_{zz}\Phi_1+\partial_z\Phi_1\partial_{zz}\Phi_0-\kappa_{\Lambda_0}(\partial_z\Phi_0)^2-\theta'(\Phi_0)\partial_z\Phi_1+\theta''(\Phi_0)\Phi_1\partial_z\Phi_0\right)\end{aligned} \tag{5.91}$$

Observe that

$$\begin{aligned}&b_k(\Phi_0,C_0)(K_{\boldsymbol{\nu},0}+K_{p,0}-\kappa_s(\Phi_0,C_0))\partial_z K_{p,0} \\ &\qquad=\partial_z\left(\frac{1}{2}b_k(\Phi_0,C_0)(K_{\boldsymbol{\nu},0}+K_{p,0}-\kappa_s(\Phi_0,C_0)^2\right) \\ &\qquad-(\frac{1}{2}(b_{k,\phi}(\Phi_0,C_0)\partial_z\Phi_0+b_{k,c}(\Phi_0,C_0)\partial_z C_0)(K_{\boldsymbol{\nu},0}+K_{p,0}-\kappa_s(\Phi_0,C_0)^2 \\ &\qquad-b_k(\Phi_0,C_0)(K_{\boldsymbol{\nu},0}+K_{p,0}-\kappa_s(\Phi_0,C_0))(\kappa_{s,\phi}(\Phi_0,C_0)\partial_z\Phi_0+\kappa_{s,c}(\Phi_0,C_0)\partial_z C_0)\end{aligned}$$

Thus if we integrate (5.91) over the interface, using the matching condition (5.69d) and using a similar argument to that used on the geometric terms of (5.87) we obtain a force balance for the tangential action of the stresses.

$$\boldsymbol{\mu}_{\Lambda_0}\cdot[\boldsymbol{\sigma}(t)]\boldsymbol{\mu}_{\Lambda_0}=[b_g(\kappa_p\kappa_{\boldsymbol{\nu}}-\kappa_d^2)]+[(b_k(\kappa_{\boldsymbol{\nu}}+\kappa_p-\kappa_s)-b_g\kappa_{\boldsymbol{\nu}})\kappa_p]-\sigma\kappa_{\Lambda_0}$$

We now consider (5.17) at order ε^{-2} from which we see

$$0=\partial_z\left(M_c(\Phi_0,C_0)\partial_z X_0\right). \tag{5.92}$$

By the positivity assumption on the mobility function, using the boundary condition (5.69b), we can infer that $\partial_z X_0=0$ which upon integration over the interfacial region gives

$$[\chi_0]=0. \tag{5.93}$$

To the next order ε^{-1}, again from (5.17), we see that

$$-\left(\boldsymbol{v}_0 - \boldsymbol{v}_{\Lambda_0}\right) \cdot \boldsymbol{\mu}_{\Lambda_0} \partial_z C_0 = M_{c,0} \left(\partial_{zz} X_1\right) \tag{5.94}$$

Here we have used the results of (5.92) and (5.74) to reduce the right hand side to this simple form. We may integrate this over the interfacial region to recover a Stefan condition.

$$-\left(\boldsymbol{v}_0 - \boldsymbol{v}_{\Lambda_0}\right) \cdot \boldsymbol{\mu}_{\Lambda_0} [c_0] = [M_{c,0} \nabla_{\Gamma(t)} \chi_0] \cdot \boldsymbol{\mu}_{\Lambda_0}. \tag{5.95}$$

Collecting all of the resulting equations gives rise to the sharp interface model (5.2.2).

5.5.7 Remarks

Planar Settings

If we make the simplifying assumption of solving the sharp interface Problem 5.2.2 in a planar setting then it reduces to the following system which can be thought of as the limit of an Allen-Cahn type Stokes flow with forcing.

$$\left.\begin{aligned} -\mu \Delta \boldsymbol{v} + \nabla \pi &= p^{\pm}_{,d_{\mathcal{S}}} \\ \nabla \cdot \boldsymbol{v} &= 0 \\ c_t + \nabla \cdot (c \boldsymbol{v}) &= \nabla \cdot (M_c^{\pm} \nabla \chi) \\ \chi &= f^{\pm}_{,c} + p^{\pm}_{,c} \end{aligned}\right\} \text{ in } \Omega^{\pm}(t) \tag{5.96}$$

$$\left.\begin{aligned} [\chi] &= 0 \\ [\boldsymbol{v}] &= 0 \\ -[c]\left(\boldsymbol{v} - \boldsymbol{v}_{\Lambda}\right) \cdot \boldsymbol{\mu}_{\Lambda} &= [M_c \nabla \chi] \cdot \boldsymbol{\mu}_{\Lambda} \\ -\omega (\boldsymbol{v} - \boldsymbol{v}_{\Lambda}) \cdot \boldsymbol{\mu}_{\Lambda} + [c]\chi &= \sigma \kappa_{\Lambda} + [p + f] \\ [\pi] &= -\sigma \kappa_{\Lambda} + \mu \left[\nabla \boldsymbol{v} \boldsymbol{\mu}_{\Lambda}\right] \cdot \boldsymbol{\mu}_{\Lambda} \end{aligned}\right\} \text{ on } \Lambda(t) \tag{5.97}$$

Where we have replaced $\boldsymbol{\sigma}(t)$ with its expanded form for comparison with the below model.

Since we solved Problem 5.2.2 on a surface without boundary we either need suitable boundary conditions, typically homogeneous Neumann type for the binder density and no flow for the fluid velocity, or the alternative, solving the system in the plane, $\mathbb{R}^2$. In either case the space, $\Omega(t) \subseteq \mathbb{R}^2$ is decomposed as $\Omega(t) = \Omega^{\pm}(t) \cup \Lambda(t)$ in a similar manner to our decomposition of the surface $\Gamma(t)$. Furthermore the surface velocity is now purely tangential, having no normal component.

Some care should be taken over what is meant by the distance $d_{\mathcal{S}}$ for a

flat case, however we leave the forcing due to the adhesion potential in it's current format, as there may be some dependence on the binder density.

Ignoring the binder density, c, for the moment, we have a type of binary fluid flow. In the literature Shen and Yang [2010]; Abels et al. [2012], phase field equations have been coupled to fluid flows for the modelling of multi-component fluids. When one phase is preferable, Allen-Cahn type phase field equations have been used Alt and Alt [2009]; Blesgen [1999] with the sharp interface limit derived for a compressible Allen-Cahn/Navier-Stokes model in Witterstein [2010]. Whenever the two phases are of equal preference Cahn-Hilliard type phase field equations have been used due to the fact that they conserve the order parameter Boyer et al. [2010]; Abels [2009]. The sharp interface limit of an incompressible Cahn-Hilliard/Navier-Stokes systems was studied in Gal and Grasselli [2010] which derived the limiting system as

$$\left.\begin{aligned} \boldsymbol{v}_t + (\boldsymbol{v}\cdot\nabla)\boldsymbol{v} &= -\nabla\pi + \tfrac{1}{Re}\Delta\boldsymbol{v} \\ \nabla\cdot\boldsymbol{v} &= 0 \end{aligned}\right\} \text{ in } \Omega^{\pm}(t) \tag{5.98}$$

$$\left.\begin{aligned} [\boldsymbol{v}] &= 0 \\ \boldsymbol{v}_\Lambda &= \boldsymbol{v} \\ [\pi] &= -\tfrac{\kappa_\Lambda}{We} + \tfrac{1}{Re}\left[\nabla\boldsymbol{v}\boldsymbol{\mu}_\Lambda\right]\cdot\boldsymbol{\mu}_\Lambda \\ [\nabla v_{\boldsymbol{\tau}}]\cdot\boldsymbol{\mu}_\Lambda &= 0 \end{aligned}\right\} \text{ on } \Lambda(t) \tag{5.99}$$

Aside from the obvious time derivative and non-linearity present in the limiting Navier-Stokes equation, the only difference between this limiting problem and that described by (5.96)-(5.97) ignoring the binder density, arrives from the conservation of the order parameter in this Cahn-Hilliard type flow, resulting in the interface being transported with the flow so that $\boldsymbol{v}_\Lambda = \boldsymbol{v}$ on $\Lambda(t)$. This contrasts the curve shortening flow from our limit which, when ignoring binder dynamics, reads as $-\omega(\boldsymbol{v}-\boldsymbol{v}_\Lambda)\cdot\boldsymbol{\mu}_\Lambda = \sigma\kappa_\Lambda$. Thus the adhered region is shrunk in the absence of binder dynamics.

Stationary Setting

Considering a stationary setting so that there is no mass transport, the system (5.96)-(5.97) further reduces to

$$\left.\begin{aligned} c_t &= \nabla \cdot (M_c^{\pm} \nabla \chi) \\ \chi &= f_{,c}^{\pm} + p_{,c}^{\pm} \end{aligned}\right\} \text{ in } \Omega^{\pm}(t) \tag{5.100}$$

$$\left.\begin{aligned} [\chi] &= 0 \\ [c]\, \boldsymbol{v}_\Lambda \cdot \boldsymbol{\mu}_\Lambda &= [M_c \nabla \chi] \cdot \boldsymbol{\mu}_\Lambda \\ \omega \boldsymbol{v}_\Lambda \cdot \boldsymbol{\mu}_\Lambda + [c]\chi &= \sigma \kappa_\Lambda + [p+f] \end{aligned}\right\} \text{ on } \Lambda(t) \tag{5.101}$$

This system has an associated free energy

$$E = \int_{\Omega^+(t)} f^+ + p^+ \int_{\Omega^-(t)} f^- + p^- + \int_{\Lambda(t)} \sigma. \tag{5.102}$$

Recall that our purpose was to extend the work of Freund and Lin [2004]. The one sided model it derives can be read as

$$\left.\begin{aligned} c &= c_0 \end{aligned}\right\} \text{ in } (-\infty, a(t))$$

$$\left.\begin{aligned} c_t &= \partial_x \left(M c \partial_x \chi \right) \\ \chi &= \delta_c \tilde{E} \end{aligned}\right\} \text{ in } (a(t), \infty)$$

$$\left.\begin{aligned} [\chi] &= 0 \\ [c]\, \boldsymbol{v}_\Lambda &= (M c \partial_x \chi)^+ \\ \boldsymbol{v}_\Lambda \delta_\Gamma \tilde{E} &\leq 0 \end{aligned}\right\} \text{ at } a(t)$$

where $(\cdot)^+$ is the one sided limit from the free region and c_0 is the minimum binder density required for adhesion and $\tilde{E}$ is the Freund and Lin models free energy.

Observe that with our specific form of the systems free energy it is the case that $\delta_c E = f_{,c}^{\pm} + p_{,c}^{\pm}$ in each region. Furthermore it should be clear that by fixing the binder density in $\Omega^1(t)$ as c_0 and defining the mobility functions $M_c^- = 0$ and $M_c^+ = Mc$ that we easily recover all of the model of Freund and Lin [2004] except for the equation $\boldsymbol{v}_\Lambda \delta_\Gamma \tilde{E} \leq 0$. This equation physically implies that the change in energy due to interfacial motion should be dissipative. By considering the time derivative of our free energy it can be shown that the last equation of (5.101) ensures this is the case.

5.6 Simulating A Reduced Model

As a first step towards producing simulations of the diffuse interface model (5.12)-(5.18), we consider a simpler reduced model. For this reduced model we suppose that there is a reduced free energy, $E_R = E_S + E_M$, which consists of a state component, $E_S = E_B + E_{GL}$, and a membrane component, $E_M = E_{SC} + E_{AD}$, where E_{SC} is a shape regularisation term given by

$$E_{SC} = \int_{\Gamma(t)} \gamma \tag{5.103}$$

where γ is a constant.

In addition we make the simplifying assumption that the adhesion potential, p, is independent of the binder density, c. In contrast with (5.2) and (5.1) where we used variations of the full system energy we postulate the following evolution laws which only depend on variations of the state energy.

$$\varepsilon\omega\partial_t^\bullet\phi = -\delta_\phi E_S(\Gamma,\phi,c) \tag{5.104}$$

$$\partial_t^\bullet c + c\nabla_{\Gamma(t)}\cdot\boldsymbol{v} = \nabla_{\Gamma(t)}\cdot\left(M_c(\phi,c)\nabla_{\Gamma(t)}\delta_c E_S(\Gamma,\phi,c)\right) \tag{5.105}$$

By assumption the membrane energy, E_M, is not affected by tangential motions of the surface and so we assume the surface motion is purely normal. To describe the evolution of the membrane we discard the complex elastic forces and instead propose a force balance between viscous forces and membrane forces, more specifically $F_M + F_{visc} = 0$. For the viscous forces, we propose they be given proportional to the surface velocity, $F_{visc} = \alpha v_{\boldsymbol{\nu}}$, and the membrane forces are given as $F_M = -\delta_\Gamma E_M$. This results in the following reduced model.

Problem 5.6.1. *Given an initial hypersurface $\Gamma(0) \subset \mathbb{R}^3$, and initial conditions for the binder density, $c(0) : \Gamma(0) \to \mathbb{R}$ and phase field variable, $\phi(0) : \Gamma(0) \to \mathbb{R}$, find $(\Gamma(t), \phi(t), c(t))$ such that at each time $t \in [0,T]$:*

$$\alpha v_{\boldsymbol{\nu}} = \gamma\kappa_m - p_{,d_S}(\phi,d)\boldsymbol{\nu}\cdot\boldsymbol{\nu}_S \tag{5.106}$$

$$\partial_t^\bullet c + c\nabla_{\Gamma(t)}\cdot\boldsymbol{v} = -\nabla_{\Gamma(t)}\cdot j_c \tag{5.107}$$

$$j_c = -M_c\nabla_{\Gamma(t)} f_{,c}(\phi,c) \tag{5.108}$$

$$-\varepsilon\omega\partial_t^\bullet\phi = \sigma\left(-\varepsilon\Delta_{\Gamma(t)}\phi + \frac{1}{\varepsilon}\theta'(\phi)\right) + g_{,\phi}(\phi,c) \tag{5.109}$$

where $\boldsymbol{v} = v_{\boldsymbol{\nu}}\boldsymbol{\nu}$ describes the evolution of $\Gamma(t)$.

The forcing term $g = f - cf_{,c}$ is the grand potential. The sharp interface limit of this system is given by

$$\left.\begin{aligned} \alpha v_{\boldsymbol{\nu}} &= \gamma\kappa_m - \partial_{d_{\mathcal{S}}} p^{\pm}(d)\boldsymbol{\nu}\cdot\boldsymbol{\nu}_S \\ \partial_t^{\bullet} c + c\nabla_\Gamma\cdot\boldsymbol{v} &= -\nabla_\Gamma\cdot j_c^{\pm} \\ j^{\pm} &= -M_c^{\pm}\nabla_\Gamma f_{,c}^{\pm}(c) \end{aligned}\right\} \text{ in } \Gamma^{\pm}(t) \tag{5.110}$$

$$\left.\begin{aligned} [c]\,\boldsymbol{v}_\Lambda\cdot\boldsymbol{\mu}_\Lambda &= [j]\cdot\boldsymbol{\mu}_\Lambda, \\ [f_{,c}] &= 0, \\ \omega\boldsymbol{v}_\Lambda\cdot\boldsymbol{\mu}_\Lambda &= \sigma\kappa_\Lambda + [g] \end{aligned}\right\} \text{ on } \Lambda(t) \tag{5.111}$$

For simulating solutions of Problem 5.6.1 we follow the ideas of Barrett et al. [2008] but using a formulation based on the grand potential. Recall χ is the chemical potential and in this example satisfies $\chi = f_{,c}(c,\phi)$. If we assume that the potential function is convex with respect to the binder density then we can write $c = c(\chi,\phi)$ and reformulate using the variables (χ, g) instead of (c, f) so that $g(\chi,\phi) = f(c(\chi),\phi) - c(\chi)\chi$. Under this set up we have that $g_{,\phi} = f_{,\phi}$ and $g_{,\chi} = -c$.

We begin with a weak formulation, observe that to increase the regularity of the solution we have added a Lagrange multiplier type term, λ_v, to the surface evolution to enforce a volume constraint on the surface.

Problem 5.6.2. *We say that a tuple $(\Gamma(t),\phi(t),g(t))$ is a weak solution of Problem 5.6.1 if it satisfies*

$$\frac{d}{dt}\int_{\Gamma(t)} g_{,\chi}\eta + \int_{\Gamma(t)} M_c\nabla_{\Gamma(t)}\chi\cdot\nabla_{\Gamma(t)}\eta = \int_{\Gamma(t)} g_{,\chi}\partial_t^{\bullet}\eta, \tag{5.112}$$

$$\varepsilon\omega\int_{\Gamma(t)}\partial_t^{\bullet}\phi\psi + \int_{\Gamma(t)}\sigma\varepsilon\nabla_{\Gamma(t)}\phi\cdot\nabla_{\Gamma(t)}\psi + \frac{\sigma}{\varepsilon}\theta'(\phi)\psi - \int_{\Gamma(t)} g_{,\phi}\psi = 0, \tag{5.113}$$

$$\int_{\Gamma(t)}\alpha\partial_t\boldsymbol{x}\cdot\boldsymbol{\nu}\zeta - \gamma\kappa_m\zeta + p_{,d_{\mathcal{S}}}\boldsymbol{\nu}\cdot\boldsymbol{\nu}_{\mathcal{S}}\zeta = \int_{\Gamma(t)}\lambda_v\zeta, \tag{5.114}$$

$$\int_{\Gamma(t)}\kappa_m\boldsymbol{\nu}\cdot\xi + \nabla_{\Gamma(t)}\boldsymbol{x} : \nabla_{\Gamma(t)}\xi = 0. \tag{5.115}$$

Here $\boldsymbol{x}(t)$ is some parameterisation of the surface, $\Gamma(t)$. The principles of the surface finite element method have been discussed in Chapter 4, however the basics of approximating the geometry and generating spatial discretisation are the same, as is the use of the method of lines for the temporal discretisation. The main difficulty in producing simulations is dealing with the unknown surface velocity, given an initially triangulated surface how should the nodes be advected and how do we assemble quantities over a future surface. We will discuss how we overcome this difficulty later and assume for now that there is some method for generating a

triangulation for all times so that we may generate our spatial discretisation using the following finite element space:

$$S_h(t) = \left\{ \eta \in C^0(\Gamma(t) \,\middle|\, \eta\big|_T \in \mathbb{P}^1 \; \forall T \in \mathcal{T}_h \right\}. \tag{5.116}$$

Following the standard practice we have discrete functions $c_h, \phi_h, \boldsymbol{x}_h \in S_h(t)$. As mentioned above the surface velocity is unknown and so at any particular time step, t_m, the approximation of the surface at the next time step, t_{m+1}, is unknown. This means that, should we want to take a time derivative, assembling any system matrices over the surface $\Gamma(t_{m+1})$ is non-trivial. The method we have employed is to solve the surface evolution equations over the current surface first and then solve the state equations using this update information.

In addition we have used an Arbitrary Lagrangian-Eulerian (ALE) method based on the work of Elliott and Styles [2012]. In our continuous problem we have a purely normal surface velocity but in practice for the discrete equations, due to the approximation of geometry, the update velocity given by $\boldsymbol{v}_a = \frac{\boldsymbol{x}_h^m - \boldsymbol{x}_h^{m-1}}{\tau}$, can have a non-zero tangential component. The purpose of the ALE scheme is to account for this drift in the field equations.

In the framework of Elliott and Venkataraman [2015], this means we have an arbitrary tangential velocity $\boldsymbol{a}_\tau = \boldsymbol{v}_a - v_{\boldsymbol{\nu}}$ which we use to transport the nodes of $\Gamma_h(t)$ and which manifests as an advection term proportional to $\boldsymbol{a}_\tau \cdot \nabla_\Gamma \eta$ (with η some test function) in the field equations. However since $v_{\boldsymbol{\nu}}$ is purely normal we may rewrite this advection term as $\boldsymbol{v}_a \cdot \nabla_\Gamma \eta$. Thus our fully discrete problem reads

as below, we have implemented this scheme in MATLAB.

$$\begin{aligned}
\frac{1}{\tau}\int_{\Gamma_h^m} I_h^m\left(g_{h,\chi}^m\eta_h^m\right) + \int_{\Gamma_h^m} I_h^m\left(g_{h,\chi}^m\frac{\boldsymbol{x}_h^m-\boldsymbol{x}_h^{m-1}}{\tau}\right)\cdot\nabla_{\Gamma_h^m}\eta_h^m \\
+\int_{\Gamma_h^m} M_{c,h}^m\nabla_{\Gamma_h^m}\chi_h^m\cdot\nabla_{\Gamma_h^m}\eta_h^m = \frac{1}{\tau}\int_{\Gamma_h^{m-1}} I_h^{m-1}\left(g_{h,\chi}^{m-1}\eta_h^{m-1}\right), \\
\frac{\varepsilon\omega}{\tau}\int_{\Gamma_h^m} I_h^m\left(\phi_h^m\psi_h^m\right) + \int_{\Gamma_h^m} I_h^m\left(\phi_h^m\frac{\boldsymbol{x}_h^m-\boldsymbol{x}_h^{m-1}}{\tau}\right)\cdot\nabla_{\Gamma_h^m}\psi_h^m \\
+\int_{\Gamma_h^m}\sigma\varepsilon\nabla_{\Gamma_h^m}\phi_h^m\cdot\nabla_{\Gamma_h^m}\psi_h^m + \int_{\Gamma_h^m}\frac{\sigma}{\varepsilon}I_h^m\left(\theta'(\phi_h^m)\psi_h^m\right) \\
=\int_{\Gamma_h^m} I_h^m\left(g_{h,\phi}^{m-1}\psi_h^m\right)+\frac{\varepsilon\omega}{\tau}\int_{\Gamma_h^m} I_h^m\left(\phi_h^{m-1}\psi_h^{m-1}\right), \\
\int_{\Gamma_h^{m-1}} I_h^{m-1}\left(\frac{\alpha}{\tau}\boldsymbol{x}_h^m\cdot\boldsymbol{\nu}_h^{m-1}\zeta_h^{m-1} - \gamma\kappa_h^m\zeta_h^{m-1}\right) + p_{h,d}^{m-1}\boldsymbol{\nu}_h^{m-1}\cdot\boldsymbol{\nu}_{\mathcal{S}}\zeta_h^{m-1} \\
=\int_{\Gamma_h^{m-1}}\lambda_v^{m-1}\zeta_h^{m-1}+\frac{\alpha}{\tau}\int_{\Gamma_h^{m-1}}\boldsymbol{x}_h^{m-1}\cdot\boldsymbol{\nu}_h^{m-1}\zeta_h^{m-1}, \\
\int_{\Gamma_h^{m-1}}\kappa_h^m\boldsymbol{\nu}_h^{m-1}\cdot\xi_h^{m-1}+\nabla_{\Gamma_h^{m-1}}\boldsymbol{x}_h^m:\nabla_{\Gamma_h^{m-1}}\xi_h^{n-1}=0.
\end{aligned}$$

We have implemented the volume constraint as a penalty method by considering an additional surface energy contribution of the form

$$E_A(\Gamma)=\frac{1}{2}p_a\left(\frac{1}{2}\int_\Gamma \boldsymbol{x}\cdot\boldsymbol{\nu}-A_0\right)^2, \tag{5.117}$$

which has variation

$$\delta E_A(\Gamma)=p_a\left(\frac{1}{2}\int_\Gamma \boldsymbol{x}\cdot\boldsymbol{\nu}-A_0\right)=:\lambda_v. \tag{5.118}$$

Here p_a is a penalty constant and A_0 is the initial enclosed volume.

In the following examples we use an interpolation method to define ϕ dependent adhesion and grand potentials. More specifically we use an interpolation function $h(\phi)=\phi^2(3-2\phi)$ and define potentials, $g^{\pm}$ and $p^{\pm}$ with

$$p(\phi,d_{\mathcal{S}})=p^+(d_{\mathcal{S}})h(\phi)+p^-(d_{\mathcal{S}})(1-h(\phi)) \tag{5.119}$$

$$g(\phi,\chi)=g^+(\chi)h(\phi)+g^-(\chi)(1-h(\phi)) \tag{5.120}$$

Although we have formulated our numerical scheme in terms of the grand potential and the chemical potential, when displaying the output we map back to the binder

Parameter	Data for Ex. 5.6.1
ϕ^-, ϕ^+	0, 1
$g^+(\chi)$	$0.5\chi^2$
$g^-(\chi)$	$0.5\chi^2$
$p^+(d_{\mathcal{S}})$	$\begin{cases} 25d_{\mathcal{S}}^2 - 10d_{\mathcal{S}} & d_{\mathcal{S}} < 0.2 \\ (5d_{\mathcal{S}} - 1)^2(5 - 10d_{\mathcal{S}}) - 1 & 0.2 < d_{\mathcal{S}} < 0.6 \\ 0 & d_{\mathcal{S}} \geq 0.2 \end{cases}$
$p^-(d_{\mathcal{S}})$	$\begin{cases} 25d_{\mathcal{S}}^2 - 10d_{\mathcal{S}} + 1 & d_{\mathcal{S}} < 0.2 \\ 0 & d_{\mathcal{S}} \geq 0.2 \end{cases}$
$\theta(\phi)$	$\phi(1-\phi)(1-2\phi)$
$M_c(c)$	0
N	20
τ	0.01
ω	1
σ	0.3
α	10
γ	0.1
ε	0.2
p_a	20

Figure 5.4: Simulation data for Section 5.6.1.

Parameter	Data for Ex. 5.6.2	Data for Ex. 5.6.3
ϕ^-, ϕ^+	0, 1	-
$g^+(\chi)$	$(0.25\chi - 0.5)\chi$	-
$g^-(\chi)$	$(0.25\chi - 0.1)\chi$	-
$p^+(d_{\mathcal{S}})$	$\begin{cases} 25d_{\mathcal{S}}^2 - 10d_{\mathcal{S}} & d_{\mathcal{S}} < 0.2 \\ (5d_{\mathcal{S}} - 1)^2(5 - 10d_{\mathcal{S}}) - 1 & 0.2 < d_{\mathcal{S}} < 0.6 \\ 0 & d_{\mathcal{S}} \geq 0.2 \end{cases}$	-
$p^-(d_{\mathcal{S}})$	$\begin{cases} 25d_{\mathcal{S}}^2 - 10d_{\mathcal{S}} + 1 & d_{\mathcal{S}} < 0.2 \\ 0 & d_{\mathcal{S}} \geq 0.2 \end{cases}$	-
$\theta(\phi)$	$\phi(1-\phi)(1-2\phi)$	-
$M_c(c)$	1	0.25
N	100	-
τ	0.01	-
ω	1	-
σ	0.3	-
α	10	0.5
γ	0.1	-
ε	0.2	-
p_a	20	10

Figure 5.5: Simulation data for Sections 5.6.2 and 5.6.3.

density as this is easier to interpret. This is done by inverting the relation described above.

5.6.1 Tangential Transport Effects

In this example we display the importance of the ALE terms in our numerical scheme. We consider the unit circle, centred at $(0, 1)$, as the initial surface. However, we do not distribute our nodal points evenly. Instead beginning with a uniform distribution of points in the parameterisation space with values $s_i = \frac{i}{N_h}$, $i = 1, ..., N_h$ we use parameterisation

$$\left\{(x, y) \in \mathbb{R}^2 \,|\, x = cos(2\pi s_i^3), y = sin(2\pi s_i^3) + 1\right\}. \tag{5.121}$$

The cubic power of the parameterisation points has the effect of clustering nodes in the top right quadrant as seen in Figure 5.6a. As initial conditions we use

$$\chi(x, y) = 0.5, \tag{5.122}$$

$$\phi(x, y) = 0.5. \tag{5.123}$$

We remove any substrate from this example so that in a continuous setting, the cell should not move. We set $M_c = 0$, and using the forms of $g^{\pm}$ in the first column of Table 5.5, there should be no change in the density or the phase field variable.

In Figure 5.6 we display the results of two simulations. In Figure 5.6b we see that without the ALE terms, due to the approximation of geometry, the nodes are transported tangentially to create a more even distribution. This tangential motion has the effect of advecting mass in the binder equation which changes the density. This does not happen to the phase variable as it is not governed by a conservation type law. In contrast in Figure 5.6c, we see that with the ALE terms, even though the nodes are still transported tangentially, the binder density remains constant.

5.6.2 Adhesion Patch Growth

As a proof of concept simulation we have looked to investigate the theoretical growth rate of an adhesion patch. In Freund and Lin [2004] it was shown for solutions of their model that the position of the interface should advance proportional to $\sqrt{t}$ relative to it's initial position. We would like our model, as an attempted generalisation of the model of Freund and Lin [2004] to exhibit similar behaviour.

To investigate the growth rate of an adhesion patch we use the parameters in the centre column of Table 5.5. We start from an initial ellipse placed just above

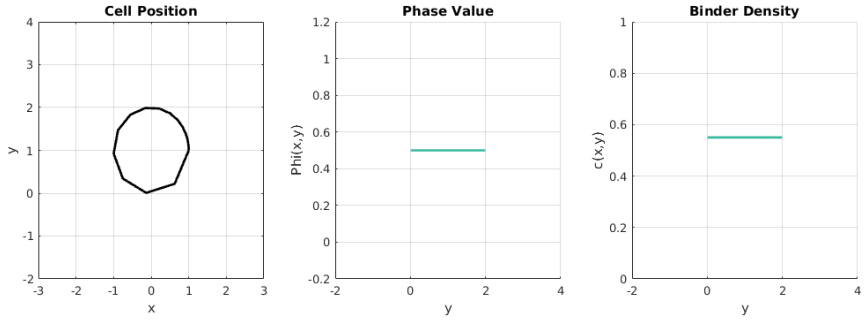

(a) $t = 0.0$

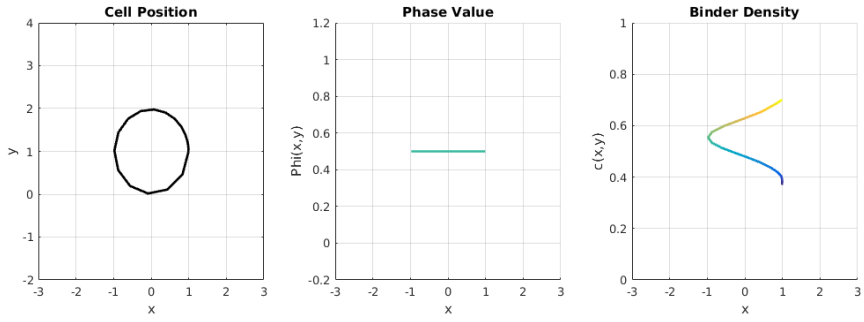

(b) $t = 1.0$, without ALE terms.

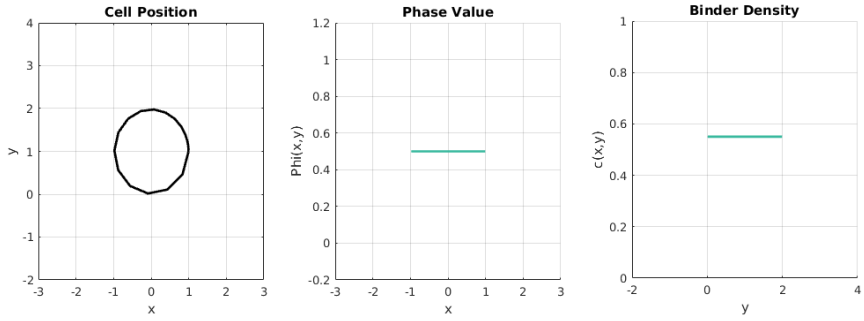

(c) $t = 1.0$, with ALE terms.

Figure 5.6: Difference in solution behaviour due to inclusion of ALE terms as discussed in Section 5.6.1. Nodal points move tangentially due to approximation of geometry (b) without ALE terms altering the binder density, (c) with ALE terms the binder density remains constant.

the x-axis, given by the parameterisation

$$\left\{(x,y) \in \mathbb{R}^2 \,|\, x = 3\cos(2\pi t), y = 0.8\sin(2\pi t) + 0.99,\, t \in [0,1]\right\} \tag{5.124}$$

then to ensure that nucleation of an adhesion patch has occured, for all points with $y < 0.2$, we move them to be such that $y = 0.2$ and so obtain $\Gamma(0)$. As initial conditions for the phase value and binder density we use

$$\chi(x,y) = \begin{cases} 0.2 & y > 0.2, \\ 0.0 & y = 0.2. \end{cases} \tag{5.125}$$

$$\phi(x,y) = \begin{cases} 1 & y > 0.2, \\ 0 & y = 0.2. \end{cases} \tag{5.126}$$

Observe that with g^+ and g^- as chosen, the density of binders is sufficiently large in the free region to allow the adhesion patch (initially given by the set of points for which $y = 0.2$) to grow. The substrate is chosen to be the x-axis for this example so that the normal to the substrate is the vector $\boldsymbol{\nu}_{\mathcal{S}} = (0,1)^T$.

We expect that the adhesion patch should grow and thus flatten the cell boundary near to the x-axis. Note it should not be strictly adhered as with the adhesion potentials we have chosen, the optimum distance between the cell and the substrate to minimise the energy should be 0.2. In addition since the cell has a finite size, and thus a finite number of binders, whatever the growth rate of the interface, it is expected to slow and reach an equilibrium profile in the long term.

As can be seen in Figure 5.7, the cell adheres at the optimal distance at all times, sitting at a distance of 0.2 away from the substrate described by the x-axis. In addition the finite size effects that we predicted can be seen from Figure 5.8a where after a relatively rapid growth the interface can be seen to be settling to some equilibrium point. By plotting the adhesion front against the square root of the time in Figure 5.8b we can see the approximately linear relation after an initial period. This initial period is due to the sharp initial conditions we have used and is a relaxation period.

Observe that we have plotted the relative distance of the front from it's original position so as to be better able to see the relation. We have also calculated the interface position as the .05 level set of ϕ_ε, during an uphill transition when traversing the nodes in an incremental manner.

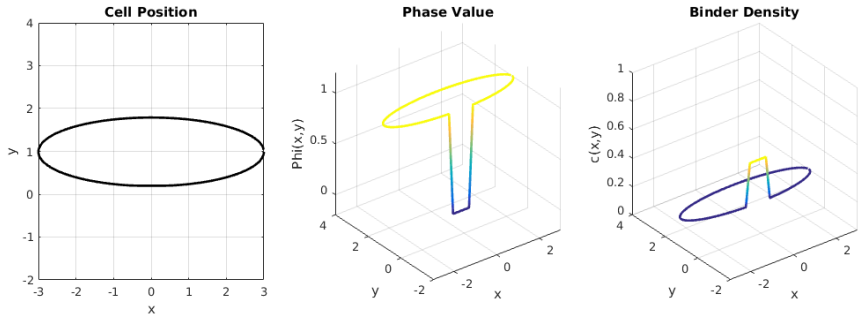

(a) $t = 0.0$

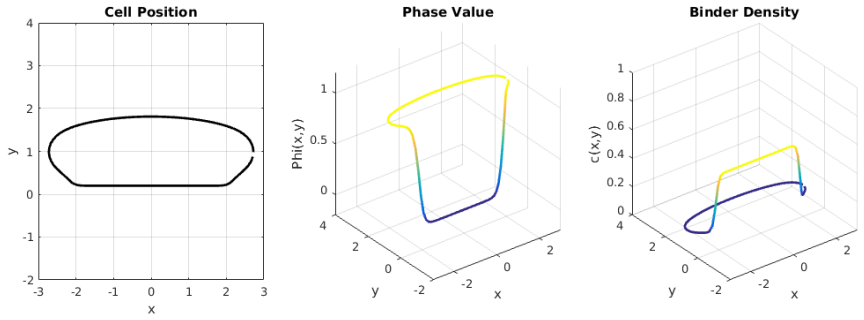

(b) $t = 40.0$

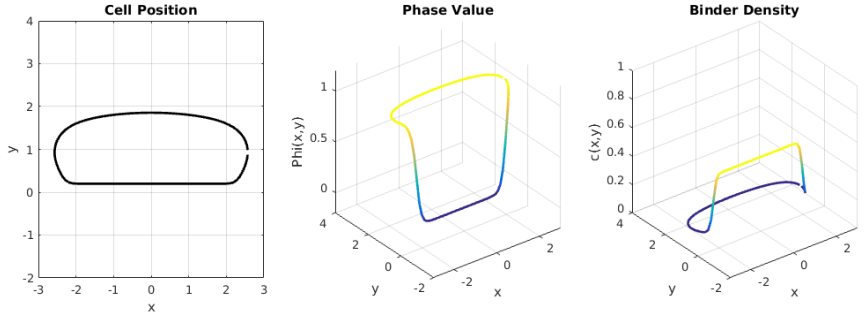

(c) $t = 80.0$

Figure 5.7: Adhesion patch growth as described in Section 5.6.2. Cell adheres to substrate as patch grows and then the curvatures relax to a more favourable state. Note that the small disconnection in the domain, near the right most point, is merely a limitation of the plotting software used and is not some form of tearing of the surface.

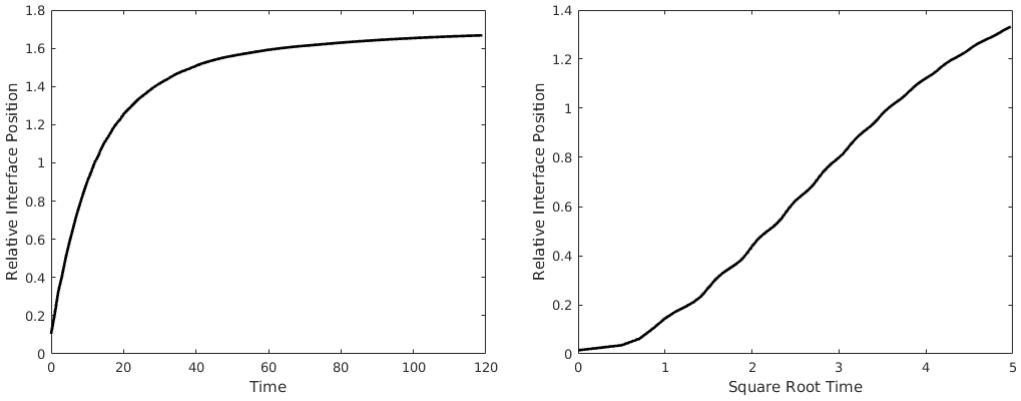

(a) (b)

Figure 5.8: Growth of an adhesion experiment as described in Section 5.6.2. Plots of the relative interface position against (a) time, showing effect of finite binder recruitment and (b) square root of time, showing approximate front advancement rate in relation to initial position.

5.6.3 Changing Topology

In this example we would like to justify our use of the phase field methodology by showing its strength in its ability to model topological changes. To do this we will look at an initial cell with two adhesion patches separated by a free region and allow the cell to relax. The parameters used in this example are the same as in the last example except where indicated by the right column of Table 5.5.

We again start from an initial ellipse placed just above the x-axis, given by a similar parameterisation as used in Section 5.6.2 but lowered:

$$\left\{(x,y) \in \mathbb{R}^2 \,|\, x = 3\cos(2\pi t), y = 0.8\sin(2\pi t) + 0.79,\, t \in [0,1]\right\}. \tag{5.127}$$

The lowering of the cell is so that we can obtain a large adhesion patch, we again use the same procedure for all points with $y < 0.2$, where by we move them to be such that $y = 0.2$ and so obtain $\Gamma(0)$. As initial conditions for the phase value and binder density we use

$$\chi(x,y) = \begin{cases} 0.1 & y = 0.2 \text{ and } 0.6 \leq |x| \leq 1.6, \\ 0.0 & \text{else.} \end{cases} \tag{5.128}$$

$$\phi(x,y) = \begin{cases} 0 & y = 0.2 \text{ and } 0.6 \leq |x| \leq 1.6, \\ 1 & \text{else.} \end{cases} \tag{5.129}$$

Note that we still have a surplus of binders but not to the same extent as in the

previous example. The substrate is again chosen to be the x-axis so that the normal to the substrate is the vector $\boldsymbol{\nu}_{\mathcal{S}} = (0,1)^T$.

By reducing α for this simulation the cell dynamics should occur at a faster rate when compared with the cell evolution in Section 5.6.2, and so we expect that the cell should move so as to be as circular as possible whilst maintaining its adhesion patches. The adhesion patches should persist as they are energetically more favourable than a free region close to the substrate. Due to the surplus of binders the adhesion patches should grow until they intersect at which point they should transition to a single adhesion patch.

In Figures 5.9-5.10 we display the resultant simulation. As can be seen, the cell wall does move so as to be near circular in the free region. Also as expected when the patches grow and the interfaces meet the patches merge to form a singular adhesion patch.

To display that the merging of the two interfaces is purely due to growth of adhesion patches and is not due to the surface geometry in some manner trying to pull the patches closer together to obtain a more energetically favourable state we consider a similar example. We use the same parameters as above but with a slightly different initial condition for the chemical potential, $\chi = 0$.

In this setting there is no longer a surplus of binders for the growth of the adhesion patches and so the two patches should not grow. Thus we expect the two patches to persist and remain adhered at their original contact points. Any motion of the surface should be to relax to the energetically favourable circular shape but constrained to being pinned at the patches.

In Figure 5.12 we display the resultant simulation for which we see the persistence of the the two separate adhesion patches for all times and may thus conclude that the topological change seen in Figures 5.9-5.10 is due to the growth of the adhesion patches. In Figure 5.11 we display the energy of the system calculated from E_R for the simulation displayed in Figure 5.12. Although we have not prescribed a strict gradient flow structure we can see that the total energy constantly reduces over time.

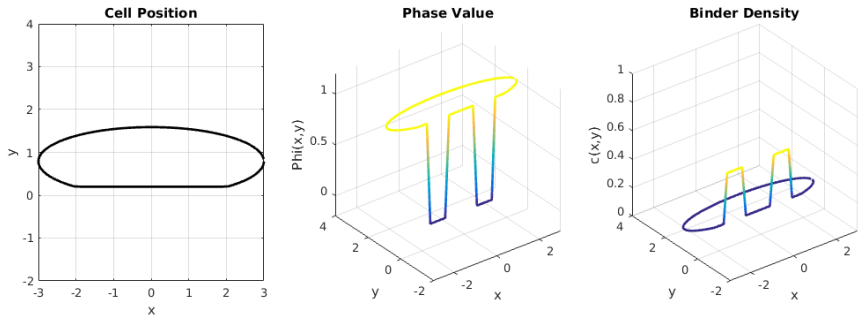

(a) $t = 0.0$

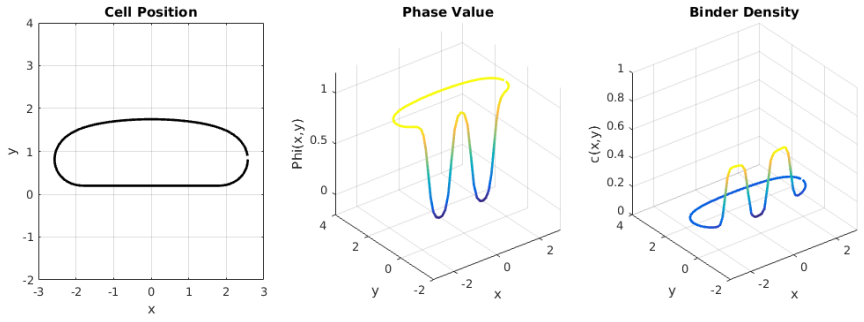

(b) $t = 5.0$

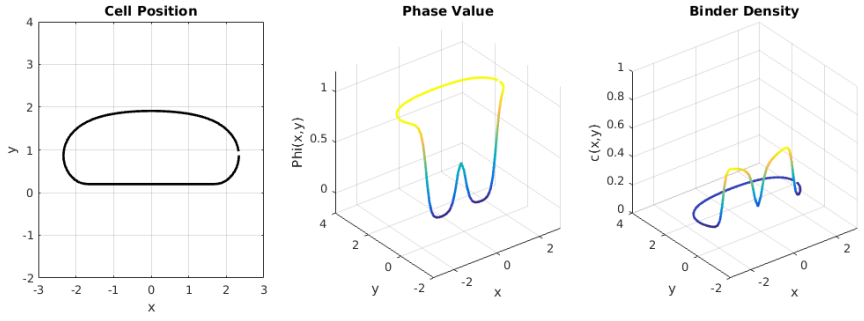

(c) $t = 10.0$

Figure 5.9: Twin adhesion patch merging as described in Section 5.6.3 during early times. Cell is adhered to substrate and merges two adhesion patches to obtain a more favourable energetic state.

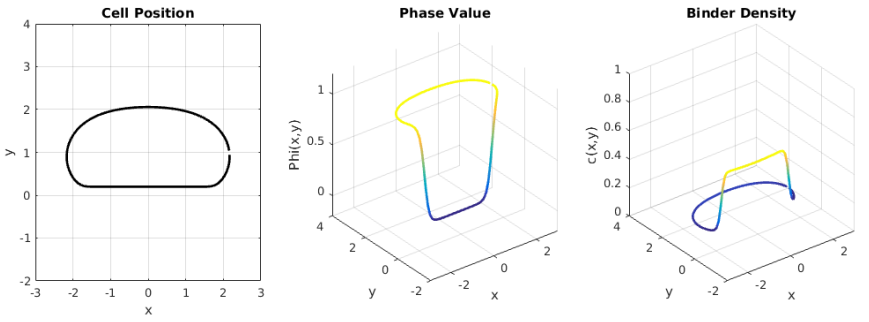

(a) $t = 15.0$

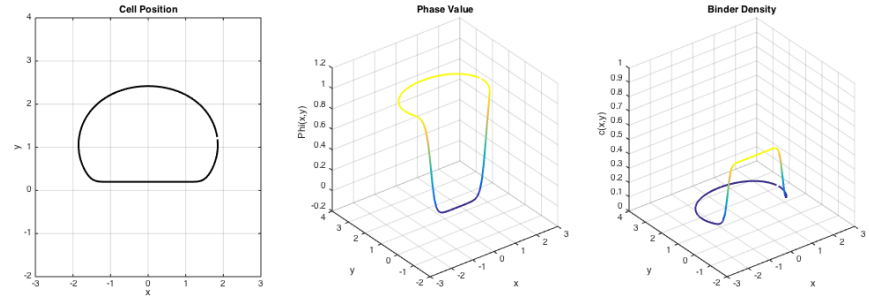

(b) $t = 30.0$

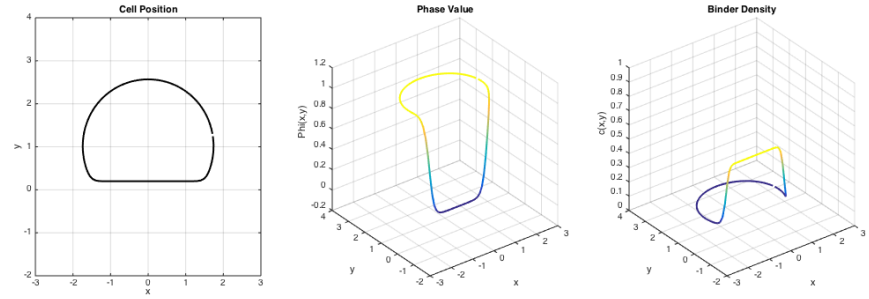

(c) $t = 45.0$

Figure 5.10: Twin adhesion patch merging as described in Section 5.6.3 during later times. Cell is adhered to substrate and merges two adhesion patches to obtain a more favourable energetic state.

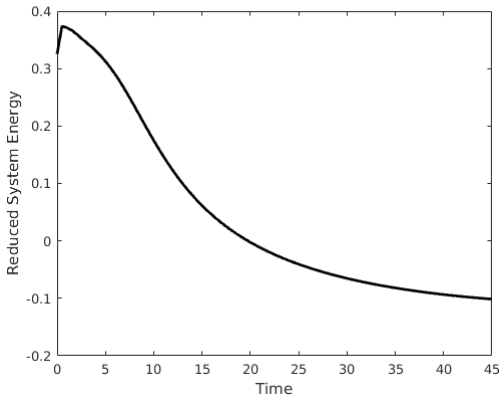

Figure 5.11: Energy profile of twin adhesion patches as described in Section 5.6.3 and displayed in Figure 5.12. Energy can be seen to be constantly decreasing.

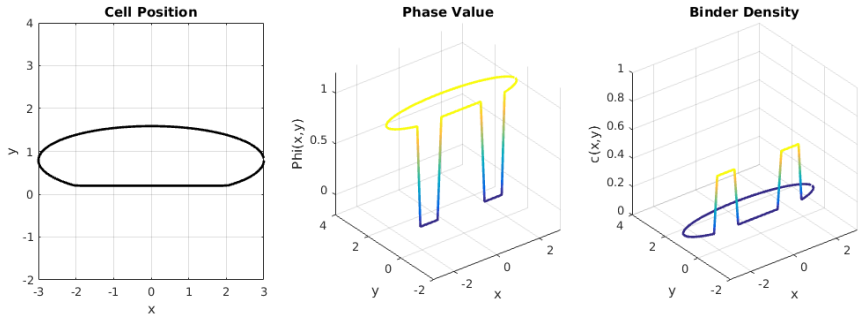

(a) $t = 0.0$

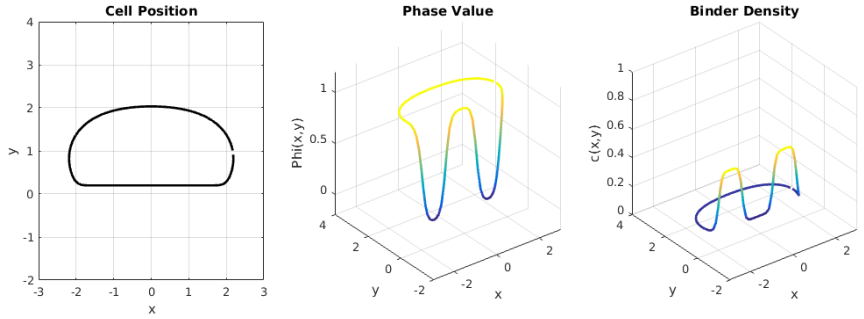

(b) $t = 15.0$

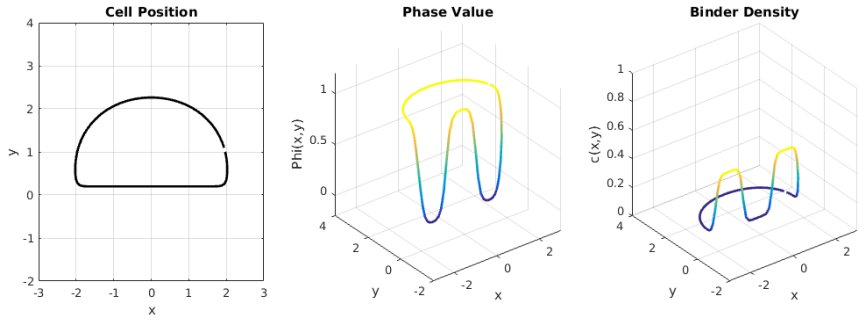

(c) $t = 30.0$

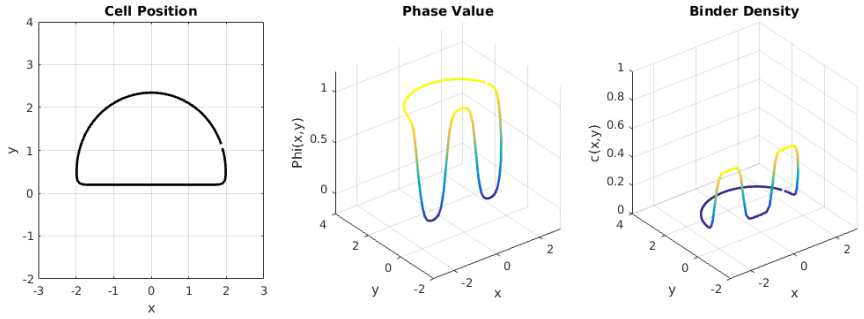

(d) $t = 45.0$

Figure 5.12: Twin adhesion patch persistant as described in Section 5.6.3. Cell is adhered to substrate and patches persist due to insufficient binder density for recruitment.

Chapter 6

Conclusion

We will now briefly summarise the results of this thesis' chapters.

6.1 Chapter 2 - Calculus on Evolving Surfaces

In this chapter the main result from our investigation was the effects of a time dependent surface on the change of variable formulae used in the inner region during our asymptotic analysis. In particular we showed that for points within a region of width $\mathcal{O}(\varepsilon)$ that the material derivative of the signed distance function could be expressed as the difference of the surface velocity $\boldsymbol{v}$ and the interfacial velocity $\boldsymbol{v}_\Lambda$ in the co-normal direction $\boldsymbol{\mu}_\Lambda$, plus order ε contributions. More specifically the result reads that when reparameterising a hypersurface locally around a predefined curve, Λ, as $\boldsymbol{x} \to (s, r)$, with s parameterising Λ and r the distance to the curve, then the time rate of change of r is given by:

$$\partial_t^\bullet r(x,t) = \big(\boldsymbol{v}(x_\Lambda,t) - \boldsymbol{v}_\Lambda(x_\Lambda,t)\big) \cdot \boldsymbol{\mu}_\Lambda(x_\Lambda,t) + \mathcal{O}(\varepsilon).$$

We argued formally for this result and thus future work would require that this argument be made more rigorous.

6.2 Chapter 3 - Asymptotics for the Evolving Surface Cahn-Hilliard Equation

In this chapter we used the results of the previous chapter alongside the method of matched asymptotic expansions to analyse the Evolving Surface Cahn-Hiliard Equation (3.1)-(3.2). We derived and analysed the ESCH equation with various forms for its mobility and potential functions and derived limiting sharp interface

problems. We restricted to smooth potentials first, excluding the case of a double obstacle potential.

Of interest is that for not all scalings of the mobility with respect to the surface velocity in relation to the parameter ε could we derive a free boundary problem. In the intermediary case that the ratio of the mobility against the velocity scales as ε^0 we were able to derive the following evolving surface Mullins-Sekerka type problem, where the unknowns are $w(t)$ and $\Lambda(t)$:

$$\left.\begin{aligned} \phi &= \phi_i \\ \nabla_{\Gamma(t)} \cdot \big(M(\phi)\nabla_{\Gamma(t)} w(t)\big) &= \phi \nabla_{\Gamma(t)} \cdot \boldsymbol{v}(t) \end{aligned}\right\} \text{ in } \Gamma^i(t),\ i = a, b, \tag{6.1}$$

$$\left.\begin{aligned} [w(t)] &= 0 \\ w(t) &= S\kappa_\Lambda(t) \\ \tfrac{1}{\phi_b - \phi_a}[M(\phi)\nabla_{\Gamma(t)} w(t)] \cdot \boldsymbol{\mu}_\Lambda(t) &= \big(\boldsymbol{v}(t) - \boldsymbol{v}_\Lambda(t)\big) \cdot \boldsymbol{\mu}_\Lambda(t) \end{aligned}\right\} \text{ on } \Lambda(t). \tag{6.2}$$

Here, $\Lambda(t)$ is the moving boundary separating the bulk phases $\Gamma^b(t)$ and $\Gamma^a(t)$, $[\cdot] = [\cdot]_a^b = (\cdot)^b - (\cdot)^a$ stands for the jump across $\Lambda(t)$, $S > 0$ is a calibration constant depending on the double-well potential F, $\kappa_\Lambda(t)$ is the geodesic curvature of $\Lambda(t)$ with respect to $\Gamma(t)$, $\boldsymbol{v}_\Lambda(t)$ is the velocity of $\Lambda(t)$, and $\boldsymbol{\mu}_\Lambda(t)$ is the co-normal of $\Lambda(t)$ with respect to $\Gamma(t)$ which points into $\Gamma^b(t)$.

For the case of a faster mobility so that the ratio of the mobility against the velocity scale as ε^{-1} we derived the following problem, the unknowns are again $w(t)$ and $\Lambda(t)$.

$$\left.\begin{aligned} \phi &= \phi_i \\ \nabla_\Gamma \cdot (M(\phi)\nabla_\Gamma w(t)) &= \phi \nabla_\Gamma \cdot \boldsymbol{v}(t) \end{aligned}\right\} \text{ in } \Gamma^i(t), i = a, b, \tag{6.3}$$

$$\left.\begin{aligned} [w(t)] &= 0 \\ w(t) &= T\kappa_\Lambda(t)^2 \\ \tfrac{1}{\phi_b - \phi_a}\,[M(\phi)\nabla_\Gamma w(t)] \cdot \boldsymbol{\mu}_\Lambda(t) &= \big(\boldsymbol{v}(t) - \boldsymbol{v}_\Lambda(t)\big) \cdot \boldsymbol{\mu}_\Lambda(t) \end{aligned}\right\} \text{ on } \Lambda(t). \tag{6.4}$$

together with the compatibility condition that $\kappa_\Lambda(t)$ is spatially constant and T is a different calibration constant. This compatibility condition is particularly restricting on the surface velocity $\boldsymbol{v}$.

Finally in this chapter we considered the case of a double obstacle potential and the difficulties that brought. Most notably that in the bulk regions we no

longer have any limiting problem and cannot use a pair of asymptotic expansions with matching conditions for the two. Instead we worked with the inner region explicitly and made assumptions on the fluxes on the boundary as in Cahn et al. [2006]. By altering the arguments used for smooth potentials we were able to recover that the limiting problem for the velocity of the interface is that of forced surface diffusion:

$$(\boldsymbol{v}(t) - \boldsymbol{v}_\Lambda(t)) \cdot \boldsymbol{\mu}_\Lambda(t) = \tilde{S}\Delta_s \kappa_\Lambda(t). \tag{6.5}$$

when dropping the term $u\nabla_{\Gamma(t)} \cdot \boldsymbol{v}$ from (3.1) to obtain a non-conservative variant.

Further work would be to consider using more involved asymptotic arguments to rigorously show the convergence of the slower mobility ($\frac{M}{\boldsymbol{v}} \sim \mathcal{O}(\varepsilon^0)$). In particular the numerical example of Section 4.4.3 suggests that this could be done under an assumption of rotational symmetric as in Stoth [1996].

6.3 Chapter 4 - Numerical Simulations

In this chapter we provided supporting evidence of the results in Chapter 3 and also displayed some examples which exhibit interesting behaviour. In Section 4.4.3 we gave a benchmark example where we considered a rotationally symmetric setting on a sphere with tangential mass transport. By comparing the energies of solutions to the evolving surface Cahn-Hilliard equation with the energy of the sharp interface solution, we were able to provide numerical evidence that the derived sharp interface limit is indeed the correct limiting problem. In the example in Section 4.4.5 we showed how a surface velocity can lead to an increase in energy for the solution when the initial and final surface are the same.

Throughout our computations we were restricted to smooth potentials and constant mobilities. Further work would provide supporting examples for non-constant mobilities and non-smooth potentials. In particular we would like to look at simulating solutions for the nESCH equation with logarithmic potential where the temperature parameter θ is scaled with ε. We would like to compare this with simulations of surface diffusion on a moving surface.

6.4 Chapter 5 - A Phase Field Model For Focal Cell Adhesion

In this chapter we extended a known model by Freund and Lin [2004] for focal cell adhesion. Building on the observations of Freund and Lin regarding the process

by which fronts propagate, we applied the phase field methodology to generate an intrinsic model on a surface that could account for topological changes of adhesion patches due to cell migration. Our derived model is based on a conservation law for binder density with a phase field variable to track the fronts between adhered and free regions. The surface evolution is derived from a force balance equation that results in a surface analogue of Stoke's flow by considering the membrane as a visco-elastic fluid subject to forcing from an array of potentials. The resultant model can be thought of as a two-phase Stokes-Allen-Cahn equation with forcing due to a surface field.

We have also analysed our model in the sharp interface limit to be able to compare it with the Freund and Lin model as well as comparing it with known literature results on two phase surface flows.

As a step towards simulating the full model, we considered a reduced model that is based on a simpler bending energy and also simplifies which components of the system energy affect the governing equations. We implemented this reduced model in MATLAB and presented some interesting results. In particular we were able to recover qualitative behaviour of the Freund and Lin model.

There are many open questions we would like to answer in regards this work, of great interest would be deriving an appropriate numerical scheme for the full model. This would allow us to produce simulations and thus compare the behaviour of solutions of our model with experimental data of the cell adhesion process. Comparisons of this nature would allow us to fit parameters to our model as well as exploring suitable expressions for some of the functions we assumed general forms of, for example the adhesion potentials p_i.

Bibliography

H. Abels. Longtime behavior of solutions of a navier-stokes/cahn-hilliard system. *Banach Center Publications*, 86(1):9–19, 2009.

H. Abels, H. Garcke, and G. Grün. Thermodynamically consistent, frame indifferent diffuse interface models for incompressible two-phase flows with different densities. *Mathematical Models and Methods in Applied Sciences*, 22(03):1150013, 2012.

S. Allen and J. Cahn. A microscopic theory for antiphase boundary motion and its application to antiphase domain coarsening. *Acta Metallurgica*, 27(6):1085–1095, 1979.

A. Alphonse, C. Elliott, and B. Stinner. An abstract framework for parabolic pdes on evolving spaces. *arXiv preprint arXiv:1403.4500*, 2014.

H. Alt and W. Alt. Phase boundary dynamics: Transitions between ordered and disordered lipid monolayers. *Interfaces and Free Boundaries*, 11(1):1–36, 2009.

M. Arnold, A. Cavalcanti, A. Elisabetta, R. Glass, J. Blümmel, W. Eck, M. Kantlehner, H. Kessler, and J. Spatz. Activation of integrin function by nanopatterned adhesive interfaces. *ChemPhysChem*, 5(3):383–388, 2004.

M. Arroyo and A. DeSimone. Relaxation dynamics of fluid membranes. *Physical Review E*, 79(3):031915, 2009.

G. Bao and S. Suresh. Cell and molecular mechanics of biological materials. *Nature materials*, 2(11):715–725, 2003.

J. Barrett, H. Garcke, and R. Nürnberg. On the parametric finite element approximation of evolving hypersurfaces in R3. *Journal of Computational Physics*, 227 (9):4281–4307, 2008.

J. Barrett, H. Garcke, and R. Nürnberg. On the stable numerical approximation of two-phase flow with insoluble surfactant. *ESAIM: Mathematical Modelling and Numerical Analysis*, 49(2):421–458, 2015.

P. Bastian, M. Blatt, A. Dedner, C. Engwer, R. Klfkorn, M. Ohlberger, and M. Sander. A Generic Grid Interface for Parallel and Adaptive Scientific Computing. Part I: Abstract Framework. *Computing*, 82(2–3):103–119, 2008a.

P. Bastian, M. Blatt, A. Dedner, C. Engwer, R. Klfkorn, M. Ohlberger, and M. Sander. A Generic Grid Interface for Parallel and Adaptive Scientific Computing. Part II: Implementation and Tests in DUNE. *Computing*, 82(2–3):121–138, 2008b.

P. Bates and P. Fife. The dynamics of nucleation for the cahn-hilliard equation. *SIAM Journal on Applied Mathematics*, 53(4):990–1008, 1993.

G. Bell, M. Dembo, and P. Bongrand. Cell adhesion, competition between nonspecific repulsion and specific bonding. *Biophysical journal*, 45(6):1051, 1984.

G. Bell et al. Models for the specific adhesion of cells to cells. *Science*, 200(4342): 618–627, 1978.

D. Betounes. Kinematics of submanifolds and the mean curvature normal. *Archive for Rational Mechanics and Analysis*, 96(1):1–27, 1986.

M. Blatt and P. Bastian. The iterative solver template library. In *Applied Parallel Computing. State of the Art in Scientific Computing*, volume 4699 of *Lecture Notes in Computer Science*, pages 666–675. Springer, 2007.

T. Blesgen. A generalization of the navier-stokes equations to two-phase flows. *Journal of Physics D: Applied Physics*, 32(10):1119, 1999.

J. Blowey and C. Elliott. The cahn–hilliard gradient theory for phase separation with non-smooth free energy part i: mathematical analysis. *European Journal of Applied Mathematics*, 2(03):233–280, 1991a.

J. Blowey and C. Elliott. The cahn–hilliard gradient theory for phase separation with non-smooth free energy part i: mathematical analysis. *European Journal of Applied Mathematics*, 2(03):233–280, 1991b.

A. Boulbitch, Z. Guttenberg, and E. Sackmann. Kinetics of membrane adhesion mediated by ligand–receptor interaction studied with a biomimetic system. *Biophysical Journal*, 81(5):2743–2751, 2001.

F. Boyer, C. Lapuerta, S. Minjeaud, B. Piar, and M. Quintard. Cahn–hilliard/navier–stokes model for the simulation of three-phase flows. *Transport in Porous Media*, 82(3):463–483, 2010.

S. Brenner and R. Scott. *The mathematical theory of finite element methods*, volume 15. Springer Science & Business Media, 2007.

G. Caginalp. Stefan and hele-shaw type models as asymptotic limits of the phase-field equations. *Physical Review A*, 39(11):5887, 1989.

J. Cahn. On spinodal decomposition. *Acta Metallurgica*, 9:795–801, 1961.

J. Cahn and J. Hilliard. Free energy of a nonuniform system. i. interfacial free energy. *J.Chem.Phys*, 28:258–267, 1958.

J. Cahn, C. Elliott, and A. Novick-Cohen. The cahn-hilliard equation with a concentration dependent mobility: motion by minus the laplacian of the mean curvature. *Euro. J. Appl. Math.*, 7:287–301, 2006.

P. Canham. The minimum energy of bending as a possible explanation of the biconcave shape of the human red blood cell. *Journal of theoretical biology*, 26 (1):61–81, 1970.

P.R. Cha, D.H. Yeon, and J.K. Yoon. Phase-field model for multicomponent alloy solidification. *Journal of Crystal Growth*, 274(12):281 – 293, 2005. ISSN 0022-0248.

D. Cuvelier, O. Rossier, P. Bassereau, and P. Nassoy. Micropatterned" adherent/repellent" glass surfaces for studying the spreading kinetics of individual red blood cells onto protein-decorated substrates. *European Biophysics Journal*, 32 (4):342–354, 2003.

S. Dai and Q. Du. Coarsening mechanism for systems governed by the cahn-hilliard equation with degenerate diffusion mobility. *Multiscale Modeling and Simulation*, 12(4):1870–1889, 2014.

A. Dedner, R. Klfkorn, M. Nolte, and M. Ohlberger. A Generic Interface for Parallel and Adaptive Scientific Computing: Abstraction Principles and the DUNE-FEM Module. *Computing*, 90(3–4):165–196, 2010.

A. Demlow and G. Dziuk. An adaptive finite element method for the laplace-beltrami operator on implicitly defined surfaces. *SIAM Journal on Numerical Analysis*, 45(1):421–442, 2007.

M. Dustin, L. Ferguson, P.Y. Chan, T. Springer, and D. Golan. Visualization of cd2 interaction with lfa-3 and determination of the two-dimensional dissociation

constant for adhesion receptors in a contact area. *The Journal of cell biology*, 132 (3):465–474, 1996.

G. Dziuk and C. Elliott. Finite elements on evolving surfaces. *IMA Journal of Numerical Analysis*, 27(2):262–292, 2007. doi: 10.1093/imanum/drl023.

G. Dziuk and C. Elliott. Finite element methods for surface pdes. *Acta Numerica*, 22:289–396, 5 2013. ISSN 1474-0508. doi: 10.1017/S0962492913000056.

C. Eilks and C. Elliott. Numerical simulation of dealloying by surface dissolution via the evolving surface finite element method. *Journal of Computational Physics*, 227(23):9727–9741, 2008.

C. Elliott and H. Garcke. On the cahn-hilliard equation with degenerate mobility. *Siam journal on mathematical analysis*, 27(2):404–423, 1996.

C. Elliott and S. Luckhaus. *A generalised diffusion equation for phase separation of a multi-component mixture with interfacial free energy.* Universität Bonn. SFB 256. Nichtlineare Partielle Differentialgleichungen, 1991.

C. Elliott and T. Ranner. Evolving surface finite element method for the cahn-hilliard equation. *ArXiv e-prints*, oct 2013.

C. Elliott and B. Stinner. A surface phase field model for two-phase biological membranes. *SIAM Journal on Applied Mathematics*, 70:2904–2928, 2010a.

C. Elliott and B. Stinner. Modeling and computation of two phase geometric biomembranes using surface finite elements. *J. Comput. Phys.*, 229(18):6585–6612, 2010b.

C. Elliott and B. Stinner. A surface phase field model for two-phase biological membranes. *SIAM Journal on Applied Mathematics*, 70(8):2904–2928, 2010c.

C. Elliott and B. Stinner. Computation of two-phase biomembranes with phase dependent material parameters using surface finite elements. *Commun. Comput. Phys.*, 13(2):325–360, 2013.

C. Elliott and V. Styles. An ale esfem for solving pdes on evolving surfaces. *Milan Journal of Mathematics*, 80(2):469–501, 2012.

C. Elliott and C. Venkataraman. Error analysis for an ale evolving surface finite element method. *Numerical Methods for Partial Differential Equations*, 31(2): 459–499, 2015.

C. Elliott and S. Zheng. On the cahn-hilliard equation. *Archive for Rational Mechanics and Analysis*, 96(4):339–357, 1986.

E. Evans. Bending resistance and chemically induced moments in membrane bilayers. *Biophysical journal*, 14(12):923, 1974.

P. Fife and O. Penrose. Interfacial dynamics for thermodynamically consistent phase-field models with nonconserved order parameter. *J. Differential Equations*, pages 1–49, 1995.

P. Fife et al. *Mathematical aspects of reacting and diffusing systems*. Springer Verlag, 1979.

L. Freund and Y. Lin. The role of binder mobility in spontaneous adhesive contact and implications for cell adhesion. *Journal of the Mechanics and Physics of Solids*, 52(11):2455 – 2472, 2004. ISSN 0022-5096.

C. Gal and M. Grasselli. Asymptotic behavior of a cahnhilliardnavierstokes system in 2d. *Annales de l'Institut Henri Poincare (C) Non Linear Analysis*, 27(1):401 – 436, 2010. ISSN 0294-1449.

S. Ganesan and L. Tobiska. A coupled arbitrary lagrangian–eulerian and lagrangian method for computation of free surface flows with insoluble surfactants. *Journal of Computational Physics*, 228(8):2859–2873, 2009.

H. Garke and B. Stinner. Second order phase field asymptotics for multi-component systems. *Interfaces and Free Boundaries*, 8:131–157, 2006a.

H. Garke and B. Stinner. Second order phase field asymptotics for multi-component systems. *Interfaces and Free Boundaries*, 8:131–157, 2006b.

S. Gross and A. Reusken. *Numerical methods for two-phase incompressible flows*, volume 40. Springer Science & Business Media, 2011.

M. Gurtin. Generalized ginzburg-landau and cahn-hilliard equations based on a microforce balance. *Physica D: Nonlinear Phenomena*, 92(3):178–192, 1996.

Z Guttenberg, B Lorz, E Sackmann, and A Boulbitch. First-order transition between adhesion states in a system mimicking cell-tissue interaction. *EPL (Europhysics Letters)*, 54(6):826, 2001.

K. Lam H. Garcke and B. Stinner. Diffuse interface modelling of soluble surfactants in two-phase flow. *arXiv preprint arXiv:1303.2559*, 2013.

C.J. Heine. *Isoparametric finite element approximation of curvature on hypersurfaces*. Citeseer, 2004.

W. Helfrich. Elastic properties of lipid bilayers: theory and possible experiments. *Zeitschrift für Naturforschung C*, 28(11-12):693–703, 1973.

P. Hohenberg and B. Halperin. Theory of dynamic critical phenomena. *Reviews of Modern Physics*, 49(3):435–479, 1977.

E. Kenneth and J. Claes. Adaptive finite element methods for parabolic problems i: A linear model problem. *SIAM Journal on Numerical Analysis*, 28(1):43–77, 1991.

S. Khatri and A.K. Tornberg. A numerical method for two phase flows with insoluble surfactants. *Computers & Fluids*, 49(1):150–165, 2011.

M.C. Lai, Y.H. Tseng, and H. Huang. An immersed boundary method for interfacial flows with insoluble surfactant. *Journal of Computational Physics*, 227(15):7279–7293, 2008.

L. Landau and V. Ginzburg. On the theory of superconductivity. *Zh. Eksp. Teor. Fiz.*, 20:1064, 1950.

N. Le. A gamma-convergence approach to the cahn–hilliard equation. *Calculus of Variations and Partial Differential Equations*, 32(4):499–522, 2008. ISSN 1432-0835.

C. Leung and M. Berzins. A computational model for organism growth based on surface mesh generation. *Journal of Computational Physics*, 188(1):75 – 99, 2003. ISSN 0021-9991.

A. Matthieu, D. Hilhorst, and H. Matano. The singular limit of the allencahn equation and the fitz-hughnagumo system. *Journal of Differential Equations*, 245 (2):505 – 565, 2008. ISSN 0022-0396. doi: http://dx.doi.org/10.1016/j.jde.2008.01.014.

W. Mullins and R. Sekerka. Morphological stability of a particle growing by diffusion or heat flow. *J. Appl. Phys.*, 34:323–329, 1963.

M. Muradoglu and G. Tryggvason. A front-tracking method for computation of interfacial flows with soluble surfactants. *Journal of computational physics*, 227 (4):2238–2262, 2008.

P. Bates N. Alikakos and X. Chen. Convergence of the cahn-hilliard equation to the hele-shaw model. *Archive for rational mechanics and analysis*, 128(2):165–205, 1994.

B. Nestler, H. Garcke, and B. Stinner. Multicomponent alloy solidification: phase-field modeling and simulations. *Physical Review E*, 71(4):041609, 2005.

A. Novick-Cohen. The nonlinear cahn-hilliard equation: Transition from spinodal decomposition to nucleation behavior. *Journal of Statistical Physics*, 38(3-4): 707–723, 1985. ISSN 0022-4715.

A. Novick-Cohen. The cahn-hilliard equation. *Handbook of differential equations: evolutionary equations*, 4:201–228, 2008.

D. O'Connor and B. Stinner. The Cahn-Hilliard equation on an evolving surface. *ArXiv e-prints*, July 2016.

K. Park, F.W. Mao, and H. Park. Morphological characterization of surface-induced platelet activation. *Biomaterials*, 11(1):24–31, 1990.

R. Pego. Front migration in the nonlinear cahn-hilliard equation. *Proceedings of the Royal Society of London. A. Mathematical and Physical Sciences*, 422(1863): 261–278, 1989.

M. Rahimi, A. DeSimone, and M. Arroyo. Curved fluid membranes behave laterally as effective viscoelastic media. *Soft Matter*, 9(46):11033–11045, 2013.

A. Ratz. A benchmark for the surface cahnhilliard equation. *Applied Mathematics Letters*, 56:65 – 71, 2016. ISSN 0893-9659.

D. Rodrigues, R. Ausas, F. Mut, and G. Buscaglia. A semi-implicit finite element method for viscous lipid membranes. *Journal of Computational Physics*, 298: 565–584, 2015.

S. Rosenberg. *The Laplacian on a Riemannian manifold: an introduction to analysis on manifolds*. Number 31 in London Mathematical Society: Student Texts. Cambridge University Press, 1997.

J. Rubinstein and P. Sternberg. Nonlocal reactiondiffusion equations and nucleation. *IMA Journal of Applied Mathematics*, 48(3):249–264, 1992.

P. Saffman and M. Delbrück. Brownian motion in biological membranes. *Proceedings of the National Academy of Sciences*, 72(8):3111–3113, 1975.

S. Serfaty. Gamma-convergence of gradient flows on hilbert and metric spaces and applications. *Discrete Contin. Dyn. Syst*, 31(4):1427–1451, 2011.

J. Shen and X. Yang. A phase-field model and its numerical approximation for two-phase incompressible flows with different densities and viscosities. *SIAM Journal on Scientific Computing*, 32(3):1159–1179, 2010.

L. Smilenov, A. Mikhailov, R. Pelham, E. Marcantonio, and G. Gundersen. Focal adhesion motility revealed in stationary fibroblasts. *Science*, 286(5442):1172–1174, 1999.

I. Steinbach, F. Pezzolla, B. Nestler, M. Seeßelberg, R. Prieler, G. Schmitz, and J. Rezende. A phase field concept for multiphase systems. *Physica D: Nonlinear Phenomena*, 94(3):135–147, 1996.

B. Stinner, B. Nestler, and H. Garcke. A diffuse interface model for alloys with multiple components and phases. *SIAM Journal on Applied Mathematics*, 64(3): 775–799, 2004.

B. Stoth. Convergence of the cahnhilliard equation to the mullinssekerka problem in spherical symmetry. *Journal of Differential Equations*, 125(1):154 – 183, 1996. ISSN 0022-0396.

J. Tiaden, B. Nestler, H.J. Diepers, and I. Steinbach. The multiphase-field model with an integrated concept for modelling solute diffusion. *Physica D: Nonlinear Phenomena*, 115(1):73–86, 1998.

S. Vey and A. Voigt. Amdis: adaptive multidimensional simulations. *Computing and Visualization in Science*, 10(1):57–67, 2007.

G. Witterstein. Sharp interface limit of phase change flows. *Advances in Mathematical Sciences and Applications*, 20(2):585, 2010.

C. Wolgemuth. Lamellipodial contractions during crawling and spreading. *Biophysical journal*, 89(3):1643–1649, 2005.

J.J. Xu, Z. Li, J. Lowengrub, and H. Zhao. A level-set method for interfacial flows with surfactant. *Journal of Computational Physics*, 212(2):590–616, 2006.

J.J. Xu, Y. Huang, M.C. Lai, Z. Li, et al. A coupled immersed interface and level set method for three-dimensional interfacial flows with insoluble surfactant. *Communications in Computational Physics*, 15(2):451–469, 2014.

X. Yang and A. James. An arbitrary lagrangian-eulerian (ale) method for interfacial flows with insoluble surfactants. *FDMP*, 3:65–96, 2007.

S. Yon and C. Pozrikidis. A finite-volume/boundary-element method for flow past interfaces in the presence of surfactants, with application to shear flow past a viscous drop. *Computers & Fluids*, 27(8):879–902, 1998.